Waseda University
Tokyo, Japan.

Single Molecule Studies of F_1-ATPase with a Truncated Gamma Subunit

ガンマサブユニットを切り欠いた
F_1-ATPaseの一分子研究

By

Mohammad Delawar Hossain

A thesis submitted to the Graduate School of Science and Engineering
for the degree of Doctor of Science

February, 2008

ACKNOWLEDGEMENTS

ACKNOWLEDGEMENTS

I would like to express my sincere gratitude to my reverend teacher and supervisor Professor Kazuhiko Kinosita Jr., Department of Physics, Waseda University, Tokyo, Japan for his valuable guidance, creative suggestions, constructive criticism, patience, encouragement and continuous financial support from his research grant during the entire period of research for my Ph.D. degree. Professor Kinosita is a person of big heart and of high level mentality. I fell very fortunate to have an opportunity to work under his superb supervision. I am also grateful to him for arranging full financial support for me during my many trips within Japan and several other countries to present my research work in different international conferences. Thanks are also due to him for lending me some money when I first came in Japan and providing many fruitful suggestions to continue my daily life in Japan. I am deeply indebted to Dr. Md. Yusuf Ali, Associate Professor, Department of Physics, Shahjalal University of Science and Technology, Sylhet, Bangladesh who has introduced me with Professor Kinosita to do present research in Japan. He also taught me some biophysical techniques in Kinosita lab.

I deeply appreciate and acknowledge to Professor Shin`ichi Ishiwata, Department of Physics, Waseda University and Professor Masasuke Yoshida, Director, Chemical Resource laboratory, Tokyo Institute of Technology, Japan for their intellectual questions and critical suggestions during my regular (half yearly) presentation in joint seminar at Waseda University that have helped greatly to improve my research as well as my Ph.D. thesis. Professor Shin`ichi Ishiwata also helped me greatly in administrative work related to my Ph.D. degree. I wish to express my warm and sincere thanks to Professor Hiromichi Nakazato, Head, Department of Physics, Waseda University, for his kind help and cooperation. Thanks are due to Dr. Mitsunori TAKANO, Associate Professor, Department of Physics, Waseda University for his interest and encouragement in this work. Thanks are also due to all the faculty members of the Department of Physics, Integrative Bioscience and Biomedical Engineering, Waseda University for their interest in this work.

I also record my thanks to Dr. Hiroyasu Itoh for his constructive comments throughout this work. Here are a few to whom I must deliver my special thanks. Dr. Kengo Adachi taught me F_1 purification and provided advices and feedback on my research at different stages. Dr. Shou Furuike with whom I mainly collaborated taught me several biophysical techniques and constantly provided suggestions throughout this work. I want to specially thank Rieko Shimo-Kon, who helped me greatly in many ways during my research work in Kinosita lab. I also thank Dr. Naoyoshi Sakaki for helping me in torque calculations and use of Video Savant program. I do not hesitate to deliver my thanks to Dr. Katsuyuki Shiroguchi for his help during making my alien registration card in Okazaki city hall and opening a Bank account as well as scientific help during my research. I would like to thank Yasuhiro Onoue for his patient assistance and fruitful suggestions during my experiment. I also thank Dr. Tetsuaki Okamoto for his help in installing Video Savant program as well as recording system with a microscope. Thanks are also due to Katsunori Yogo for his interest about my research. Thanks are due to Dr. Digambara Patra and Dr. Akilan Palanisami for their scientific and personal cooperation during my research work. I gratefully acknowledge the kind help and cooperation from Mikiko Fukatsu who cordially did huge official work for me. Thanks a lot to Hitomi Umezawa and Yuta Shimamoto for their cordial help in filling and checking the Ph.D. application forms. I am also grateful to Keiko Sakamaki for her official help. I remember all the undergraduate and Masters students of Kinosita lab with whom I mixed and enjoyed social life.

I am thankful to all the people with whom I came in contact during my research in Kinosita lab at the center of integrative bioscience, Okazaki National Research Institutes of Natural Sciences, Japan. I am specially thankful to the officers of Yamate Lodge where I lived about two years who made my life easy and enjoyable therein. I am also thankful to the officers of STEP 21 and Waseda Machi guest house for their kind help and cooperation in various ways.

I feel it my profound privilege to express my sincere thanks to Professor M. Habibul Ahsan, Head, Department of Physics, Shahjalal University of Science and Technology, Sylhet, Bangladesh for his constructive advice and official help

during the period of study leave abroad. I also thank Professor Mominul Huq, BUET, Dhaka, Bangladesh for his inspiring suggestions and cooperation.

Thanks a lot to the authority of Shahjalal University of Science and Technology, Sylhet, Bangladesh for granting me the necessary study leave to complete my Ph.D. research in Japan. This research work was supported in part by grants-in-aid from the Ministry of education, Culture, Sports, Science and Technology of Japan.

Mohammad Delawar Hossain

Dedicated to my beloved son:
Nabil Mahmud

ABSTRACT

ABSTRACT

This thesis deals with the elucidation of the role of rotor-stator interactions in rotation as well as the mechanism of torque generation by F_1-ATPase with emphasis on the role of the γ subunit. An $\alpha_3\beta_3\gamma$ sub-complex of F_1-ATPase derived from thermophilic *Bacillus* PS3 (TF_1) was used and expressed in *Escherichia coli*. Three groups of mutants were constructed genetically by successive truncation of amino acid residues from either carboxy (C) terminus or from both amino (N) and carboxy (C) termini of the γ subunit: **A** in which the tip of the γ subunit is absent, **B** in which only a single amino-terminal helix swings freely in the stator cavity and **C** where the rotor remains outside the cavity and simply sits on the concave entrance of the stator orifice. Purification procedures were adjusted depending on the stability of the mutant complexes. Wild type and group **A** mutants were purified with heat treatment and using an affinity column, a hydrophobic-interaction column and a size-exclusion column (4 °C). For group **B**, the hydrophobic-interaction column and heat treatment were omitted. For group **C**, the same method as **B** was used except that the size-exclusion column chromatography was done at room temperature. The ATP hydrolysis activity of F_1-ATPase in bulk solution was measured with a spectrophotometer at 23 °C. Rotation of F_1-ATPase was observed on an inverted microscope by attaching plastic beads or gold particles to the γ subunit. Bead images were captured with a high speed charged-coupled device camera.

The rotary characteristics of the group **A** mutants monitored by using a 0.49 μm bead duplex did not differ greatly from those of the wild-type over the ATP concentrations of 20 nM-2 mM, the most conspicuous effect being 50 % reduction in torque and 70 % reduction in the rate of ATP binding. The ATP hydrolysis activity estimated in bulk samples was more seriously affected. The shortest mutant in which twenty one amino acid residues from the carboxy terminus is absent, in particular, was > 10 times less active compared to the wild type, but this is likely due to instability of this complex. Time courses of ATP hydrolysis of the mutants were complicated involving lag and slow inactivation. The use of a

surfactant such as lauryldimethaylamine oxide (LDAO) in the hydrolysis assay stimulated ATP hydrolysis activity of both wild type and the mutants. Inactivated states of mutants became activated and followed simple Michealis-Menten kinetics. The rotary torque produced by the wild type and mutant F_1-ATPase in the presence of LDAO remained unaffected. The effect of another surfactant sodium dodecyl sulfate (SDS) on the mutants was also explored. The SDS study apparently indicates that the shortest mutant as mentioned above showed relatively poor ATP hydrolysis activity due to its very weak structure.

Group **B** mutants and several of group **C** mutants monitored by using a 0.29 μm bead duplex produced ~50 % of wild type torque but the hydrolysis activity was reduced to ~3 % in some mutants. These mutants could be used for rotation only while fresh, within three days after purification when kept at room temperature. All the mutants of group **B** and **C** carrying a gold particle rotated in the correct direction, though some mutants exhibited moments of irregular motion. This implies that neither a pivot nor an axle is needed for rotation of F_1-ATPase. The time-averaged rate of rotation as well as the rate of ATP hydrolysis were low in the mutants compared to the wild type, indicating that the interactions between the rotor tip and the bottom stator support is important for the rapid progress of catalysis. A mutant in group **C** lacking most of the rotor shaft and with the remaining rotor portion merely sitting on the concave entrance of the stator cylinder still rotates in the correct direction for >100 turns. This suggests that most of the interactions between the rotor and the stator cylinder are not essential for rotation.

CONTENTS

CONTENTS

CHAPTER 1
INTRODUCTION

CHAPTER 1
INTRODUCTION

1.1 Why Single Molecule?

Bio-molecules such as protein motor molecules act as molecular machines and they take part in various activities in biological cells. These machines work stochastically rather than in a synchronized manner. Thus, to understand their mechanisms it is essential to study their behavior individually. Single-molecule studies allow us to image the behavior of a bio-molecule in real time under an optical microscope by attaching a probe to the molecule. By single molecule experiment we can closely observe and manipulate an individual protein molecule, trace the trajectory of its motion, measure the speed, torque and study the mechanism of chemo-mechanical or mechano-chemical energy transduction.

1.2 Rotary Protein Motor

Protein motors convert the chemical energy derived from the hydrolysis of adenosine triphosphate (ATP) into mechanical work to carry out a unique function in biological cells. Rotary motors do their mechanical work by physically rotating some specialized part of the protein. One of the most important rotary protein motor is ATP synthase that synthesizes ATP in animals, bacteria and plants in the process of oxidative phosphorylation or photophosphorylation[1-4]. ATP powers nearly every energy consuming process in the cells that make up biological bodies. ATP synthase consists of two motors: F_o and F_1 as depicted in Fig.1.1. When protons flow through the membrane-embedded F_o motor due to the electrochemical potential gradient across the membrane, ATP is synthesized from ADP and inorganic phosphate in F_1. The ATP synthase is a reversible molecular machine in which ATP hydrolysis in F_1 pumps back protons through F_o. The two reactions, the proton flow in F_o and hydrolysis/synthesis in F_1, have been proposed to be coupled by mechanical rotation[5-6]. Both F_o and F_1 are rotary motors, F_o being driven by proton flow and F_1 by ATP hydrolysis, and the rotary shaft is common to the two motors yet their functional rotary directions are opposite to each other. Thus, when the proton motive force is high and F_o wins, F_1 is forcibly rotated in its

reverse direction, resulting in ATP synthesis by the reversal of the hydrolysis reaction. When F_1 wins, F_o is rotated in reverse and protons flow back. Isolated F_1 hydrolyzes ATP and is called F_1-ATPase. The minimal subcomplex of F_1 that works as an ATP driven rotary motor consists of $\alpha_3\beta_3\gamma$ subunits[7] which is referred to here in this thesis also as F_1 unless ambiguity arises. A brief description of F_1 structure is given in the next section.

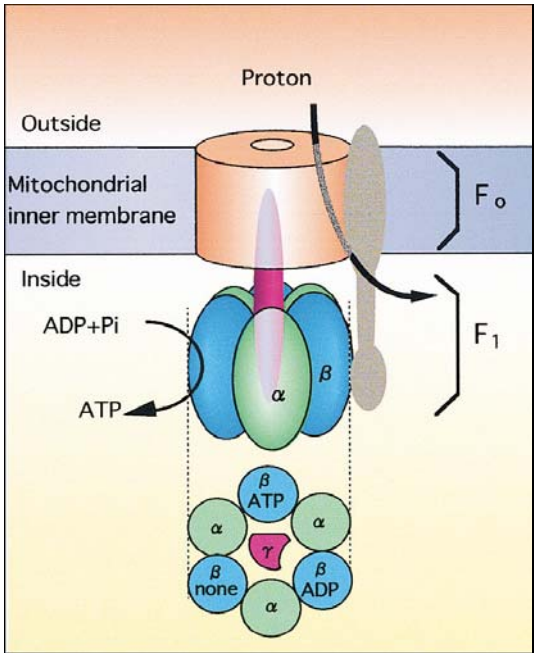

Figure1.1 A simplified schematic view of ATP synthase[2, 8]. The magenta rod at the center represents the common shaft (the γ subunit). The orange cylinder in the membrane rotates together with the γ shaft and the grey part serves as the stator. The bottom diagram shows a top view of the F_1 part with catalytic nucleotides as found in the crystal.

1.3 Structure of F_1

A high resolution structure of bovine mitochondrial F_1-ATPase (MF_1) has revealed that three α- and three β-subunits are alternately arranged to form a stator cylinder[9] as shown in Fig.1.2. An α-helical coiled coil made of the amino (N)- and carboxy (C)-termini of the γ-subunit deeply penetrates the central cavity of the stator cylinder and is held by the cylinder wall at two positions, at the orifice and the bottom. Three β subunits bind and hydrolyze ATP whereas three α subunits bind ATP without hydrolysis. Three catalytic sites reside at α-β interfaces, primarily hosted by a β-subunit. In the original structure, one site (hosted by β_{TP}

and α_{TP}) bound an ATP analog, another (β_{DP} and α_{DP}) ADP and the third (β_E and α_E) none. The central γ-subunit breaks the three-fold symmetry seen in the empty $\alpha_3\beta_3$ barrel[11], laying the basis for unidirectional rotation. The non-catalytic sites, residing at other α-β interfaces and hosted primarily by an α-subunit, bound the ATP analogue.

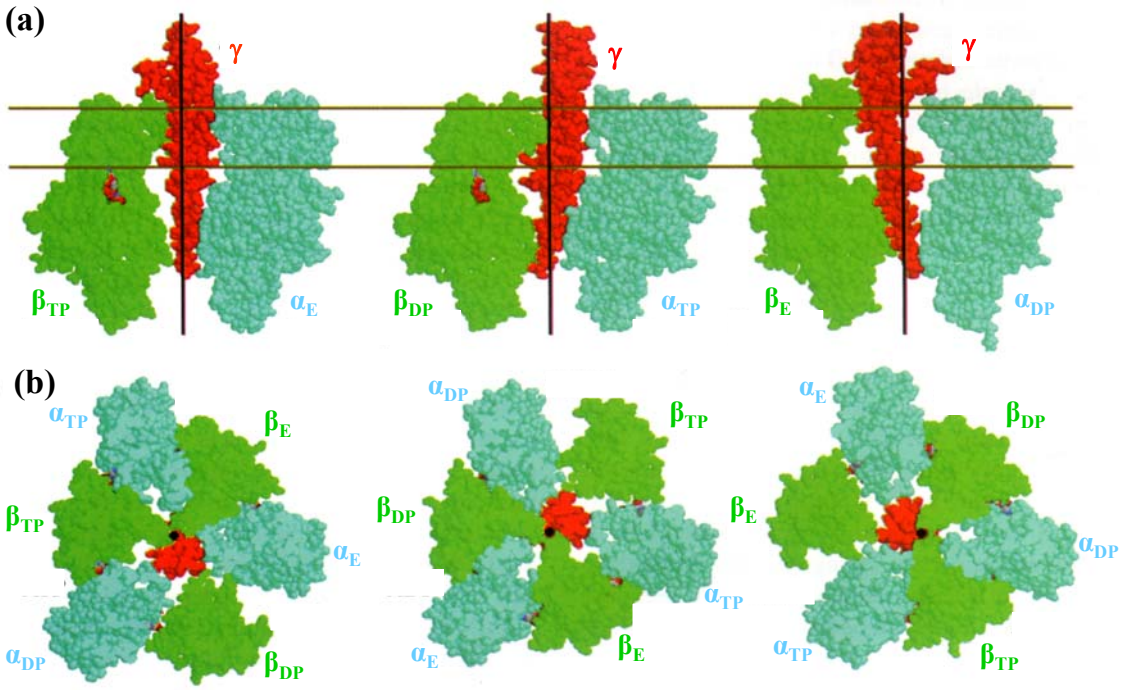

Figure1.2 An atomic structure of MF_1 in which nucleotide dependent conformational changes have been shown[2, 9]. (**a**) The central γ, one β to the left of γ, and one α to the right are selected and shown. The black lines indicate the rotation axis suggested by Wang and Oster[10]. The lower half of MF_1 retains an approximate three fold symmetry around this axis. Nucleotides are shown in CPK colors. (**b**) Top view of sections of MF_1 between the gold lines in (**a**).

This structure is asymmetric due to differences in the relative orientations of the domains of α and β subunits and in their interactions with γ subunit. The non-catalytic nucleotide binding sites in α_{DP} and α_E are very similar whereas in α_{TP} the site is more open. The conformation of β_E differs substantially from the other two in the central domains where a nucleotide is bound with β_{TP} and β_{DP}. In β_E, the C-terminal half of this central domain together with the bundle of six α-helices that forms the C-terminal domain has rotated from the six fold peudo-symmetry axis. This disruption of the central domain abolishes the capacity of the β_E subunit to bind nucleotides. Therefore, the crystal structure exhibits the asymmetry required

by the binding change mechanism[3] and three different conformations of the subunits β_E, β_{TP} and β_{DP} were considered to represent "open", "loose" and "tight" states respectively.

The structure of the $\alpha_3\beta_3$ complex of F_1 derived from a thermophilic *Bacillus* PS3 (TF_1) was determined at 3.2 Å in the absence of nucleotide[11]. This complex is symmetric and has only low affinity nucleotide binding sites[12] in the absence of the γ subunit. It is the central asymmetric γ subunit that forces the surrounding subunits into different conformations and thereby mediates cooperative interactions among the three catalytic sites in TF_1. The β subunits adopt a conformation essentially identical to that of β_E of MF_1 and the α subunits in both structures also have similar conformations. This structural homology between the $\alpha_3\beta_3$ assemblies in TF_1 and MF_1 together with the conservation of key residues at the catalytic sites strongly implies a common mechanism for the two enzymes. The present work has been done on TF_1.

1.4 Present State of the Mechanism of F_1 Rotation and Aim of the Thesis

Elucidation of the role of rotor-stator interactions in rotation as well as torque generation is a central matter in order to understand the molecular mechanism of F_1. In the structure of MF_1 as shown in Fig. 1.2, the tip of the carboxy-terminus of the γ-subunit held by the bottom of the stator cylinder was suggested to play important roles in rotation of γ-subunit. A single molecule experiment has shown that the γ-subunit rotates uni-directionally inside the cylinder of $\alpha_3\beta_3$ subunits upon ATP hydrolysis[7]. Rotation of the γ-subunit occurs in 120° steps, each accompanied by hydrolysis of one ATP molecule[13-14]. The asymmetric γ-subunit dictates which of the three basically equivalent sites binds the next ATP molecule[15]. ATP binding to that site drives the first 80-90° of a 120° step and release of hydrolysis product drives most of the remaining 40-30° [16]. Based on the MF_1 structure, a push-pull mechanism[10] for rotation was proposed in which the upper part of a β-subunit that takes part in making the orifice of the stator cylinder bends toward and pushes the curved γ-subunit upon binding of an ATP whereas β

retracts and pulls γ upon product release. In this mechanism, the tip of γ-subunit held in the bottom of the stator cylinder essentially acts as a pivot for the conical rotation. However, whether the tip of γ subunit plays any role in rotation as suggested in the MF_1 structure or as a pivot as required by the push-pull mechanism remains an intriguing question. In addition, the functional roles of the γ-subunit in chemo-mechanical energy conversion have not yet been clearly explored.

Interactions between the protruding portion of γ and the top surface of β near the orifice seem less important, because the highly conserved and charged DELSEED sequence that touches γ in the β_{TP} form can all be replaced with alanine without affecting rotational torque[17]. If the penetrating portion of γ is essential for rotation, as the structure suggests, its truncation should at some point lead to loss of torque. In an early study[18], up to 10 residues at the C-terminus of *Escherichia coli* F_1 (EF_1) were truncated, resulting in reduced but significant ATPase activity; deletion of 18 residues gave an inactive enzyme. With chloroplast F_1 (CF_1), truncation up to 20 C-terminal residues did not result in the complete loss of hydrolysis activity[19]. Retention of ATPase activity, however, does not necessarily imply active rotation, because rotation and ATP hydrolysis may be decoupled in a defective enzyme. With single-molecule observation, Müller et al.[20] have shown that up to 12 C-terminal residues of EF_1 can be truncated without affecting torque, although hydrolysis activity was gradually diminished at longer deletions. Deletion of 15 or more residues was also attempted, but the enzyme apparently failed to assemble. Motivated by this work the present research has been undertaken.

The aim of this thesis is to elucidate the role of rotor-stator interactions in rotation as well as torque generation by F_1 with emphasis on the role of the γ-subunit. An $\alpha_3\beta_3\gamma$ sub-complex of F_1 derived from thermophilic *Bacillus* PS3 (TF_1) was expressed in *Escherichia coli*. The γ-subunit was genetically truncated both at its amino- and carboxy- termini step by step until the remaining rotor head would be outside the stator cavity and simply sit on the concave entrance of the

stator orifice. Rotation of the wild type and mutants were observed adopting single molecule techniques.

It was found that all truncation mutants rotated in the correct direction, though the average rotary speeds were low compared to the wild type and some mutants exhibited moments of irregular motion. These results suggest that neither a pivot nor an axle is needed for rotation of F_1.

1.5 Organization of the Thesis

Chapter 2 summarizes basic knowledge about **Enzyme Kinetics**. Chapter 3 describes **Materials and Methods** used in the thesis. Chapter 4 is devoted to **Results and Discussion** and Chapter 5 presents **Conclusion**s.

CHAPTER 2

ENZYME KINETICS

CHAPTER 2

ENZYME KINETICS

2.1 Introduction

Enzymes such as F_1 enhance the rates of chemical reactions and kinetic analysis is essential for characterization of enzymes. The kinetics required to understand how F_1 functions during ATP hydrolysis reaction is discussed in this chapter.

2.2 Basic Terminologies

An **enzyme** acts as a catalyst that increases the rate of a chemical reaction without changing itself by the process. A reaction that involves a catalyst is called a **catalyzed reaction** and the process is called **catalysis**. A **substrate** is a reactant (not catalyst) in a catalyzed reaction. An **inhibitor** is a substance that reduces the rate of a catalyzed reaction and the process is called **inhibition.** An **activator** increases the rate of the reaction. For example, F_1 can hydrolyze ATP by the following simple reaction.

$$F_1+ATP \rightleftharpoons F_1.ATP \longrightarrow F_1+ADP+P_i$$

$$E+S \underset{k_{-1}}{\overset{k_1}{\rightleftharpoons}} E.S \xrightarrow{k_2} E+P \qquad \text{.....(2.1)}$$

In this reaction, F_1 is an enzyme (E) that acts as a catalyst. It reacts with the substrate ATP (S) to form a complex F_1.ATP (ES) that is finally converted into the product ADP+P_i (P) keeping the enzyme F_1 as it is. Back reaction after product formation is ignored. During above reaction often MgADP acts as an **inhibitor** that slows down or stops the reaction whereas addition of lauryldimethaylamine oxide (LDAO) enhances this reaction. That means it acts as an **activator**.

2.3 Michaelis-Menten Kinetics

Leonor Michaelis and Maud Menten proposed a model for enzyme kinetics in 1913. It describes the rate of enzyme catalyzed reactions for many kinds of enzymes. In equation (2.1) the enzyme E combines with substrate S to form an

enzyme-substrate complex ES with a rate constant k_1. The complex ES can either dissociate to individual components E and S with a rate constant k_{-1} or it can break down to yield the product P with a rate constant k_2. The number of reactions catalyzed by an enzyme per second is called the rate of catalysis or enzyme velocity (V) and it varies with the substrate concentration [S]. The Michaelis-Menten equation describing the enzyme velocity V as a function of substrate concentration [S] is given by

$$V = V_{max} \frac{[S]}{[S] + K_M} \quad \text{.....(2.2)}$$

where $$K_M = \frac{k_{-1} + k_2}{k_1} \quad \text{.....(2.3)}$$

The velocity V rises linearly with the increase of substrate concentration and gradually levels off to approach a maximum value V_{max} when a constant rate of product formation is achieved (Fig. 2.1) due to saturation of enzyme active sites with substrate. The following conclusions can be achieved from equation (2.2) at different substrate concentrations.

(a) When $[S] << K_M$, $V=(V_{max}/K_M)[S]$ which implies that the enzyme velocity V is linearly proportional to the substrate concentration.

(b) When $[S] >> K_M$, $V=V_{max}$ which implies that the enzyme velocity V is maximum and the enzyme active sites are fully saturated with substrate.

(c) When $[S] = K_M$, $V=V_{max}/2$ which implies that the enzyme velocity V reaches half its maximum value at a substrate concentration equal to K_M. This K_M value is called the Michaelis-Menten constant and it is the substrate concentration at which half of the enzyme active sites are filled.

The K_M value of an enzyme for a particular substrate depends on several parameters such as pH, temperature and ionic strength[21]. In equation (2.3), if $k_{-1} >> k_2$ then K_M represents the dissociation constant of the complex ES and it acts

as an inverse measure of the binding affinity between the enzyme E and the substrate S. A low K_M indicates a strong affinity of binding and a high K_M indicates a weak affinity of binding. The rate constant k_2 is referred to as the catalytic constant k_{cat} at full saturation when the enzyme velocity is V_{max}. k_{cat} is also called the turnover number of an enzyme. It is the number of substrate molecules that are converted into product by an enzyme molecule per second at full saturation of the enzyme with substrate.

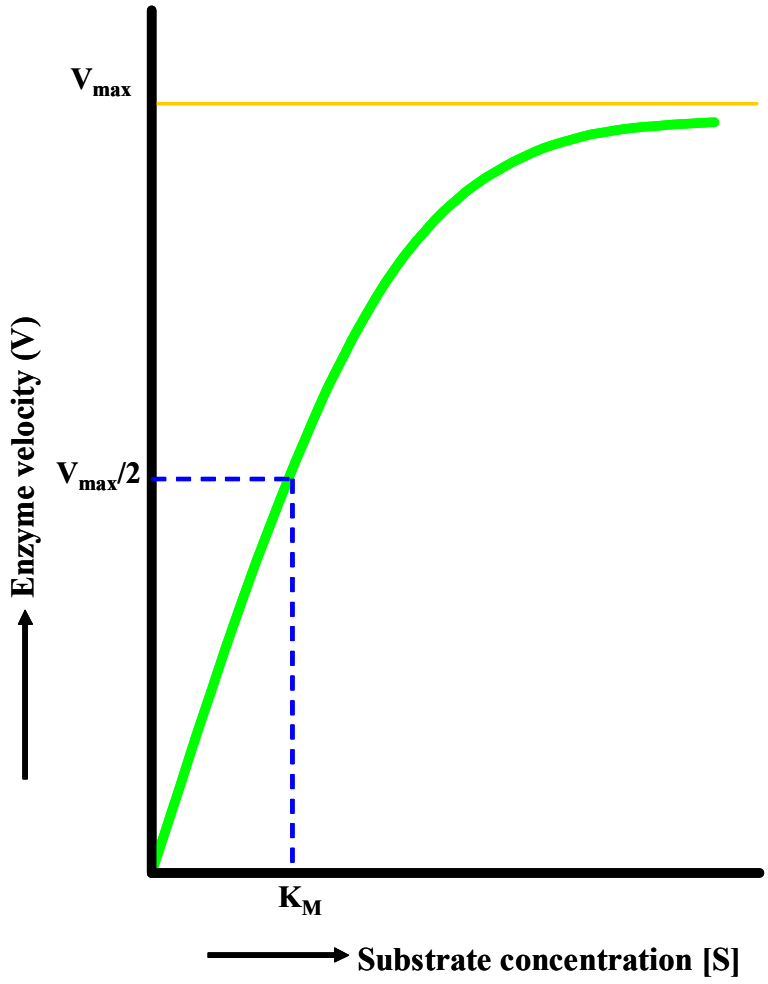

Figure 2.1 The substrate concentration [S] dependence of the enzyme velocity (V). The Michaelis-Menten constant (K_M) is the substrate concentration giving a velocity of $V_{max}/2$.

CHAPTER 3

MATERIALS AND METHODS

CHAPTER 3
MATERIALS AND METHODS

3.1 Introduction

This chapter is devoted to a brief description of the main biophysical and biochemical techniques as well as equipments used in this work. This chapter also includes details of the required experimental procedures. ATP hydrolysis activity of F_1 in bulk solution was measured with a spectrophotometer at 23 °C. Rotation of F_1 was observed on an inverted microscope by attaching plastic beads or gold particles to the γ subunit. Bead images were captured with a high speed charged-coupled device camera. Details are described below.

3.2 Experimental Techniques and Equipments

3.2.1 Sodium Dodecyl Sulfate-Polyacrylamide Gel Electrophoresis (SDS-PAGE)

a. Principle: Electrophoresis is based on the fact that charged molecules move in an electric field. This is a powerful analytical method to identify proteins, DNA or RNA. The polyacrylamide is a continuous matrix composed of the polymer and pores. Proteins or macromolecules are forced to move through the pores of the gel when the electric current is applied across the gel. Sodium dodecyl sulfate (SDS) is an anionic detergent that denatures proteins. It coats proteins with negative charges and linearizes them. The negatively charged protein molecules with different sizes will be pulled to the positive end by the current but will be resisted by the pores of the gel. The protein molecules larger than the size of pores will be obstructed whereas the molecules smaller compared to the size of pores will easily pass through the gel. The molecules of intermediate sizes will partially move through the gel because they can fit inside some but not all the pores of the gel. The SDS-denatured proteins will move through the gel in a series of bands.

The mobility of the protein through the gel is inversely proportional to its size. A mixture of standard proteins in parallel with an unknown protein is run through the gel and a linear standard curve is obtained by plotting the log of the molecular

weight of the standards vs. the distance they migrated through the gel. The apparent molecular weight of the unknown protein can be determined from this curve.

b. Preparation of Gels: A polyacrylamide gel is composed of two separate components. The lower part of the gel is called the **separating gel** having a higher polyacrylamide content (~13 %) and is more basic (pH 8.8). The upper part of the gel is the **stacking gel** with low polyacrylamide content (~5 %) and is slightly acidic (pH 6.8). This gel contains several regularly spaced lanes into which samples are loaded. The stacking gel concentrates protein samples before they enter the separating gel. An assembly of two cleaned glass plates (one notched) with two side spacers and clamps was made and stood upright. The separating gel was made at first by gently mixing all reagents (13 % acrylamide bis, 0.4 M Tris-HCl pH 8.8, 0.01 % SDS, a little ammonium persulfate and 0.1 % N, N, N′, N′-tetramethylethylenediamine) in a 15 ml test tube and quickly poured into the assembly so that about 2 centimeters remain below the bottom of the sample comb to be used in the stacking gel. Several drops of ultra pure water (Millipore-RX45) were overlaid on the top of the gel very carefully to remove bubbles and to prevent drying. The gel assembly was kept in room temperature for about 30-40 minutes to polymerize completely. Added water from the top of the gel was removed after polymerization. The stacking gel (5 % acrylamide bis, 0.13 M Tris-HCl pH 6.8, 0.1 % SDS, a little ammonium persulfate and 0.1 % N, N, N′, N′-tetramethylethylenediamine) was made and poured on the top of the separating gel. A sample comb was then inserted to make lanes and the assembly was allowed another 30-40 min for complete polymerization. After this duration, the sample comb, spacers and clamps were removed and the gel between the two glass plates was cleaned with little ultra pure water to make ready for electrophoresis.

c. Preparation of Sample Buffer and F_1 Protein Sample

The sample buffer (0.4 % SDS, 2 % 2-mercaptoethanol, 0.12 M Tris-HCl pH 6.8, 5 % glycerol, 0.01-0.05 % bromophenol blue) was made and stored in small aliquots (200 µl) in the refrigerator at ~ -20 ^{0}C. Usually an aliquot was taken out of the refrigerator and kept at room temperature before use. Molecular weight standard (marker) or protein F_1 was mixed with the sample buffer at the ratio of 1:1.

d. Sample Injection and Electrophoresis of the Gel

The SDS-PAGE running buffer (25 mM Tris, 192 mM glycine and 0.1 % SDS) was made before electrophoresis and poured into the upper and lower tanks of the electrophoresis apparatus. Both tanks contain electrodes that are connected to the power supply. The upper electrode serves as a **cathode** and the lower electrode serves as an **anode w**hen the power is supplied to the apparatus. The protein sample was loaded into the sample lanes of the stacking gel by a pipetman. Markers were also loaded into some other lanes of the gel. Then the circuit between the two electrodes was completed by the flow of electric current (30 mA) through the slab gel. The blue dye, (bromophenol blue) involved in the protein sample and marker is very small and highly charged so that it moves down through the gel at a faster rate than the proteins in the sample and marker. This dye is called the **tracking dye** because it indicates the progress of electrophoresis. The electrophoresis was stopped when the blue dye reaches the bottom of the gel.

e. Staining and De-staining of the Gel to Visualize the Protein

The gel was removed from between the glass plates after electrophoresis was completed and was taken in a plastic container to stain with a dye solution, Coomassie Briliant blue (CBB). It binds to the proteins within the gel and allows to directly visualize them. CBB was taken in the container and was placed inside a micro-oven to heat the gel (170 W) for 1 min. The gel was then shaken on a Cradle Shaker (ATTA, AE-3605) for 5 min. This procedure was repeated three times. Unbound dye was removed by extensive washing of the gel with de-stain buffer (10 % Methanol and 7 % acetic acid). The gel was de-stained (washed)

three times and finally kept in the buffer under continuous shaking for overnight. Protein in the gel thereafter appeared as blue bands.

f. Drying the Gel and Preservation

The stained gel so obtained was washed well with ultra pure water and made ready to dry it on an electric dryer under vacuum (ATTA, AE-3711). A filter paper (Advantec) was wet with several drops of ultra pure water and the gel was taken on it. This was placed on a larger sheet of filter paper covering the metal screen on the dryer platen. The top of the gel was covered with a cellophane sheet and any air bubble seen was removed. A thick rubber sheet cover flap was then placed over it and the chamber door was closed. Vacuum system was applied to seal the flap and the power of the heater was turned on. Upon completion of gel drying at 70 °C (and at a pressure of about 0.1 MPa) a tense sound was heard so that vacuum was disconnected and power was turned off respectively. After cooling down to room temperature the gel was pasted on a note book for storage and analysis.

3.2.2 Western Blotting

An SDS polyacrylamide gel was run normally to resolve F_1 complexes and markers. While running, filter paper (4 sheets, BIO RAD) and the membrane (Sequi-Blot ^{TM} PVDF, BIO RAD) were cut exactly to fit the resolving part of the SDS gel. Plastic gloves were worn during handling of the membrane to prevent contamination. After the SDS gel being carried out, a sandwich assembled in the order of filter paper (2 sheets) soaked in transfer buffer (SDS-PAGE running buffer and 20 % methanol), a pre-wet membrane (in methanol), resolving SDS gel and filter paper (2 sheets) soaked in transfer buffer was placed in the electroblotting system so that the membrane remains on the anode side. Care was taken to avoid air bubbles between any layers of the sandwich. The system was then subjected to an electric current (200 mA) for 60 min. The system was disassembled after electrophoresis being done and SDS gel was stained and de-stained normally. The membrane was wet in methanol and then shaked gently in 15 ml blocking buffer (20 mM Tris-HCl pH 7.5, 500 mM NaCl, 0.05 % Tween

and Blotting One solution supplied by Nacalai tesque, Japan) for 30 min. A primary antibody (anti-γ antibody) was diluted with blocking buffer and following incubation in this antibody for 60 min with gentle shaking on the Cradle Shaker, the membrane was washed with 3x20 ml of blocking buffer. A secondary antibody (peroxidase labeled goat anti- rabbit IgG human serum adsorbed, Kirkegaard & perry laboratories, 2 Cessna Court, Gaithersburg, Maryland 20879 USA) was diluted with blocking buffer. The pre-washed membrane was then incubated by a secondary antibody for 60 min. After that, solution was discarded and the membrane was washed with 2X20 ml of blocking buffer as before. Then it was washed further with 2X20 ml of blotting buffer (20 mM Tris-HCl pH 7.5, 500 mM NaCl and 0.05 % Tween) only. The γ subunit was detected with (50 ml) immunostaining HRP-1000 Kit (KONIKA MINOLTA, Seikagaku Corporation, Japan) and colored bands were seen. The membrane was dried in air and stored.

3.2.3 Column Chromatography

The column chromatography is an analytical technique used to separate the components of a complex mixture. This system involves a **mobile phase** that flows through the bed of a **stationary phase** in a column by either gravity or external pressure (Fig. 3.1). The column is usually made of a glass or plastic or metal tube of appropriate dimension. The mixture will then be eluted down the column using a suitable **eluent**.

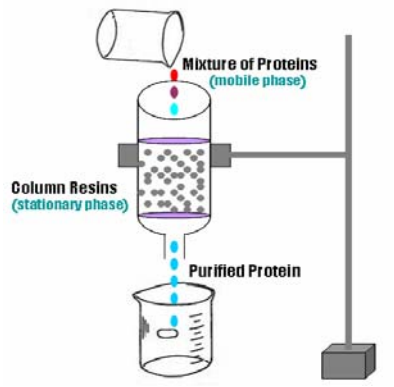

Figure 3.1 An illustration of column chromatography.

The individual components of the mixture are collected from the bottom of the column. There are many varieties of column chromatography depending on the

nature of the stationary and mobile phases. The basic principle of four columns that have been used in the present work will be briefly described in the following sections.

3.2.3.1 Immobilized Metal Affinity Chromatography (IMAC): Ni-NTA Column

a. Principle: This method is used to purify polyhistidine-tagged recombinant proteins. A polyhistidine-tag is an amino acid motif in proteins that involves at least six histidine (His) residues and provided either at the amino (N)- or carboxy (C) -terminus of the target protein. The histidine forms a complex with divalent metals. The metal ions are immobilized on a chromatographic resin by chelation that allows the separation of the histidine-tagged proteins from the untagged proteins.

A popular IMAC is based on the affinity of His-tag proteins for Ni^{2+} ions bound in a complex of Nitrilotriacetic acid (NTA) immobilized on a chromatographic support. NTA is a tetradentate chelating adsorbent that occupies four of the six ligand binding sites in the coordination sphere of the nickel ion leaving two sites free to interact with the 6xHis tag (Qiagen Handbook). NTA binds metal ions stably allowing use of stringent washes and after unbound proteins are washed away, the target protein is eluted with high concentration of imidazole.

b. Preparation of Ni-NTA Column: Ni-NTA Superflow resin (Qiagen, Hilden, Germany) was used in this work to purify F_1. This NTA coupled Superflow consists of highly cross-linked (6 %) agarose beads whose size range is 60-160 µm. It is a blue (50 %) suspension in 30 % ethanol pre-charged with Ni^{2+}. A Superflow bottle stored at 4 °C was taken out and resin was gently mixed well. Prior to use in the column the resin was washed three times with ultra pure water in such a way that 20 ml resin taken in a test tube was kept in room temperature (23 °C) for precipitation within several minutes. Then ethanol solution deposited on the top of the resin was discarded and same amount of ultra pure water was mixed with precipitated resin. A plastic column tube was washed with ultra pure

water and a suitable filter cleaned with an ultrasonic cleaner (VS-100) was fixed in the column at the bottom. After clamping the column with a stand the pre-washed resin was poured to fill it. Ultra pure water was flown out through the orifice at the bottom of the column leaving the resin and again the same suspension was applied. This procedure was repeated until the column was filled up to 10 ml with only resin and another cleaned filter was placed on its top. The bottom orifice was closed and some ultra pure water was poured on the top of the column so that it cannot be dried. The column is now ready for use.

3.2.3.2 Hydrophobic-Interaction Chromatography (HIC): Butyl Column

a. Principle: This is based on hydrophobic attraction between the stationary phase made of immobilized hydrophobic ligands (e.g. butyl or phenyl) covalently attached to the hydrophilic polymer backbone (e.g. cross linked Toyopearl or agarose) and the hydrophobic residues on the surface of the protein molecules. The protein sample is loaded onto the column with a high concentration of a non-denaturing salt like ammonium sulfate. Selective elution of bound proteins is then carried out by applying a decreasing salt gradient.

b. Preparation of Toyopearl Butyl Column: Toyopearl-Butyl-650M resin (Tosoh, Tokyo, Japan) supplied as modified methacrylate copolymer white slurry in 20 % ethanol was used to remove endogenously bound nucleotides from F_1. The resin packed in virgin polyethylene container with polypropylene cap is stored at 4 °C. Toyopearl is a methacrylic polymer that incorporates high mechanical and chemical stability. Particle size range is 40-90 μm. Before use the resin is to be washed. To do this 25 ml resin was taken in a 250 ml glass beaker to gently mix with 75 ml ultra pure water and kept at room temperature for 30-40 minutes to precipitate. After precipitation is completed the liquid at the top of resin was removed and 100 ml ultra pure water was mixed to keep it at room temperature for 30-40 minutes to again precipitate. This procedure was done for further one time. In the final stage the washed resin was mixed with 20 ml ultra pure water and a 10 ml column was made following the same procedure as for Ni-NTA column.

3.2.3.3 Size Exclusion Column: High Pressure Liquid Chromatography (HPLC)

a. Principle: Here the column is filled with polymer beads having precisely controlled pore sizes. The protein sample applied to the top of the column is filtered according to its molecular size. The protein molecules that are larger than the pores cannot enter the bead and stay in the solution surrounding the bead. They quickly pass through a smaller accessible volume within the column and are eluted first. The molecules smaller compared to the size of pores can enter the beads so that they are distributed in the solution both inside the beads and between the beads. They move slowly through a larger accessible volume within the column and are eluted later. The protein molecules of intermediate size may enter the porous beads to some extent and will be eluted between the large and small proteins.

b. Description and Instrumentation of HPLC: A Superdex^{TM} 200 HR 10/30 pre-packed size exclusion column (Amersham pharmacia, piscataway, NJ) was used in this work at the intermediate stage of F_1 purification to remove DTT, denatured protein and unbound biotin. Superdex 200 is made by the covalent bonding of dextran to highly cross-linked porous agarose beads having nominal size of 13 µm. The separation properties of the composite medium are predominantly determined by the dextran component. The column volume is around 24 ml. The stationary phase is composed of micrometer size porous particles so that a high external pressure is necessary to move the mobile phase through the column. This is why an instrumentation system is used with the column to control external pressure and other parameters. The column is connected with the automated AKTA^{TM} design system that is controlled by UNICORN^{TM} program. The HPLC therefore consists of mainly a pump, a reservoir of mobile phase, injector, column, detector, fraction collector and a recorder/data processing system. The liquid sample is introduced into a sample loop of the injector with a syringe. Separation of the sample components occurs as the analytes and mobile phase are pumped (~1.5 MPa) through the column. Each component is eluted from the column as a peak on the recorder and eluted fractions are collected on the collector. The response of the detector to each

component in the column effluent is recorded by detecting a change in refractive indices at UV-VIS absorption at a pre-set wavelength and is displayed on the computer monitor which is known as a chromatogram. This HPLC is always stored and operated at 4 °C.

3.2.3.4 Reverse-Phase HPLC

a. Principle: Its stationary phase is made of a non-polar liquid immobilized on an inert matrix. A more polar liquid acts as the mobile phase. Polar sample molecules interact least with the stationary phase so that they are eluted first and non-polar molecules are attracted by stationary phase and are eluted later.

b. Description and Instrumentation of Reverse Phase HPLC: A pre-packed TSK gel ODS-80Ts column (Tosoh, Japan) was used in this work to measure the nucleotides (ADP) bound with F_1. The column is made of spherical silica gel porous particles that have been derivatized with octadecaylsilane (ODS) reagent. The particle size is 5.0 µm and column volume is 2 ml. In similar to size exclusion HPLC this column is also connected with an automated AKTA^{TM} design system but stored and operated at room temperature.

3.2.4 Single Molecule Imaging and Recording System

A single molecule imaging and recording system (Fig. 3.2) was used in the present work that consists of an inverted microscope, two CCD (charge-coupled-device) cameras and a video cassette recorder with a monitor and an image acquiring system connected with a personal computer (PC). Rotation of beads attached to an F_1 molecule is observed under a microscope (IX70/IX71, Olympus, Tokyo) using a Plan Apo 100x/1.4 oil objective. In one set of experiment, bead images for wild type and group A mutants were captured using CCD1 (CCD-72X, Dage-MTI, Michigan, IN, USA) camera at 30 frames s^{-1} and recorded with a video cassette recorder (EVO-9850, Sony, Tokyo) on the video tape. The Video Savant program was used to make an 8-bit AVI file for each bead image. In another set of experiment, bead images for wild type and group A (in the presence of lauryl dimethylamine oxide), B and C mutants were captured using CCD2 (IPX-210M, Lynx) and a frame grabber (R64-CL, Bit flow) plugged in the PC. The images

were acquired by Video Savant software (version 4.0, IO industries) installed in the PC at a rate of 500 frames s^{-1} to make an 8-bit AVI file for each bead image. For a 40 nm gold particle, bead rotation was observed at 23 °C by laser dark-field microscopy[16] with some modifications (by S. Furuike), on an inverted microscope (Olympus IX70). Images were captured with a high-speed CMOS camera (FASTCAM-DJV, Photron, Tokyo) at 125 to 8,000 frames s^{-1} as an 8-bit AVI file. In all cases, centroid of the image was calculated as described elsewhere[16].

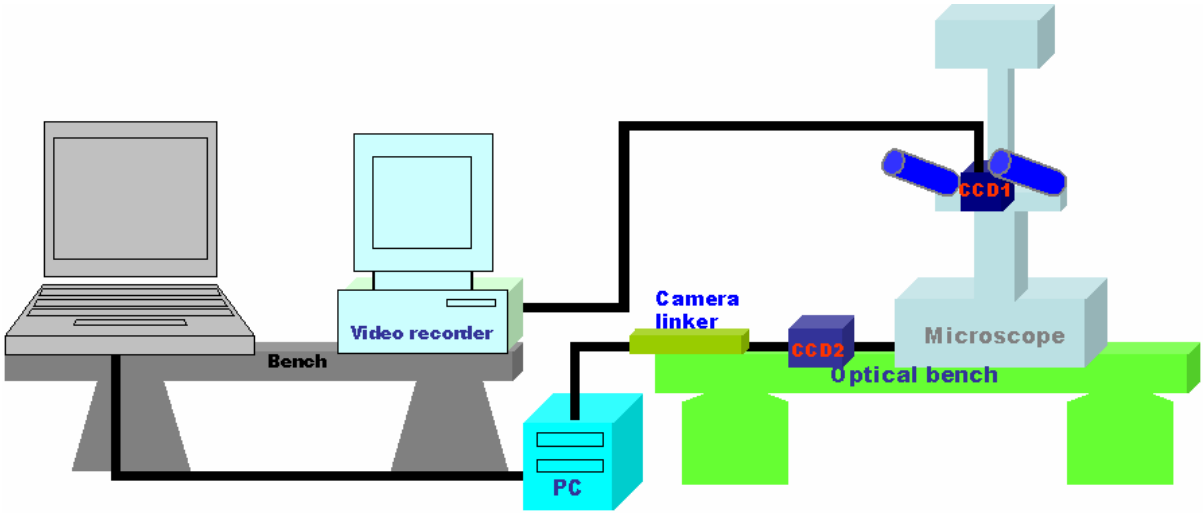

Fig. 3.2 A block diagram of single molecule imaging and recording system.

3.2.5 UV-Vis Spectrophotometer

A spectrophotometer measures the intensity of light as a function of wavelength. Ultraviolet and visible (UV-Vis) absorption spectroscopy usually works at the spectral range of approximately 190 to 900 nm. A double beam spectrophotometer measures the ratio of the light transmitted through a blank to the light transmitted through an absorbing sample. In the present work two double beam spectrophotometers (UV 3101 PC, Shimadzu and U-3100, Hitachi, Tokyo, Japan) were used.

3.2.6 Centrifuge

In biophysical/biochemical experiments, a centrifuge separates cells, viruses, large molecules such as proteins and nucleic acids and plastic or metal beads in a solution according to their size, shape, density, viscosity of the medium and rotor speed. Several types of centrifuge machines were used and will be mentioned in the experimental procedures.

3.2.7 Pipetman

A pipetman is a device used to transfer a very small volume of solution with a high degree of accuracy and precision. A set of Gilson pipetman was used in this study.

3.3 Experimental Procedures

3.3.1 Construction of Mutants

Three groups of mutants were constructed genetically: **A** in which the tip of the γ-subunit is absent, **B** in which only a single amino-terminal helix swings freely in the stator cavity and **C** where the rotor remains outside the cavity and simply sits on the concave entrance of the stator orifice. Details are given below:

a. Mutants A

Molecular Genetics

The mutants of group **A** are: γ-ΔC14, γ-ΔC17, γ-ΔC21 and γ-ΔC25. These mutants were constructed by deleting the amino acid residues from only carboxy (C)-terminus of the γ subunit as described below.

A mutant (α-C193S, β-His_{10} at amino terminus, γ-S107C, γ-I210C) $\alpha_3\beta_3\gamma$ subcomplex derived from a thermophilic *Bacillus* PS3 as wild-type F_1 (TF_1) was used. The wild type and deletion mutants were expressed with plasmid pKABG1/HC95 that carries genes for the α-(C193S), β-(His_{10} at amino terminus), and γ-(S107C, I210C) subunits of TF_1 [16, 22] in *E. coli* (*Escherichia coli*) strain JM103 Δ(uncB-uncD) which has lost the ability to express authentic F_oF_1-ATPase[23]. Plasmids for deletion mutation were prepared in *E. coli* strain JM109[24]

(obtained from Takara Bio Inc., Otsu, Japan). Culture was in a Terrific Broth[25] containing ampicillin (~50 μg ml^{-1}) or kanamycin (~50 μg ml^{-1}).

For deletion, *Bgl*II-*Mlu*I fragment, containing a C-terminal region of the γ subunit, of plasmid pKABG1/HC95 was transferred to plasmid pET-42b(+) (Novagen, Tokyo), in which *Xho*I-*Eco*RI region had been replaced with a fragment lacking a *Hind*III site. The resultant plasmid contained a sole *Hind*III-*Nhe*I region, which encompassed the γ C-terminus. Deletions were introduced by polymerase chain reaction (PCR), with pKABG1/HC95 as template and with the forward primer 5′-GGAAGCTTCTGCCGCTCACTGAC-3′ that included a *Hind*III-site. The reverse primer was, for γ-ΔC14 with deletion of 14 C-terminal residues, 5′-GGGCTAGCTTATTACGTAATCGCCGCTTGGCGAG-3′ that would eliminate 42 nucleotides (14 amino acid residues) before the γ stop codon and that also contained a *Nhe*I-site;

for γ-ΔC17, 5′-GGGCTAGCTTATTACGCTTGGCGAGCGCGGTTGTAG-3′ that would eliminate 51 nucleotides;

for γ-ΔC21, 5′-GGGCTAGCTTATTAGCGGTTGTAGGAAAGCGTCAATGTGC-3′ that would eliminate 63 nucleotides;

for γ-ΔC25, 5′-GGGCTAGCTTATTAAAGCGTCAATGTGCGAATGAGCTCG-3′ that would eliminate 75 nucleotides. The *Hind*III-*Nhe*I portion of the amplified fragment was transferred to the modified pET-42b(+) and its *Bgl*II-*Mlu*I fragment was introduced into pKABG1/HC95 to produce the expression plasmid. Mutations were confirmed by DNA sequencing (Takara Custom Service, Yokkaichi, Japan).

b. Mutants B

Molecular Genetics and Confirmation of Truncation

The mutants of group **B** are: γ-ΔC25, γ-ΔC29, γ-ΔC32, γ-ΔC36, γ-ΔN4C25, γ-ΔN7C25 and γ-ΔN4C29. These mutants were constructed by deleting the amino acid residues either from carboxy (C) terminus or from both amino (N) and carboxy (C) termini of the γ subunit as described below.

Mutations were made on plasmid pKABG1/HC95 that carries genes for the α-(C193S), β-(His_{10} at amino terminus) and γ-(S107C, I210C) subunits of TF_1[16, 22]. We introduced γ C-terminal truncations in pKABG1/HC95 as described in the previous section (Mutant **A**). First, we transferred a *Bgl*II-*Ml*uI fragment of plasmid pKABG1/HC95 containing the region coding γ (thick arrow in Fig. 3.3) into a plasmid derivative of pET-42b(+) (Novagen, Tokyo) in which *Xho*I- *Eco*RI region had been replaced with a fragment lacking an *Hin*d site. The resultant plasmid contained a sole *Hind*III-*Nhe*I region, which encompassed the γ C-terminus. To mutate this region, we prepared an *Hind*III-*Nhe*I fragment with a desired γ truncation by PCR amplification using pKABG1/HC95 as template and the following primers. A forward primer containing an *Hin*d-site:

5′-GGAAGCTTCTGCCGCTCACTGAC-3′

Reverse primers containing an *Nhe*I-site:

for γ-ΔC25, 5′-GGGCTAGCTTATTAAAGCGTCAATGTGCGAATGAGCTCG-3′

for γ-ΔC29, 5′-GGGCTAGCTTATTAGCGAATGAGCTCGTTCGCATTG-3′

for γ-ΔC32, 5′-GGGCTAGCTTATTACTCGTTCGCATTGTCCGTTGC-3′

for γ-ΔC36, 5′-GGGCTAGCTTATTAGTCCGTTGCGTTCTTCATCGC-3′

for γ-ΔC40, 5′-GGGCTAGCTTATTACTTCATCGCCGTCATCCGG-3′

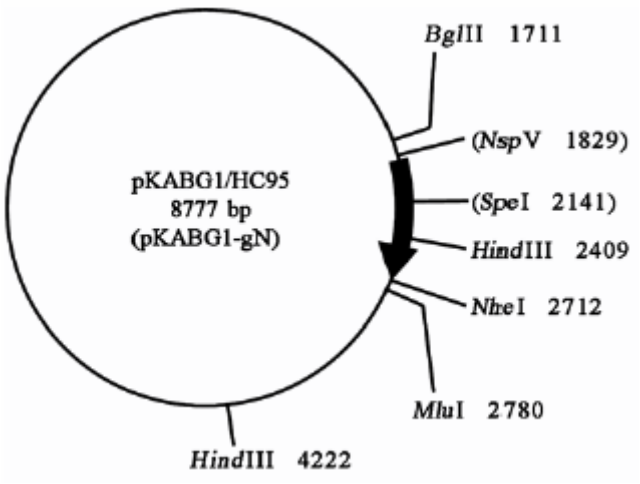

Fig. 3.3 A plasmid showing deletion site.

The *Hind*III-*Nhe*I portion of the amplified fragment was transferred back to the modified pET-42b(+), and its *Bgl*II-*Ml*uI fragment was introduced into pKABG1/HC95 to produce the expression plasmid pKABG1/HC95(γ-ΔC).

For N-terminal truncations, an *Ns*pV site was first introduced into pKABG1/HC95 immediately upstream the γ-coding region and an *Sp*eI site ~300 bases down stream by silent mutations using QuickChange XL Site-Directed Mutagenesis kit (Stratagene, CA).We refer to this plasmid as pKABG1-gN. Primers used for the *Ns*pV site were:

5′-CGCCTGTTAGAACCCGTGTTCGAAAAAGGAGGTGAAACCCATGGC-3′

and

5′-GCCATGGGTTTCACCTCCTTTTTCGAACACGGGTTCTAACAGGCG-3′,

and those for the *Sp*eI site were :

5′-GCAACGTGTTGCGACTAGTGTACCAAACGATCCAAAAACG-3′

and

5′-CGTTTTTGGATCGTTTGGTACACTAGTCGCAACACGTTGC-3′

where underscores show mutations. Then γ-ΔC25 mutation was introduced into pKABG1-gN by replacing its *Sp*eI-*Ml*uI portion with a truncated sequence. The latter was obtained by PCR using pKABG/HC95(γ-ΔC) above as template and a forward primer containing an *Sp*eI site: 5′-GCAACGTGTTGCGACTAGTGTACC-3′ and a reverse primer containing an *Ml*uI site: 5′-CTTGGATAACGCGTCCTCTTGTC-3′.

Finally, an N-terminal truncation was introduced by replacing the *Ns*pV-*Sp*eI portion that encompasses the γ N-terminus with a truncated sequence. The truncated sequences were obtained by PCR using pKABG1-gN as template and following primers.

A reverse primer containing an *Sp*eI site:

5′-GGTACACTAGTCGCAACACGTTGC-3′

Forward primers containing an *Ns*pV site:

For γ-ΔN4C25,

5′-GAACCCGTGTTCGAAAAAGGAGGTGAAACCCATGGATATTAAAACGCGC-3′

for γ-ΔN7C25,

5′-GAACCCGTGTTCGAAAAAGGAGGTGAAACCCATGACGCGCATCAATGCG-3′.

All mutations were confirmed by DNA sequencing (Shimadzu Biotech, DNA Sequence Service, Kyoto, Japan). In *E. coli* strain JM103 Δ(uncB-uncD) which has lost the ability to express authentic F_oF_1-ATPase[23], all mutants were expressed to a level similar to wild type, as seen in Fig. 3.4. The N-terminal five residues of expressed proteins were confirmed by Edman degradation (APRO Life Science Institute, Inc., Naruto, Japan). The initiation residue Met-1 was absent in the wild type, but it was not removed in γ-ΔN4C25. The mutants γ-ΔC36 and γ-ΔN4C25 were also checked by MALDI-TOF mass spectrometry (APRO Life Science Institute). γ-ΔC36 contained three major components with masses of 54700 (expected mass for α, 54714.8), 53340 (expected mass for β, 53355.9), and 27770 (expected mass for γ Ala-2 to Asp-247, 27785.1); γ-ΔN4C25 contained three major components of masses 54720 (α, 54714.8), 53360 (β, 53355.9), and 28720 (γ Met-5 to Leu-263, 28728.2).

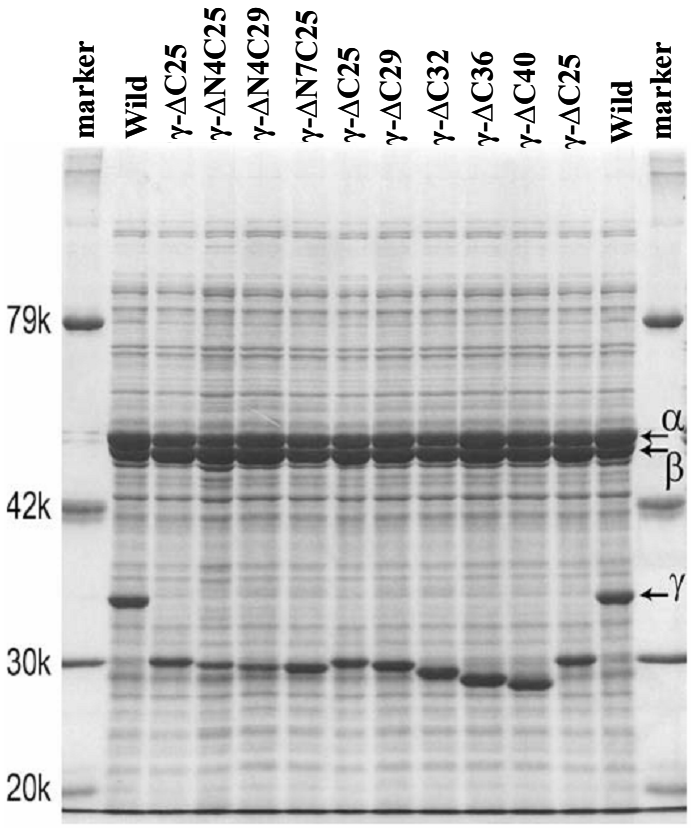

Figure 3.4 Expression of αβγ subunits of TF_1 in *E. coli*. *E. coli* pellets were dissolved in 2 % SDS and, after centrifugation to remove insoluble materials, applied to 10 % polyacrylamide gel containing 0.1% SDS. Stained with Coomassie Brilliant Blue R-250.

c. Mutants C

Molecular Genetics and Confirmation of Truncation

The mutants of group **C** are: γ-ΔN4C25, γ-ΔN7C29, γ-ΔN11C32, γ-ΔN14C36, γ-ΔN18C40 and γ-ΔN22C43. These mutants were constructed by truncating the amino acid residues from both amino (N) and carboxy (C) termini of the γ subunit. The procedures for γC-terminal truncation mutants (γ-ΔC25, γ-ΔC29, γ-ΔC32, γ-ΔC36 and γ-ΔC40) or for γ-ΔN4C25 mutant are described in the previous section (Mutants B). For γ-ΔC43, a reverse primer 5'-GGGCTAGCTTATTACGTCATCCGGGCGGCGTGTT-3' containing an *Nhe*I site was used. For γN-terminal truncation, a reverse primer containing an *Spe*I site: 5'-GGTACACTAGTCGCAACACGTTGC-3' and following forward primers containing an *Nsp*V site were used:

for γ-ΔN7C29,

5'-GAACCCGTGTTCGAAAAAGGAGGTGAAACCCATGACGCGCATCAATGCG-3'

for γ-ΔN11C32,

5'-GAACCCGTGTTCGAAAAAGGAGGTGAAACCCATGGCGACGAAGAAGACAAGCC-3'

for γ-ΔN14C36,

5'-GAACCCGTGTTCGAAAAAGGAGGTGAAACCCATGAAGACAAGCCAAATTACAAAAGCG-3'

for γ-ΔN18C40,

5'-GAACCCGTGTTCGAAAAAGGAGGTGAAACCCATGATTACAAAAGCGATGG-3'

for γ-ΔN22C43,

5'-GAACCCGTGTTCGAAAAAGGAGGTGAAACCCATGATGGAAATGGTCTCG-3'.

The mutant lacking γ entirely, the $\alpha_3\beta_3$ complex, was produced by introducing into pKABG1-gN two *Xho*I sites, one between *Nsp*V site and the beginning of the γ coding region and the other between the end and *Nhe*I site, and then removing the *Xho*I-*Xho*I portion. The replacement sequence was obtained by PCR using

pKABG1-gN as template and a reverse primer containing an *Nhe*I and an *Xho*I sites

5'-AAATTTGCTAGCCTCGAGCTCGTTCGCATTGTCCGTTGC-3'

and a forward primer containing an *Nsp*V and an *Xho*I sites

5'-GAACCCGTGTTCGAAAAAGCTCGAGGTGAAACCC-3'

where underscores show mutations.

The above mutations were confirmed by DNA sequencing (FASMAC Co.,Ltd., DNA sequencing services, Atsugi, Japan). In *E. coli* strain JM103 Δ(uncB-uncD) which has lost the ability to express authentic F_oF_1-ATPase[23], all mutants were expressed to a level similar to wild type, as seen in Fig. 3.5. The N-terminal five residues of expressed γ were confirmed by Edman degradation (APRO Life Science Institute, Inc., Naruto, Japan) as shown in Table 3.1. The initiation residue Met-1 was absent in the wild type, γ-ΔN7C29 (~30 % had Met-1), and γ-ΔN11C32. The mutants γ-ΔN4C25, γ-ΔN7C29, γ-ΔN11C32 and γ-ΔN14C36 were also checked by MALDI-TOF mass spectrometry (APRO Life Science Institute) as shown in Table 3.1. Peaks corresponding to α, β, and γ subunits were obvious except for γ-ΔN14C36, for which the γ peak appeared on a side of the β (z=2) peak.

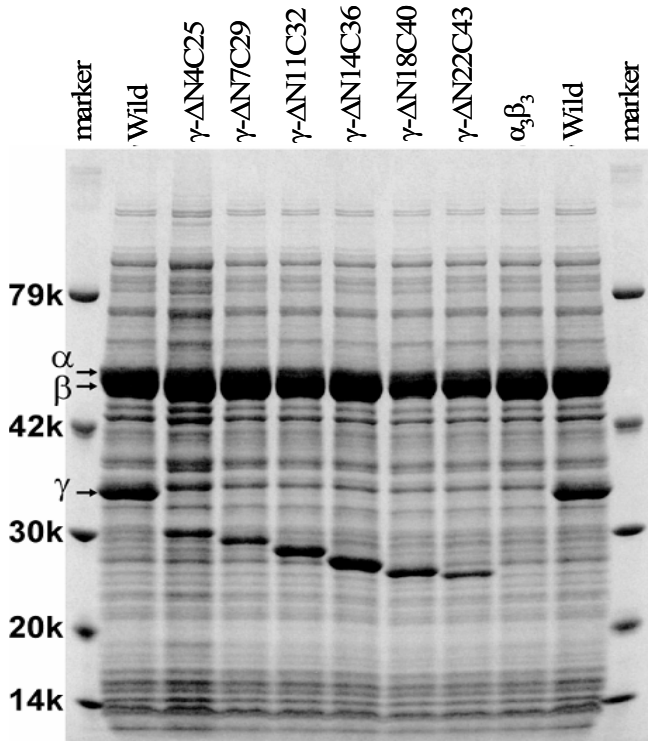

Figure 3.5 Expression of αβγ subunits of TF_1 in *E. coli*. *E. coli* pellets were dissolved in 2 % SDS and, after centrifugation to remove insoluble materials, applied to 12.5 % polyacrylamide gel containing 0.1 % SDS. Stained with Coomassie Brilliant Blue R-250.

Table 3.1 Confirmation of γ truncations

Mutant	Amino acid sequence at N-terminus of γ (right to left)*	Experimental mass *m/z* (*z* = 1)			Expected mass of γ	
		α	β	γ	*m/z*	sequence
Wild type	-DRLSA	54714.8 (expected)	53355.9 (expected)			
γ-ΔN4C25	-TKID*M*	54720	53360	28720	28728.2	Met5-Leu258
γ-ΔN7C29	-ANIRT (~70%) -NIRT*M* (~30%)	54720	53360	27800	27812.0	Thr9-Arg254
γ-ΔN11C32	-TKKTA	54720	53360	26940	26945.0	Ala13-Glu251
γ-ΔN14C36	-QSTK*M*	54720	53360	26350	26347.4	Met15-Arg247
γ-ΔN18C40	-AK(T)I*M* (T: unclear)					
γ-ΔN22C43	-VMEM*M*					

*Italic *M* indicates undigested Met-1.

The amino-acid sequence here, in Fig. 4.17**c** and in Fig. 4.20**B** (Chapter 4) is taken from ref 41, except that our numbering starts from Met-1, which is absent in the expressed wild type. Recently we have found that the actual sequence of TF_1 that we used here is slightly different from the original one in ref. 41 and that the C-terminus of the wild type in this work is Gln-285 and not Gln-283, counting from Met-1 (T. Suzuki and M. Yoshida, unpublished). Because the differences are not in the N- and C-termini, we adopt the published sequence for description of truncation. The expected masses mentioned for mutants **B** and in Table 3.1 for mutants **C**, however, have been calculated on the basis of the actual sequence.

3.3.2 Preparation of Agar Plate

A solution that contains the nutrients necessary for survival and growth of bacteria is called a **culture medium**. The culture media can be either a liquid form called **BROTH** or a solid form called **AGAR**. An **agar plate** is a sterile Petri dish made of a shallow glass or plastic cylindrical dish used for bacterial culture. It contains agar and some nutrients. A small plastic container was placed on the platform of a balance (PR8002 DeltaRange^R) and calibrated to zero. Each reagent was directly taken in the container from its bottle with utmost care to take correct amount and to reduce contamination. Measured reagents were poured into a conical flask and 100 ml ultra pure water was added to make a 2xYT solution with gentle shaking. Agar (1.5 g) was then added in this solution and mixed well. The flask was sealed with a cotton plug followed by loose wrapping with a SUMIKEI aluminium foil to sterilize in an autoclave (BS-325, TOMY) at 121 °C for 20 minutes. Sterilization is performed for killing other bacteria or microbes present in the media so that only desired bacteria can grow on it. The agar is dissolved by the heat of sterilization.

Both hands were sterilized with 70 % ethanol in order to work on the CLEAN BENCH. A packet of IWAKI clinical test ware containing 10 dishes was taken on the CLEAN BENCH. Light was switched on and gas burner was made ready to use. Dishes were partially uncovered and kept staked in a row, three or four per stack, on the BENCH. After sterilization was completed, the agar medium was

taken out and kept on the CLEAN BENCH until the flask can be handled with bare hands (60<temperature>40 °C). The bottom of the flask containing the agar solution was heated to sterilize it by the gas burner and ampicilline was added with a pipetman having sterilized tip to a final concentration of 50 μg/ml and mixed well. The cover of one Petri dish was opened with the left hand wide enough to pour the media while holding the neck of the flask with right hand. Then immediately the agar solution (about 10 ml) was carefully poured into each of the stacked dishes so that bubble cannot be formed and in this way 10 Petri dishes were made rapidly before the solution is converted into a gel. Dishes were at first fully covered for 3 minutes and then partially uncovered (~20 %) to keep under UV exposure for 15 minutes for sterilization. Dishes were exposed to visible light for another ~15 minutes and care was taken to ensure that agar gels remain soft enough to use. After completion of making agar plates they were fully covered and wrapped with PARAFILM tape. Preparation date was written on them and stored upside down in the cold room at 4 °C until use.

3.3.3 Drawing of *E. coli* on the Agar Plate

An instrument called an inoculating **wire loop** was used to transfer bacteria from a glycerol stock culture to the agar plate (Fig. 3.6). *E. coli* bacteria were streaked by the loop on the agar plate to obtain isolated colonies. Hands were cleaned and sterilized with 70 % ethanol at first. The CLEAN BENCH was also wiped with 70 % ethanol and then an agar plate was taken from the cold room (4 °C) and kept on the BENCH to let it come to room temperature. Gas burner was set up with a gentle blue flame to have a sterile environment in the vicinity.

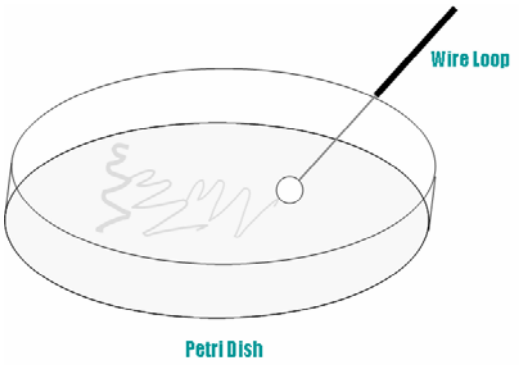

Figure 3.6a An wire loop was used to draw S-like line on the Petridish.

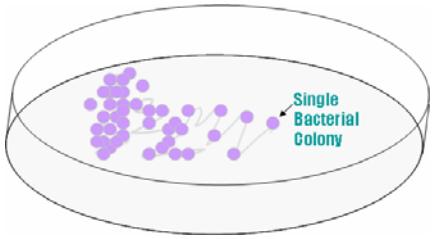

Figure. 3.6b Individual colonies have been grown on the drawn line.

A stock culture of *E. coli* bacteria was taken from the deep freezer (-80 °C) on the CLEAN BENCH. The cover of the agar plate was opened. The wire loop was flamed red hot in the gas burner to sterilize it and immediately inserted into the *E. coli* bacterial culture bottle to take some bacteria. A thick S-like line was then drawn on the agar gel with the loop containing bacteria without tearing into it (Fig. 3.6a). This line contains many bacteria but we need single bacterial colonies so that we have to dilute. To do this the loop was again flamed to kill any remaining bacteria on it and touching at a region of the first line a second line was drawn that contained smaller number of bacteria compared to the first line. In similar method several other lines were drawn to get single colonies. Finally the stock culture was restored in the freezer (-80 °C) and the wire loop was re-flamed to keep aside. The Petri dish was then sealed with a layer of PARAFILM around the edge that keeps the agar from drying out during incubation in the incubator (SLI-170D, EYELA). The plate was incubated at 37 °C until (~12 hours) individual colonies are seen (Fig. 3.6b). The agar plate was then stored upside down in the cold room at 4 °C to prevent condensing water from falling down on the growing colonies that allow them to run together. After completion of work on the CLEAN BENCH it was sterilized by exposing on UV light for 30 minutes. Used bacterial colony plates were autoclaved to kill the bacteria and to make the plates safe for disposal in a trash bag.

3.3.4 Purification of F_1 and Measurement of its Concentration

The wild type F_1 was purified according to the following procedures[26] with some modifications. The *E. coli* cells containing DNA of wild type F_1 were grown on an agar plate as individual colonies using the method discussed above. To inoculate a colony into the autoclaved start culture (2xYT), hands were sterilized with 70 % ethanol and the CLEAN BENCH was made ready to work on it.

A single bacterial colony from the agar plate was picked up with a sterile toothpick and dropped it into each of two separate test tubes containing 3 ml of (2xYT) start culture solution treated with 50 μg/ml ampicillin. This medium was incubated at 37 °C with shaking (215 rpm) by a shaker (EYELA, Tokyo Rika kikai, Japan) for 12 hours and the growth of *E. coli* was confirmed by SDS-PAGE analysis. While the start culture (2xYT) was being incubated, a Terrific Broth (500 ml) was prepared in two flasks (IWAKI) and autoclaved. Then 1.5 ml of start culture was introduced into each of the two flasks filled with 250 ml of Broth containing 50 μg/ml ampicillin. The flasks were then placed in the shaker to incubate for 16 hours to grow *E. coli* cells in large scale. After completion of incubation, to harvest the cells, the medium containing *E.coli* cells was poured into two separate bottles for centrifugation at 6000 rpm, 4 °C for 10 minutes using a centrifuge machine (Kubota) to spin down the *E.coli* cells at the bottom of the bottle.

Pellets after centrifugation of the culture were mixed well with 20-30 ml of buffer A (50 mM Imidazole-HCl pH 7.0 and 100 mM NaCl in addition to 50 mM sodium phosphate, pH 7.0) and was spun at the above condition to wash the pellets. This procedure was repeated for further one time to get the final pellet (about 4 g). The pellet was then mixed well with the same buffer for sonication with a sonicator (UR 20P, Tokyo Seiko co. Japan) for 15-20 minutes on ice to mechanically break the *E. coli* cells and thereby allowing the protein out of the cells. After being sonicated, the liquid was poured into a tube and was subjected to ultracentrifugation for 30 minutes at 40,000 rpm, 4 °C (Beckman, USA) to bring the cell debris including some DNA, membranes and insoluble proteins down to

the bottom of the tube and leaving the protein of interest and other liquids on the top as supernatant. The decanted supernatant was then treated by heat shock in a hot water tank (TAI TEC) at 65 °C for 8-10 minutes to separate F_1 complex from other proteins quickly. The sample was then again ultra-centrifuged at the same condition. The obtained supernatant was filtered and loaded onto a (10 ml) Ni^{2+}-NTA superflow column (Qiagen, Hilden, Germany) pre-equilibrated with 50 ml of buffer A. After collection of sample through, the column was washed with 50 ml of this buffer and then the enzyme was eluted with 50 ml of buffer B (300 mM imidazole-HCl pH 7.0 and 100 mM NaCl). Using SDS PAGE the eluted fractions containing the enzyme were selected. Ammonium sulfate was added to these fractions (10 ml) to a final concentration of 10 % saturation and the sample was applied to a (10 ml) butyl-Toyopearl column (Tosoh, Japan) pre-equilibrated with buffer C (100 mM KPi pH 7.0 and 2 mM EDTA) and 10 % saturated ammonium sulfate.

The column was washed with 40 column volumes (400ml) of the same buffer containing 10 % saturated ammonium sulfate to remove endogenously bound nucleotides. The enzyme was then eluted successively with 50 ml of buffer C, each containing 5 %, 3 %, 1 % and 0 % ammonium sulfate salt. All fractions (10 ml each) taken from the column were analyzed by SDS PAGE. The protein was usually obtained in 1 % and 0 % ammonium sulfate fractions. Ammonium sulfate (70 %) and 2 mM dithiothreitol (DTT) were added to the purified protein to store it as *precipitant* in the buffer at 4 °C in a cold room. Before use, this enzyme precipitant was dissolved well and spun at 15000 rpm, 4 °C for 20 minutes. The supernatant was discarded and the precipitant containing F_1 complex was mixed with an appropriate amount of (filtered and degassed under vacuum) buffer C and spun again at the same condition, and the supernatant was passed through a computer controlled size exclusion column (Superdex 200 HR 10/30, Amersham Pharmacia Biotech Piscataway, NJ) pre-equilibrated with the above buffer to remove DTT and possible denatured enzyme. The F_1-protein was identified as in a large peak in the elution profile (Fig. 3.7) that consisted of four fractions 18, 19, 20 and 21 having different concentrations.

Purification procedures for the mutants were adjusted depending on their stability. Wild type and group **A** mutants were purified with heat treatment and using affinity column, hydrophobic-interaction column and size-exclusion column (4 °C). For group **B**, the hydrophobic-interaction column and heat treatment were omitted. For group **C,** the same method as **B** was used except that the size-exclusion column was done at room temperature.

The concentration of the collected protein was measured using a computer aided spectrophotometer (U-3300, Hitachi, Japan). The spectrophotometer was turned on 30 minutes before starting a measurement. A properly washed and dried quartz cuvette was fitted well into the holder of the spectrophotometer and the base line was corrected against buffer. The buffer was then replaced by five times diluted F_1 and absorbance for each fraction was determined from its spectrum at 280 nm by 'UV solutions' program and finally F_1 concentration was calculated (ε_{280}= 0.154/μM). The protein fraction having A_{280}/A_{260} >1.95 was usually taken for the measurement of hydrolysis activity[27].

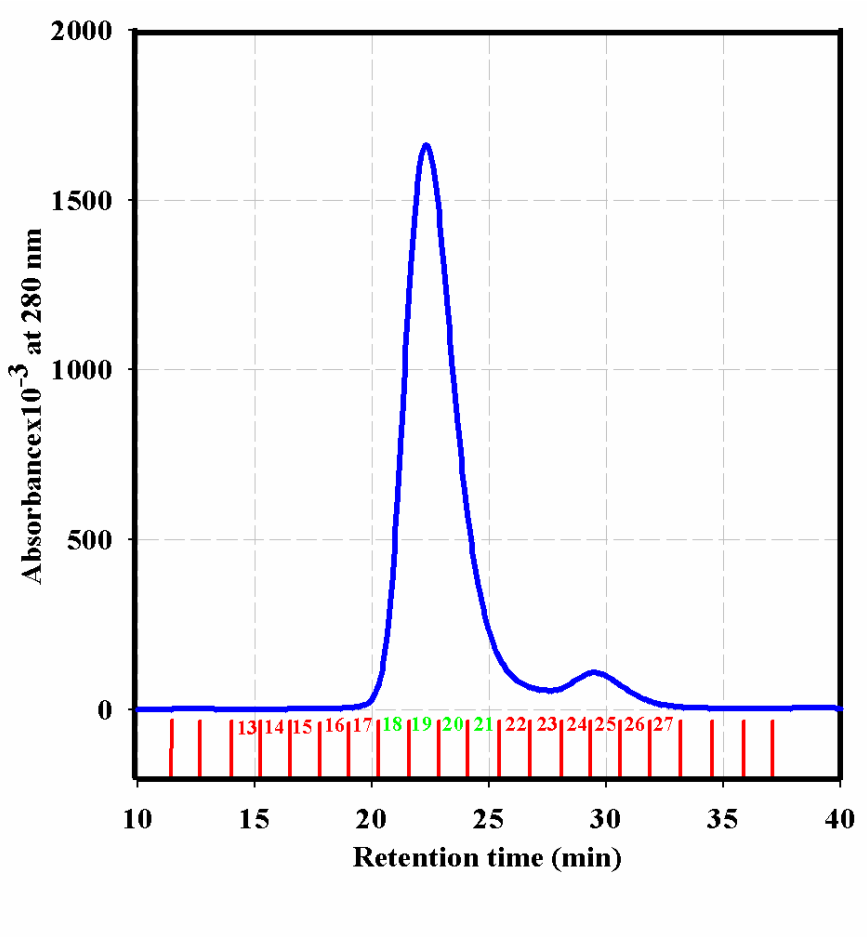

Figure 3.7 An elution profile of F_1 from high pressure liquid chromatography (HPLC). The fractions containing F_1 are marked by green color.

3.3.5 Biotinylation of F_1

To observe the rotation, F_1 was biotinylated at the two cysteines (γ-107C and γ -210C) by incubation with fourfold molar excess of 6-{N′-[2-(N-maleimide) ethyl-N-piperazinylamide}hexyl-D-bitinamide (Dojindo, Kumaoto, Japan) for 30 minutes at room temperature. The solution was then passed through a size exclusion (Superdex 200 HR 10/30, Amersham Pharmacia Biotech Piscataway, NJ) column pre-equilibrated with buffer C to remove unbound biotin. Biotinylated F_1 was frozen with liquid nitrogen and stored at -80 °C in a freezer.

3.3.6 Measurement of Turbidity to Determine Doubling Time

In order to investigate the speed of growth of *E.coli* containing genes of wild type F_1 and group **A** mutants, 1.5 ml of small culture (2xYT) was transferred into 250 ml of large culture (Terrific Broth). The solution was immediately set on the shaker to grow *E. coli* at 37 °C. The initial transparent medium progressively became more and more cloudy and opaque upon shaking at 215 rpm. The growth of *E. coli* over 17 hours was monitored by measuring the turbidity at 600-nm wavelength using a spectrophotometer (UV 3101 PC, Shimadzu). The turbidity gives a quantitative measurement of the cell number. Absorbance measurement during *E. coli* growth was carried out every two hours in a 2 ml quartz cuvette placed in the holder of the spectrophotometer. The doubling time was determined in the log phase (Fig 3.8).

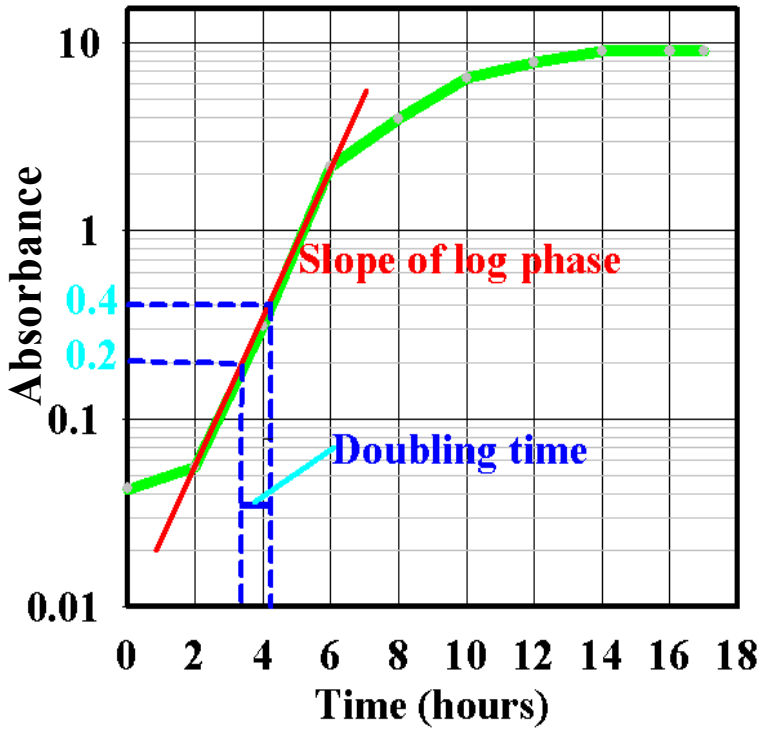

Figure 3. 8 A growth curve for *E. coli* bacteria. In the log phase cells are dividing regularly by binary fission and the growth is exponential, doubling in number every few minutes.

3.3.7 Estimation of Yield of F_1

The yield of wild type or group A mutant F_1 was determined using the following equation.

$$Yield\ (\%) = \frac{Net\ amount\ of\ \ purified\ F_1(g)}{Wet\ weigt\ of\ \ E.coli\ \ pellet\ (g)} \cdots\cdots\cdots\cdots (3.1)$$

3.3.8 Measurement of Amount of Bound Nucleotides

The amount of nucleotides (ADP) remaining in the wild type or group A mutant F_1 was determined as follows[28]. Four ADP (pH 7.0) samples of various concentrations were taken so that the final amount to be injected into the reverse phase HPLC becomes 5, 10, 20 and 50 pmols respectively. To denature F_1 complex for which the amount of bound nucleotide was to be determined, 100 µl was taken into an eppendorf tube and 5 µl of perchloric acid of final concentration 24 % (v/v) was mixed well by pippeting. The same treatment was done for each of the four ADP samples. All five samples were then incubated on ice for 30 minutes. After incubation, white residue was seen only at the bottom of the tube containing F_1 complex. The samples were then set for centrifugation for 15 minutes at 15000 rpm, 4 °C. For neutralization purpose, 80 µl of supernatant from each sample was mixed with 24 µl of 1M Na_2HPO_4 and incubated on ice for 10 minutes. Finally, the samples were centrifuged as before. A portion of the supernatant (50 µl) from each sample was then injected directly to a reversed-phase column (HPLC, Pharmachia biotech) pre-equilibrated with 20 ml of (filtered and degassed under vacuum) 100 mM sodium phosphate (pH 6.8) buffer. Absorption peak of ADP at 259 nm corresponding to each injected ADP or F_1 sample was monitored in the HPLC elution profile and the peak area (mAU*ml) was calculated by the UNICORN program. A calibration curve was made by plotting this area against the injected amount of ADP (Fig. 3.9).

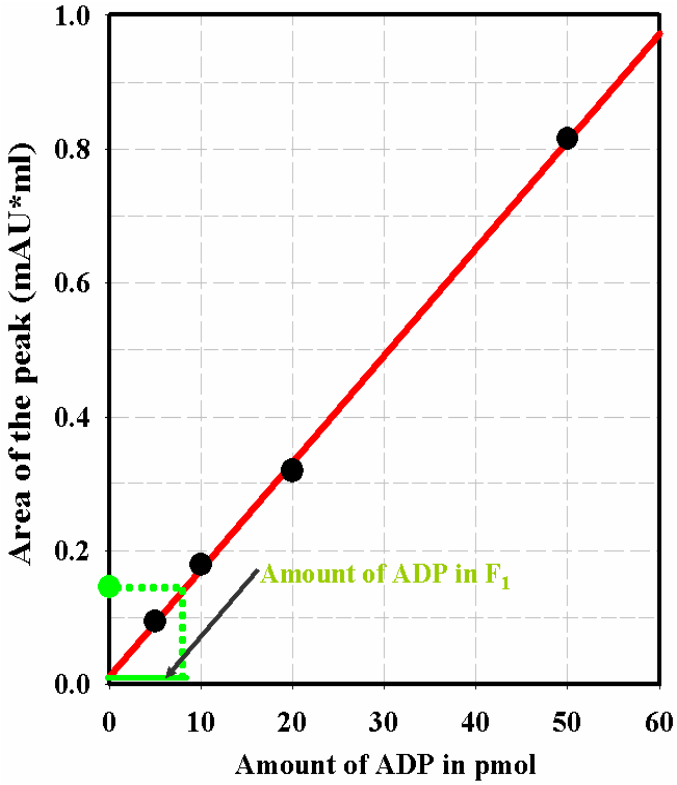

Fig. 3.9 Calibration curve for the determination of amount of ADP corresponding to the peak for F_1 in the HPLC elution profile.

The peak area for F_1 obtained from the HPLC profile was plotted on this calibration curve and corresponding amount of ADP was determined. Finally, the amount of ADP remaining in F_1 molecule was calculated from the following equation.

$$Amount\ of\ nucleotide\ bound\ with\ F_1\ molecule = \frac{Total\ amount\ of\ nucleotide\ in\ F_1\ from\ calibration\ curve\ (pmol)}{Total\ amount\ of\ F_1\ injected\ into\ the\ HPLC\ (pmol)} \quad \text{.....(3.2)}$$

3.3.9 Measurement of ATP Hydrolysis Activity of F_1

The ATP hydrolysis activity of F_1 was measured at different MgATP concentrations in the range of 2000-0.02 μM using a spectrophotometer (U-3300, Hitachi, Japan) equipped with a thermostat. An ATP-regenerating system was used for this measurement that contained buffer D (10 mM MOPS-KOH pH 7.0, 50 mM KCl, 2 mM $MgCl_2$), 0.2 mM NADH, 1mM phosphoenol pyruvate, 250

μg/ml pyruvate kinase (rabbit muscle solution in glycerol, Roche Dignostics, Mannheim, Germany) and 50 μg/ml lactate dehydrogenase (hog muscle, Roche). Typically, 1.95 ml of ATP re-generating solution was poured into a quartz-cuvette fitted in the holder of the spectrophotometer and appropriate amount of MgATP was rapidly mixed. The reaction was then started in the dark by the addition of F_1 to a final concentration of 5-10 nM. The measurement was carried out at 23 °C and hydrolysis rate was determined from the absorbance decrease of NADH at 340 nm[29] using the following equation.

$$ATPase\ (1/s) = \frac{Decreasing\ \ rate\ of\ \ absorbance\ \ of\ \ NADH\ \ (at\ 340\ nm)}{[F_1] \bullet \varepsilon_{340}^{NADH} \bullet Light\ \ path\ (1cm)} \cdots\cdots\cdots (3.3)$$

Where ε_{340}^{NADH} = 6220 $M^{-1}cm^{-1}$ and $[F_1]$ = Concentration of F_1. The rate of absorbance (A_{340}) decrease was taken from the slope of initial burst or lag and steady state conditions for the wild type and the mutants. The enzyme steady state condition was determined from the derivative dA_{340}/dt. The hydrolysis activity was also measured in the presence of lauryldimethylamine oxide (LDAO) or sodium dodecyl sulfate (SDS).

3.3.10 Ni^{2+}-Nitrilotriacetic Acid (Ni-NTA) Glass Preparation

Glass coverslips (NEO Micro Cover Glass, No.1, 24x32 mm^2, Matsunami, Osaka, Japan) were set vertically and separately on a ceramic glass holder to immerse them in 12 N KOH for 24 hours to clean the surfaces[30]. Then the coverslips along with the holder were extensively washed with ultra pure water. Taking 100 ml ultra pure water in a glass beaker containing a small stirrer bar, 0.02 % (v/v) acetic acid was added and mixed well on a magnetic stirrer at 60 °C in a fume hood (RFA 180). About 2 % (v/v) 3-mercaptopropyltrimethoxysilane (TSL8380, Toshiba GE silicone, Tokyo, Japan) was then added with a glass pipette and mixed. The pre-washed holder holding cover slips was placed carefully in the silane solution and stirring was continued for further 15-20 minutes. The hot glass beaker containing the silane solution and coversilps was taken out from the fume hood and was placed in the chamber of a constant temperature oven to incubate the coverslips for two hours at 90 °C. After being incubated, the

coverslips were taken out to cool them down in the fume hood for about 30 minutes and were washed vigorously with ultra pure water. Then the glasses were placed on a clean wipe paper on a working table to write the preparation date and glass number on the edge of each glass and a total of six pairs were made out of 12 glasses. Only one face (opposite to the face where the date and number were written) of each glass pair was incubated for 20 minutes in room temperature with 20 µl of 1M DTT (to a final concentration of 100 mM) in 10 mM MOPS-KOH (pH 7.0) to reduce SH groups of the silane on the glass surface. The cover glasses were vigorously washed with ultra pure water and each pair (as previous) was incubated within Maleimide-C_3-NTA (Dojindo) in 10 mM MOPS-KOH, pH 7.0 to the final concentration of 10 mg/ml for 30 minutes at room temperature. After incubation, the glasses held in the ceramic holder were washed in usual manner and incubated at room temperature in 100 ml of 10 mM $NiCl_2$ for 20 minutes. Finally, the glasses in the holder were washed and stored in 100 ml of ultra pure water at room temperature. They were used within a few weeks.

3.3.11 Observation of Rotation of F_1

For observation of rotation of wild type or mutant F_1 a flow chamber was constructed using a Ni-NTA coated bottom coverslip (24x32 mm^2) and a top uncoated coverslip (18x18 mm^2) separated by two greased strips of Parafilm cover sheet. The rotation assay was made in buffer D containing an ATP regenerating system consisting of 0.2 mg/ml creatine kinase (rabit muscle, Roche) and 2.5 mM creatine phosphate (Roche). Streptavidin coated beads of diameter 0.49 µm (Bangs laboratories, Inc.) or 0.287 µm (Seradyn, Inc.) was washed three times with buffer D containing 5 mg/ml BSA (Fluka, Biochemika) through centrifugation at 15000 rpm, 10 minutes and 4 °C to remove preservatives. The concentration of the beads was finally adjusted to 0.1 % (w/v) with 5 mg/ml BSA. One flow chamber volume of 500 pM-100 nMF_1 was infused into the chamber and was incubated at room temperature for 2 minutes so that F_1 complex was fixed on the Ni-NTA coated cover glass through histidine tags. After incubation, the chamber was washed three times with 5 mg/ml BSA and incubated for 5 minutes. One chamber volume of

pre-washed streptavidin coated beads was infused into the chamber and kept for 15 minutes at the room temperature so that beads were attached with the biotinylated γ subunit of the $\alpha_3\beta_3\gamma$ complex. After incubation, the flow cell was washed three times with buffer D to remove unbound beads.

Finally, five chamber volumes of a desired amount of MgATP was infused into the chamber and the chamber was sealed with silicon grease to avoid evaporation. The chamber was then used for observation of rotation under a microscope. When necessary, an appropriate amount of LDAO was also added with ATP regenerating system. For clear identification of rotation, a bead duplex was always used.

For 40 nm gold particle rotation, the surface of 40-nm gold beads (EM.GC40, a suspension at 9×10^{10} particles ml^{-1}, BB International, Cardiff, UK) was modified with polyethylene glycol (PEG) and PEG-biotin by adding 0.2 mM 2-aminoethanthiol (Tokyo Chemical Industry, Tokyo), 0.1 mM NHS-m-dPEG (molecular weight: 1214, Quanta BioDesign, Powell) and 0.1 mM NHS-dPEG4-Biotin (Quanta BioDesign) to the bead suspension and letting the reaction proceed at room temperature for more than one day. Before use, we washed the gold beads extensively with buffer E (10 mM Mops-KOH, pH 7.0, 50 mM KCl) to remove free biotin.

Biotinylated TF_1 (10-100 nM) in 10 mM Mops-KOH, 20 mM imidazole-HCl, pH7.0, 400 mM KCl, or in buffer E for wild type, γ-ΔC17 and γ-ΔC21 was infused into an observation chamber made of Ni-NTA coated bottom and uncoated top coverslips. After washing out unbound TF_1 with buffer E, we infused 10 mg ml^{-1} BSA in buffer E to prevent nonspecific binding and then 40 μg ml^{-1} streptavidin (Pierce, Rockford) in buffer E. After extensive washing with buffer E, we infused the modified gold beads and washed away excess beads with buffer E. Finally, we infused buffer E containing 2 mM MgATP, 2 mM $MgCl_2$, and an ATP regenerating system (0.2 mg ml^{-1} creatine kinase and 2.5 mM creatine phosphate). Microscopy for observation of rotation of F_1 using plastic bead or gold particle and the recording systems have been described in section 3.2.4.

CHAPTER 4
RESULTS AND DISCUSSION

CHAPTER 4
RESULTS AND DISCUSSION

4.1 Introduction

The results obtained from the experimental work are presented and thoroughly discussed in this chapter. First the rotational and hydrolytic properties of the wild type and mutants **A** are discussed. The effects of surfactants like lauryldimethylamine oxide (LDAO) or sodium dodecyl sulfate (SDS) on them are also described. Then the results of the study on the mutant groups **B** and **C** are discussed.

4.2 Wild Type and Mutant A

4.2.1 Expression and Assembly of the Wild and Mutant F_1

Deletion mutants of TF_1, γ-ΔC14, γ-ΔC17, γ-ΔC21 and γ-ΔC25 in which 14, 17, 21 or 25 amino acid residues from the C-terminus of the γ subunit were removed, were expressed in *E. coli* apparently normally. The doubling time of the *E. coli* that lacks its authentic F_1 genes was almost the same whether a gene encoding wild type or γ-deleted TF_1 was incorporated (Table 4.1), suggesting that all these mutations were not harmful to the cells.

Table 4.1 Doubling time, yield and bound nucleotide for the wild type and mutants.

Type of F_1	Doubling time* (min)	Yield (weight %)	Bound nucleotide (mol %)
TF_1 (wild)	45 ± 1	0.042	6.7
TF_1 (γ-ΔC14)	54 ± 0	0.057	5.1
TF_1 (γ-ΔC17)	50 ± 2	0.039	6.5
TF_1 (γ-ΔC21)	45 ± 3	0.050	3.3
TF_1 (γ-ΔC25)	55 ± 8	0.0	-

*Mean ± SD range for two or three samples.

The yield of the assembled subcomplex $\alpha_3\beta_3\gamma$, the total amount of the subcomplex after final purification versus wet weight of *E. coli* pellet, did not

differ significantly up to γ-ΔC21, but we were unable to obtain γ-ΔC25, which eluted from the size exclusion column apparently as dissociated subunits (Table 4.1). As discussed below, γ-ΔC21 also appears to be unstable. Deletions were confirmed on the DNA sequence and, except for γ-ΔC25, from the sodium dodecyl sulfate (SDS)-gel pattern of purified subcomplexes (Fig. 4.1). The purified samples contained 0.03-0.07 mol of tightly bound nucleotide per mol of F_1.

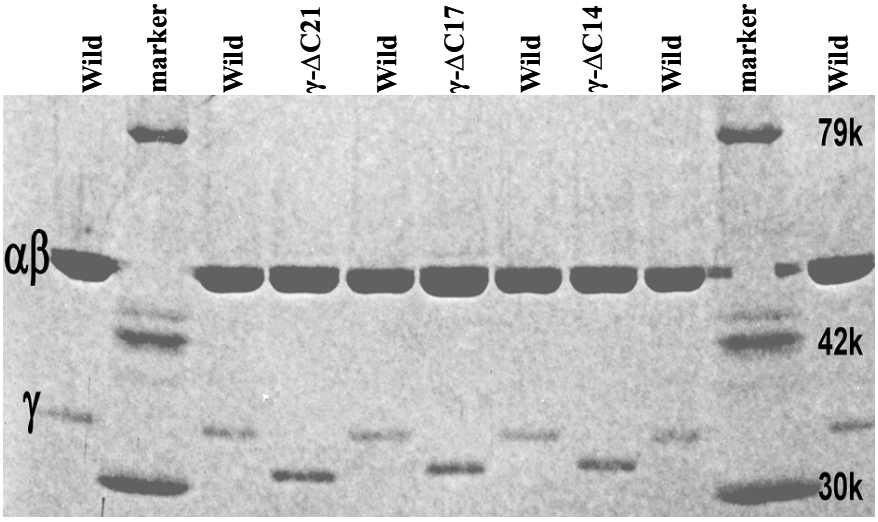

Figure 4.1 Confirmation of γ-deletions by SDS-polyacrylamide gel electrophoresis (10 % gel containing 0.1 % SDS; stained with Coomassie Brilliant Blue G-250). The α and β subunits were unresolved on this gel.

4.2.2 Rotation

For the analysis of rotation, we chose those F_1 molecules that happened to carry a duplex of 0.49-μm beads and that rotated fast without irregular intermissions over at least 25 revolutions. For the estimation of torque, in particular, we tried to choose those duplexes in which the outer bead was slightly above the inner bead, to minimize interaction with the glass surface. Time courses of rotation at various ATP concentrations ([ATP]s) are plotted in Fig. 4.2, where a fast and smoothly rotating portion over seven revolutions at each [ATP] is selected as shown in the insets. All rotations, whether of wild type or of truncated mutants, were counterclockwise. At 20 and 60 nM ATP, rotation was clearly stepwise, showing an ATP-waiting dwell every 120° (not so clean in γ-ΔC21). In this ATP-limited regime, the mutants showed a somewhat lower stepping rate, consistent with a

slower rate of ATP hydrolysis in these mutants (see below). At 2 μM ATP and above, rotation was basically continuous and the speed was independent of [ATP], indicating that the viscous friction on the beads limited the rotary speed. A closer look reveals that, even in this friction-limited regime, the bead duplex tended to fall in occasional short pauses at angles separated by 120°.

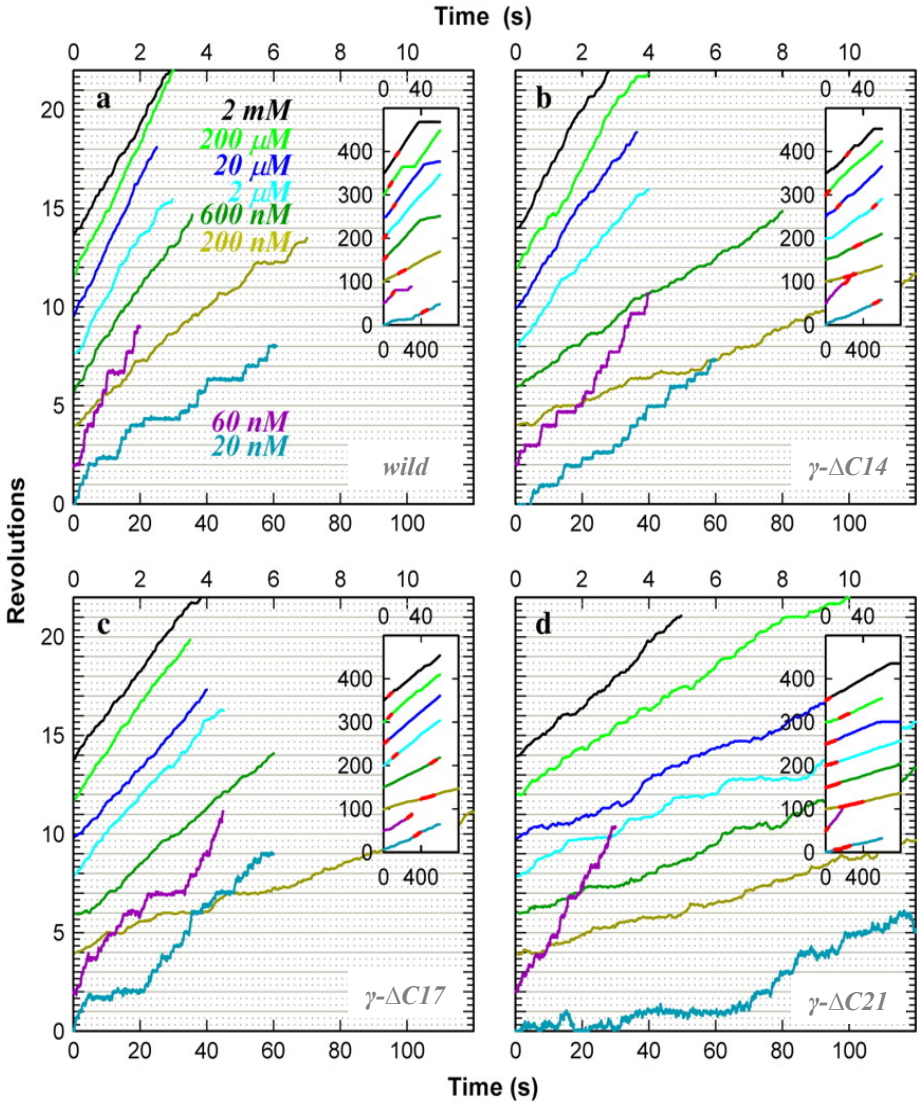

Figure 4.2 Time courses of rotation of a 0.49-μm polystyrene bead duplex attached to the γ subunit. (**a**) wild type; (**b**) γ-ΔC14; (**c**) γ-ΔC17; and (**d**) γ-ΔC21. Top time axes apply to [ATP] at 200 nM and above, and bottom axes to 20 nM and 60 nM ATP. Records showing the highest average speed over >7 consecutive revolutions are selected and shown. Insets show the whole time courses, where the selected portions are shown in red. Average rotation frequency in Fig. 4.3 and torque in Fig. 4.5 were calculated on such selected portions containing >7 consecutive revolutions. Horizontal lines (solid and dotted) are separated by 120°, and each time course has been adjusted such that frequent pauses fall on a horizontal line.

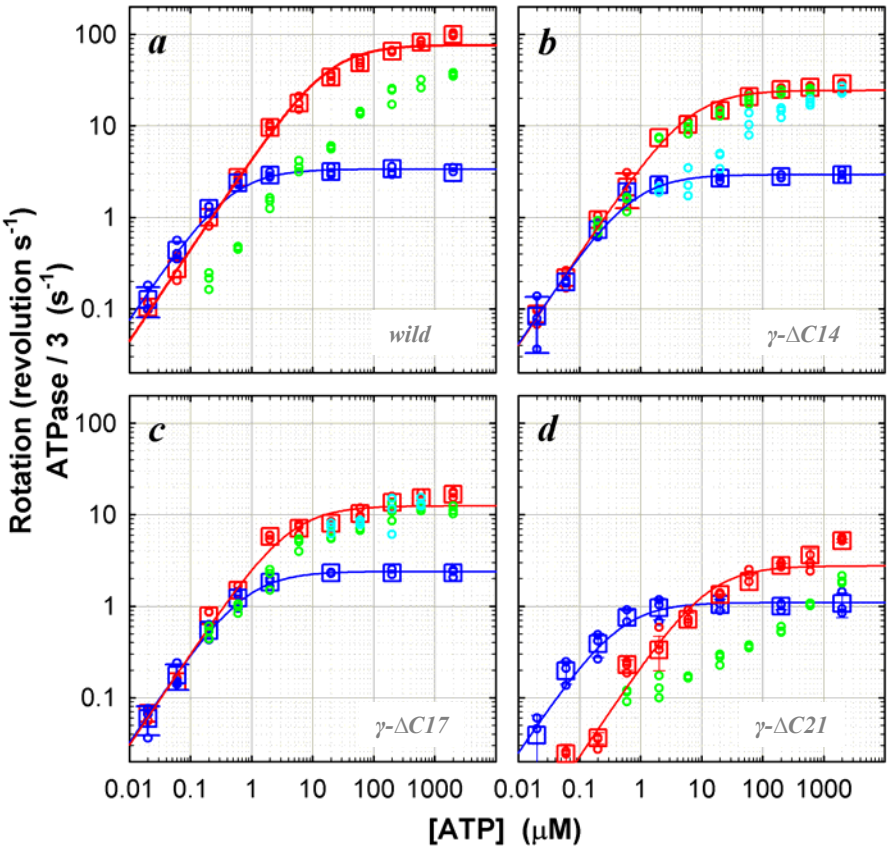

Figure 4.3 Comparison of hydrolysis and rotation rates. (**a**) Wild type; (**b**) γ-ΔC14; (**c**) γ-ΔC17; and (**d**) γ-ΔC21. For comparison with rotation, hydrolysis rates are divided by three. Circles are from individual time courses and squares show the average over three points, error bars being standard deviation larger than the size of the square. [F_1] was 5 nM except at 60 and 20 nM ATP where [F_1] was 10 nM. (Cyan) the initial hydrolysis activity estimated at 2-7 s after mixing (2 μM ATP and above), 2-15 s (600 and 200 nM ATP) or from the entire 360-s portion (60 and 20 nM ATP; 200 and 60 nM ATP for γ-ΔC21). Values at 60 and 20 nM ATP have been corrected for a small decline in absorbance observed in the absence of F_1. (Green) the steady-state hydrolysis activity estimated from the final 200-s portion of a time course; not estimated at 60 and 20 nM ATP (and 200 nM ATP for γ-ΔC21) where the activity was low from the beginning. (Red) the maximal hydrolysis activity in a time course: it was equal to the initial activity in the wild type and γ-ΔC21; in γ-ΔC14 and γ-ΔC17 at intermediate [ATP]s, the maximal activity was observed after an initial lag and its value was estimated as a slope over a 5s interval. (Blue) rotation frequency estimated over >7 consecutive revolutions (Fig. 4.2). Red and blue curves show a fit with Michaelis-Menten kinetics: $V = V_{max}[\mathrm{ATP}]/(K_m + [\mathrm{ATP}])$. For hydrolysis (red), V_{max} (not divided by three) and K_m are 230 s^{-1} and 17 μM (wild), 75 s^{-1} and 6.1μ M (γ-ΔC14), 38 s^{-1} and 4.1 s^{-1} (γ-ΔC17); 8.3 s^{-1} and 12 μM (γ-ΔC21); for rotation (blue), 3.4 s^{-1} and 0.43 μ M (wild), 2.9 s^{-1} and 0.70 μM(γ-ΔC14), and 2.4 s^{-1} and 0.73 μM (γ-ΔC17), 1.1 s^{-1} and 0.43 μM (γ-ΔC21).

These pauses likely represent load-dependent stumbling of a chemical reaction at ~80° ahead of an ATP-waiting angle[28], or short inhibition at a similar angle caused by tight binding of MgADP[31]. The rotary speed in the friction-limited regime is determined primarily by the motor torque, and thus the lower speed at longer truncation indicates a lower torque.

The [ATP] dependence of the time-averaged rotation rate is summarized in Fig. 4.3, together with the rate of ATP hydrolysis. The rotation rate (blue) can be fitted with a Michaelis-Menten kinetics, the saturation being due to the hydrodynamic friction[13]. From the fit, the apparent rate of ATP binding at [ATP] below 1 μM is obtained as $k_{on}^{ATP} = 3V_{max}/K_m$. The rate for the wild type of 2.4×10^7 $M^{-1}s^{-1}$ agrees with the previous estimates of 2.6×10^7 M^{-1} s^{-1} under negligible friction[16] and 1.7×10^7 M^{-1} s^{-1} for F_1 bearing an actin filament[13]. The mutants showed a lower rate: 1.2×10^7 $M^{-1}s^{-1}$ in γ-ΔC14 (52 % of the wild type), 0.99×10^7 $M^{-1}s^{-1}$ in γ-ΔC17 (42 %), and 0.77×10^7 $M^{-1}s^{-1}$ in γ-ΔC21 (32 %). Because the rate of ATP hydrolysis in solution (red squares in Fig. 4.3) parallels the rate of rotation at [ATP] below 1 μM, the lower rate of ATP binding in the mutants is genuine, not the result of bead attachment. The extremely low rate of ATP hydrolysis in γ-ΔC21 is presumably due to instability of this sub-complex, as discussed later.

4.2.3 Estimation of Torque

To see whether γ-truncation leads to reduction in the torque, the torque N was estimated from the instantaneous rotary speed ω (in radian s^{-1}) during a 120° step using the following equations[13, 28]:

$$N = \omega\xi \quad \text{.....(4.1)}$$

where ξ is the frictional drag coefficient given, for the case of a duplex of spherical beads, by

$$\xi = 2\times8\pi\eta a^3 + 6\pi\eta a x_1^2 + 6\pi\eta a x_2^2 \quad \text{..... (4.2)}$$

where a is the bead radius, x_1 and x_2 are the radii of rotation of the two beads, and η is the viscosity of the medium (~0.93×10^{-3} $N\cdot s\cdot m^{-2}$ at 23 °C). The drag in Eq.

4.2 is likely an underestimate[13, 32], but our purpose here is the comparison between the wild type and mutants.

The angular speed ω was estimated by averaging twenty one consecutive 120° steps, avoiding the ATP-waiting dwells at low [ATP]s and occasional pauses at high [ATP]s (*thick cyan* curves in Fig. 4.4). The slopes, shown in red lines in Fig. 4.4, indicate that the γ truncation does not seriously impair torque production in TF_1. Torque values estimated as in Fig. 4.4 are summarized in Fig. 4.5. Wild type TF_1 gave ~40 pN·nm of torque over ATP concentrations of 20 nM to 2 mM, in agreement with the previous estimate with an actin filament[13, 33] and a bead duplex[28].

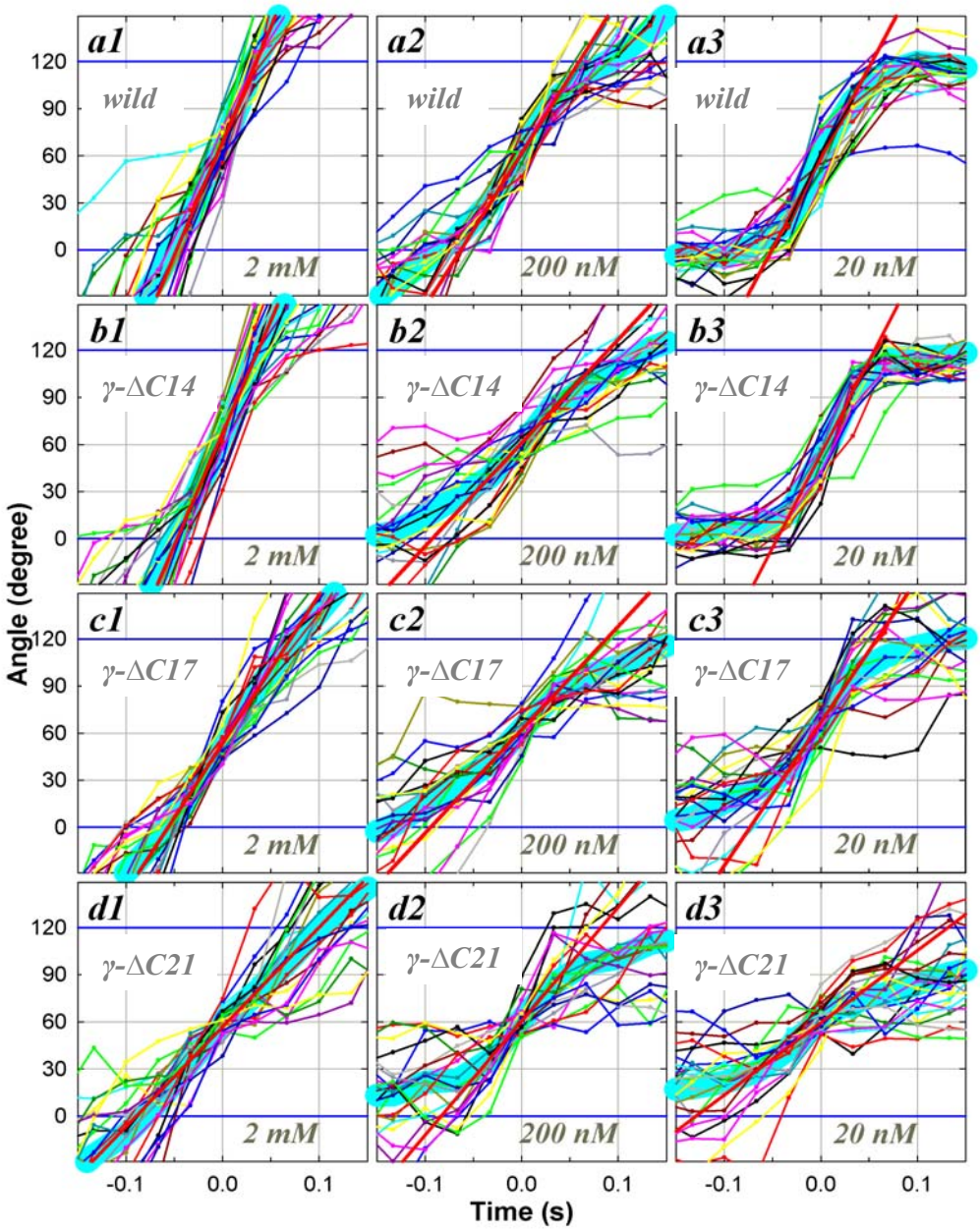

Figure 4.4 Stepping records for torque estimation. (**a**) wild type; (**b**) γ-ΔC14; (**c**) γ-ΔC17; and (**d**) γ-ΔC21. (1) at 2 mM ATP; (2) 200 nM ATP; and (3) 20 nM ATP. Thin lines with dots show 21 consecutive steps selected from a rotation time course, thick cyan line being the average. Individual step records have been shifted vertically by a multiple of 120° to obtain the overlap. Angle zero was chosen such that most of the pauses in the time course fall on a multiple of 120°. Time zero for each step record was assigned by eye to the data point closest to 60°. Straight red lines indicate the slope of the average step record judged by eye.

Truncation progressively diminished the torque, but γ-Δ21 still produced ~20 pN·nm of torque. It is noticeable in Fig. 4.5 that, for both the wild type and mutants, the torque appears somewhat low at 200 and 600 nM ATP. At this moment we cannot suggest a probable reason, nor are we 100% sure that this trend is statistically meaningful. Rotation at these [ATP]s tends to be irregular (Fig. 4.4), suggesting susceptibility to surface obstruction. The small anomaly apart, the major conclusion in this study is that the deletion up to 21 C-terminal residues, or the loss of most of the contacts between the γ tip and the lower part of the $\alpha_3\beta_3$ cylinder (Fig. 4.7**a**), does not affect the driving torque significantly (at most ~50 %).

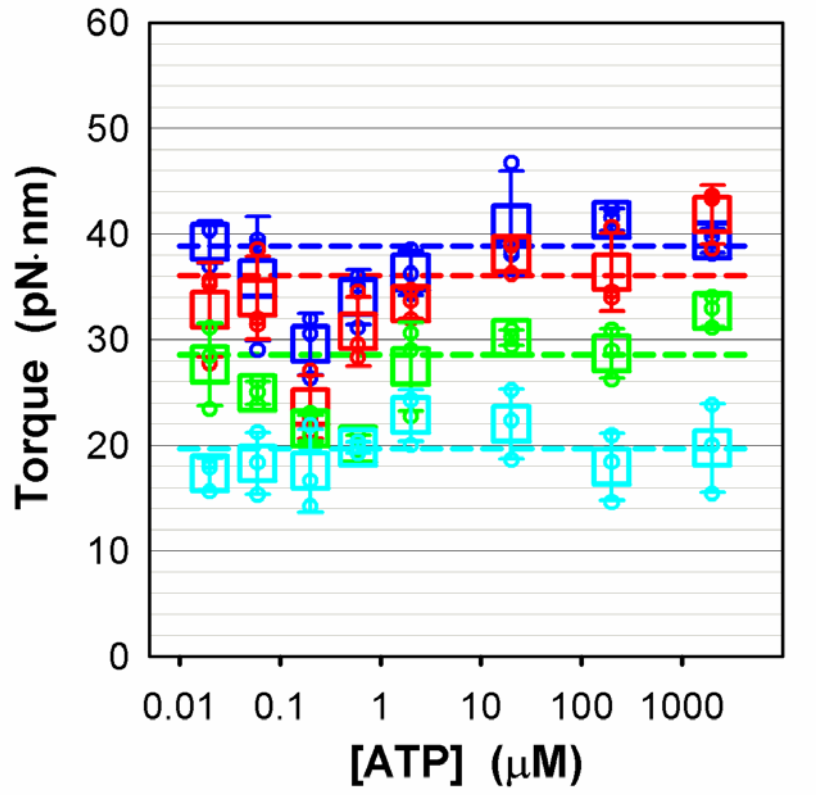

Figure 4.5 ATP dependence of the rotary torque. (Blue) wild type; (red) γ-ΔC14; (green) γ-ΔC17; and (cyan) γ-ΔC21. Three highest torque values at each [ATP] are plotted in small circles and the average of the three in a large square, the error bar being ±S.D. Dashed lines show the average over all torque values excluding data at 200 nM and 600 nM ATP.

4.2.4 Hydrolysis Activity

Typical time courses of hydrolysis activity at different [ATP]s are shown in Fig. 4.6. The slope of the curves is proportional to the rate of hydrolysis. In the wild type, an initial high activity was gradually replaced with a lower steady-state activity as MgADP inhibition proceeded[29, 31, 34]. Mutants exhibited peculiar behaviors. In γ-ΔC14, a conspicuous initial lag was observed at intermediate [ATP]s, in spite of the removal of most of the bound nucleotide which, if present in the wild type, would form MgADP-inhibited enzyme and result in a severe lag. The mutant γ-ΔC17 also showed a small lag which is not readily discerned in Fig. 4.6. The activity of γ-ΔC21 was very low, and tended to decrease with time as in the wild type. We did not explore the causes of these different kinetic behaviors. We simply note that, in all the truncation mutants and at all [ATP]s except possibly at 60 nM or below, at least part of the enzyme population was capable of actively hydrolyzing ATP. The rotating F_1 molecules that we observed under the microscope must belong to this actively hydrolyzing population.

In Fig. 4.3, the maximal hydrolysis activity in a time course, initial in the wild type and γ-ΔC21, near initial in γ-ΔC17 and near steady-state in γ-ΔC14, is plotted in red squares. Except for γ-ΔC21, the maximal activity can approximately be fitted with a Michaelis-Menten kinetics (red curves), suggesting that these maximal values best represent the activity of an active enzyme. The small deviation seen in the wild type is due to the carryover of phosphate which modulates the hydrolysis activity in an [ATP]-dependent manner (R. Shimo-Kon, unpublished): careful removal of phosphate results in a simple Michaelis-Menten kinetics[28].

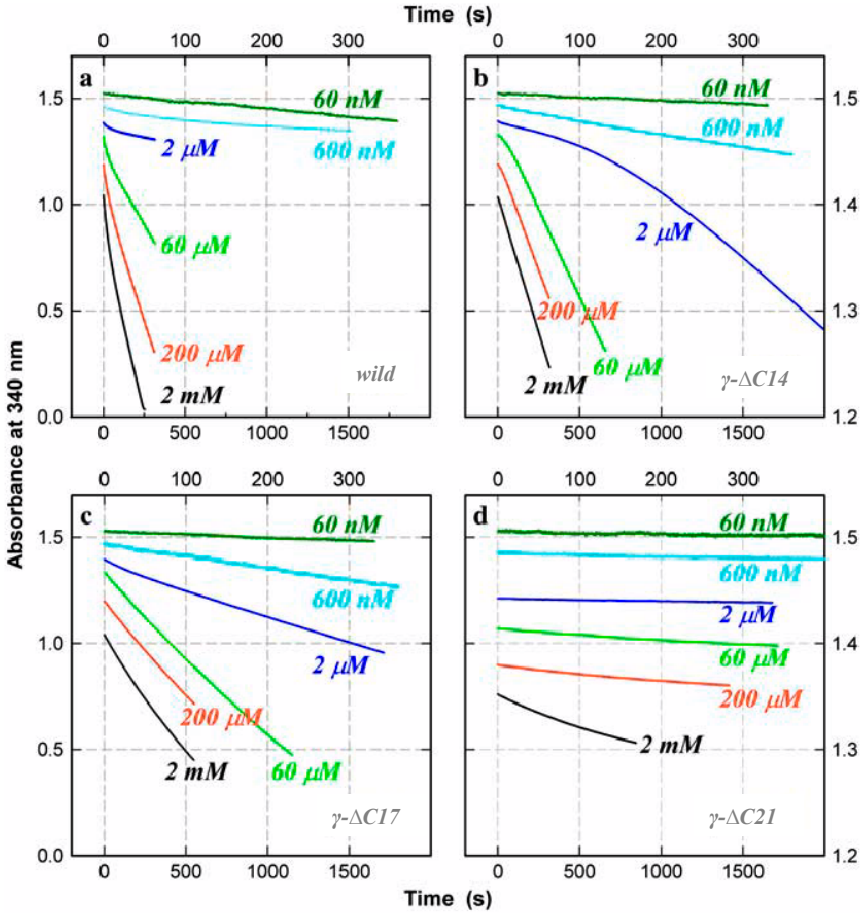

Figure 4.6 Time courses of ATP hydrolysis at indicated [ATP]. (**a**) Wild-type; (**b**) γ-ΔC14; (**c**) γ-ΔC17; and (**d**) γ-ΔC21. The decrease in absorbance is proportional to the amount of ATP hydrolyzed. Top and right axes apply to curves for 600 nM and 60 nM ATP. The wild-type showed an initial high activity followed by a steady-state activity (constant slope). At [ATP] ~ 10 μM, a low-activity phase appeared before reactivation to the final steady state (see 60μM). Mutant γ-ΔC14 showed an initial lag at and above 2 μM ATP. This was less conspicuous with γ-ΔC17, for which a slight initial lag was observed between 600 μM and 20 μM ATP (not clear on the chosen timescale). The activity of γ-ΔC21 was very low and was characterized by an initial activity followed by a lower steady-state activity. To avoid overlap, the curves are vertically shifted by an arbitrary amount. [F_1] = 5 nM except at 60 nM ATP where [F_1]= 10 nM.

The hydrolysis activity of γ-ΔC21 was extremely low, particularly at low [ATP]s where the hydrolysis rate was several times lower than expected from the rotation rate. The implication is that most of the enzyme was inactive from the beginning. With this mutant, the probability of finding a rotating bead duplex was also significantly low at low [ATP]s compared to other mutants. The simplest explanation would be that the γ-ΔC21 subcomplex is unstable and tends, for example, to partially dissociate in the absence of nucleotides. In support of this

possibility, patterns of native SDS polyacrylamide gel electrophoresis (not shown) indicated a tendency of γ-ΔC21 to dissociate into subunits under the electrophoretic conditions, and γ-ΔC17 also showed some tendency toward dissociation. A γ-ΔC21 subcomplex that happens to retain its integrity would rotate, and addition of ATP might help restore the integrity. We did not pursue further the precise reason why the bulk hydrolysis activity of γ-ΔC21 was so low. Presumably, the subcomplex of γ-ΔC25 was more unstable and could not withstand the purification procedure.

In Fig. 4.3, except for γ-ΔC21, the Michaelis-Menten fit for the maximal hydrolysis activity (red curves) overlaps with that for rotation (blue curves) at low [ATP]s, indicating that three ATP molecules are consumed per turn as expected. In the wild type, the rotation rate was somewhat higher as in previous studies, suggesting that a portion of the enzyme was already inhibited from the beginning. The F_1 in the rotation assay was labeled with streptavidin and beads, but the attachment of beads and/or streptavidin is unlikely to increase the hydrolysis activity. Biotinylation could in principle modify the activity, but biotinylated cysteines are both on the protruding portion of the γ subunit. At least at 2 mM ATP, biotinylation of either wild type (R. Shimo-Kon, unpublished) or γ-ΔC14 did not change the hydrolysis activity significantly.

As already noted, the apparent rate of ATP binding estimated from either rotation or hydrolysis activity is lower in the mutants than in the wild type. Larger differences were observed in V_{max}, the hydrolysis activity at saturating [ATP] or the rate of catalysis, γ-ΔC17 being about six-fold less active than the wild type. These differences in the rates of ATP binding and catalysis are solely related to the structural differences in the γ subunit: the loss of contacts between γ and $\alpha_3\beta_3$ cylinder somehow affects the hydrolysis kinetics in the catalytic sites remote from the γ subunit.

4.2.5 Discussion

A crystal structure of the $\alpha_3\beta_3\gamma$ subcomplex of TF_1 (Yasuo Shirakihara, Structure Biology Center, National Institute of Genetics, Mishima 411-8540, Japan, personal communication, 2005) shows close similarity to published structures of MF_1[9,35].and EF_1[36]. In particular, positions of the corresponding residues at the C-terminus of the γ subunit (Fig.4.7**c**) are essentially the same among these F_1 structures, although, near the top orifice of the $\alpha_3\beta_3$ cylinder, the γ-subunit of TF_1 and EF_1 are slightly rotated counterclockwise compared to MF_1, making the coiled coil of bacterial γ less twisted than that of MF_1.

In Fig. 4.7**a** and **b**, dark green and blue atoms on the β- and α-subunits, respectively, are those within 5 Å from an atom of γ (hydrogen atoms excluded). The structural similarity above implies that the contacts between the γ tip and $\alpha_3\beta_3$ cylinder, shown in the dark colors, are essentially the same among MF_1, EF_1, and TF_1. As seen in Fig. 4.7**a** and **b**, most of the contacts at the γ tip, below the central cavity in Fig. 4.7**a**, should be lost upon deletion of the 21 residues in TF_1 (up to and including the residues in magenta). Only a few residues of α_E and β_E remain within 5 Å from an atom of γ, and Fig. 4.7**b** suggests that the tip of the truncated γ would be allowed a considerable motional freedom in the central cavity. In spite of this loose pivot, the γ-ΔC21 mutant rotates in the correct direction with little mistakes (Fig. 4.2**d**), and its torque is still 50 % of the wild type (Figs. 4.4 and 4.5). It seems that the generation of torque, and of rotary motion, largely depends on mechanical interactions at the top orifice of the $\alpha_3\beta_3$ cylinder.

That the tip of γ is not crucial to mechanical rotation has been suggested by Junge and colleagues: deletion of 12 residues from the C-terminus of the γ subunit in EF_1 (yellow in Fig. 4.7) did not affect the torque[20], and cross linking γ-A285, after substitution with cysteine, to a residue on an α subunit in EF_1 did not impair rotation[37]. (The cross linking result, though, might simply imply that the very end of the C-terminal α-helix easily melts into a random coil). Our γ-ΔC21 here is

eight residues shorter than their 12-deletion mutant (Fig. 4.7**c**), confirming and further strengthening the unimportance of the γ tip.

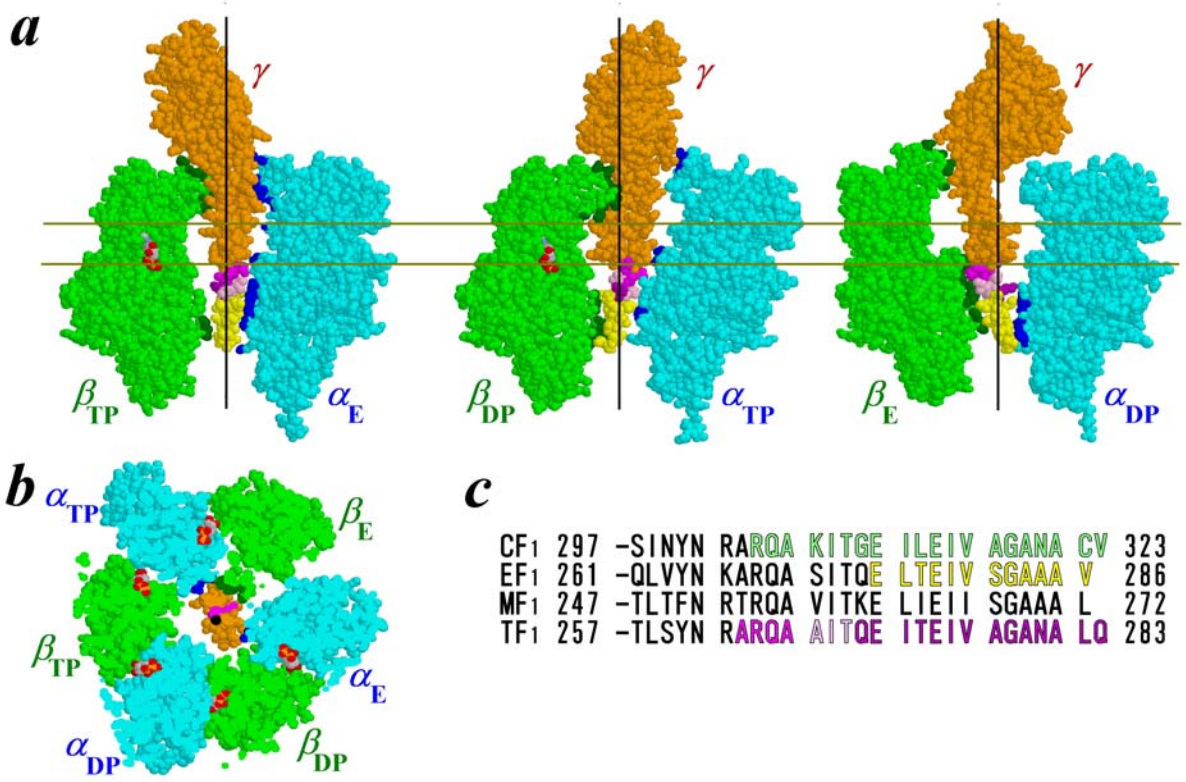

Figure 4.7 An atomic structure of bovine mitochondrial F_1 (MF_1)[35] (PDB 1E79). α-subunits are shown in light blue, β-subunits in green, and the γ-subunit in orange. The C-terminus of γ that was truncated in the present and previous works is colored according to the scheme in **c**. Those atoms of α and β subunits that are within 0.5 nm from an atom of γ (excluding hydrogens) are colored blue and dark green, respectively. Nucleotides are shown in CPK colors. The black lines in **a**, and the black dot in **b** represent a putative rotation axis[10]. (**a**) Side views showing the central γ and an opposing α-β pair. The membrane-embedded F_o portion would be above the γ subunit. (**b**) Bottom view of the section between the pair of gold lines in **a**. (**c**) Amino-acid sequences at the C-terminus of F_1 of different origins (CF_1, EF_1, and MF_1 from Nakamoto et al.[40], TF_1 from Ohta et al.[41], except that the numbering here starts from Met-1). Colored portions indicate truncations that did not kill the hydrolysis and/or rotation activities: 20 residues in CF_1[19], 12 residues in EF_1[20], and up to 21 residues in TF_1 (this work).

Previously it has been shown that forced, reverse rotation of γ in an $\alpha_3\beta_3\gamma$ subcomplex resulted in ATP synthesis, i.e., the reversal of chemical reactions in the three catalytic sites[30]. The simplest interpretation of this reversibility is a γ-dictator mechanism, in which the rotary angle of γ dictates which of the chemical reactions (binding of a substrate, synthesis or hydrolysis of ATP, and release of a product) is to occur in each site, or that the equilibrium constants for the chemical reactions are each a function of the γ angle[3]. Truncation of the γ subunit may well impair the communication from γ to catalytic sites, leading to altered kinetics of hydrolysis and rotation, even though the effect on the production of mechanical torque is minimal. Previous reports and this study indicate that the hydrolysis activity diminishes with the extent of truncation, suggesting that contacts at the γ tip plays some, though not vital, roles in the communication. Thus, for example, membrane bound EF_1 with a γ C-terminal truncation of 4 or 10 residues had 63% and 14% of wild type activity, respectively[18]. Isolated EF_1 lacking 3, 6, 9, and 12 C-terminal residues each showed an activity 70 %, 50 %, 30 %, and 24 % of a control[20]. With CF_1, Mg-ATPase activity in the presence of an activating anion sulfite was 73, 45, 31, 20, 13, and 18 % of the wild type for the deletions of 10, 12, 14, 16, 18, and 20 residues[19] respectively.

Of the contacts at the γ tip, hydrogen bonds between γ-R254 and β_E-D316 (in the MF_1 sequence) and between γ-Q255 and β_E-T318[9] have been shown to be important for catalytic activity in a mutation study: when γ-R268 or γ-Q269 of EF_1, corresponding to R254 and Q255 in MF_1 (Fig.4.7**c**), was mutated to leucine, the hydrolysis activity dropped to 12 % and 1 %, respectively, of a control[38]. With CF_1, though, the mutant with 20-residue deletion including R304 and Q305 was 18 % active[19]. The tolerance in CF_1 is remarkable, in that the N-terminus of γ, the shorter pair of the coiled coil, can also be truncated without complete loss of hydrolysis activity[39]. Whether the apparent tolerance in CF_1 may result from decoupling, i.e., hydrolysis without rotation, remains to be seen. More important is the question whether γ truncation in various F_1s leads to failure in the γ-dictated

synthesis, i.e., clockwise (reverse) rotation failing in ATP synthesis. Further studies are needed to answer these questions.

4.2.6 Hydrolysis Activity in the Presence of Lauryldimethaylamine Oxide (LDAO)

During ATP hydrolysis by F_1 MgADP is occasionally trapped in a catalytic site, rendering the enzyme into an inactive state. In the presence of ATP, tightly bound MgADP is spontaneously released and the enzyme goes through cycles of inhibition and inactivation. This so called MgADP inhibition has been commonly observed in F_1 from mitochondria[42], chloroplast[43] and bacteria[31, 44, 45]. A neutral detergent LDAO has been shown to be a good activator that stimulates F_1 by releasing inhibitory MgADP[46]. In the previous sections it has been found that time courses of ATP hydrolysis by the mutants γ-ΔC14, γ-ΔC17 and γ-ΔC21 was complicated, involving lag and slow inactivation. In order to obtain insights into the possible causes of such behaviors of mutants the hydrolysis kinetics of mutants and wild type was compared in the presence of LDAO as described below.

4.2.6.1 Time Courses

Typical time courses of hydrolysis activity measured at different [ATP]s for wild type and mutant complexes are displayed in Fig. 4.8. The data in the absence of LDAO described have been used as control. The time course data at several [ATP]s where LDAO produces a marked difference are shown. The wild type complex hydrolyzes 2 mM-60 μM ATP at almost a constant rate from the beginning when 0.03 % LDAO was added in the assay producing uniphasic time courses, compared to biphasic time courses in the control, as shown in Fig. 4.8**a**. The slope of constant rate in the presence of LDAO is very close to the slope of initial burst in the absence of LDAO. At other [ATP]s time courses are of similar pattern. Upon reduction of [ATP]s the length of initial burst phase in the wild type gradually decreases. At the start of hydrolysis reaction, MgADP-free wild type hydrolyzes ATP very rapidly and as the reaction continues the enzyme gradually accumulates MgADP to reach a stable steady-state that represents dynamic

equilibrium between active and MgADP-inhibited forms[31]. Since LDAO prevents MgADP inhibition, the initial high rate continues until NADH in the assay medium is completely consumed.

Time courses for mutant complexes are very peculiar and complex. The structure of γ subunit in each mutant is different from that of the wild type and this introduces different kinetic characteristics. In the case of γ-ΔC14 mutant as shown in Fig. 4.8**b**, addition of 0.15 % LDAO completely abolishes the initial lags in the time courses of control and converts the lags into burst at 2 mM-2 μM [ATP]s. As seen, the length of the initial lag in the absence of LDAO gradually increases with decrease of MgATP down to 2 μM. The nature or cause of this lag is unknown. Either the enzyme binds ATP very slowly or is incapable of rapid catalysis possibly due to MgADP inhibition. The entrapment of this inhibitory MgADP may occur during mixing time of ~2.0 s. When 0.15 % LDAO was added the enzyme is prevented from entrapping MgADP at the catalytic sites and consequently the lag phase completely changes into a burst phase with an increased activity.

Time courses for γ-ΔC17 mutant are shown in Fig. 4.8**c**. The curve for the control at 2 mM ATP consists of a very small initial burst whereas in the range of 600-20 μM, the initial part of time course consists of a lag phase. In the presence of 0.1 % LDAO initial bursts have been found in all cases. For γ-ΔC21 mutant as shown in Fig. 4.8**d**, 0.1 % LDAO gives similar curves as control but with higher slopes at initial burst. Because lags in the mutants are converted into burst in the presence of LDAO that stimulates F_1 by removing MgADP from catalytic site, the slow activation of catalysis in these mutants likely results from MgADP inhibition.

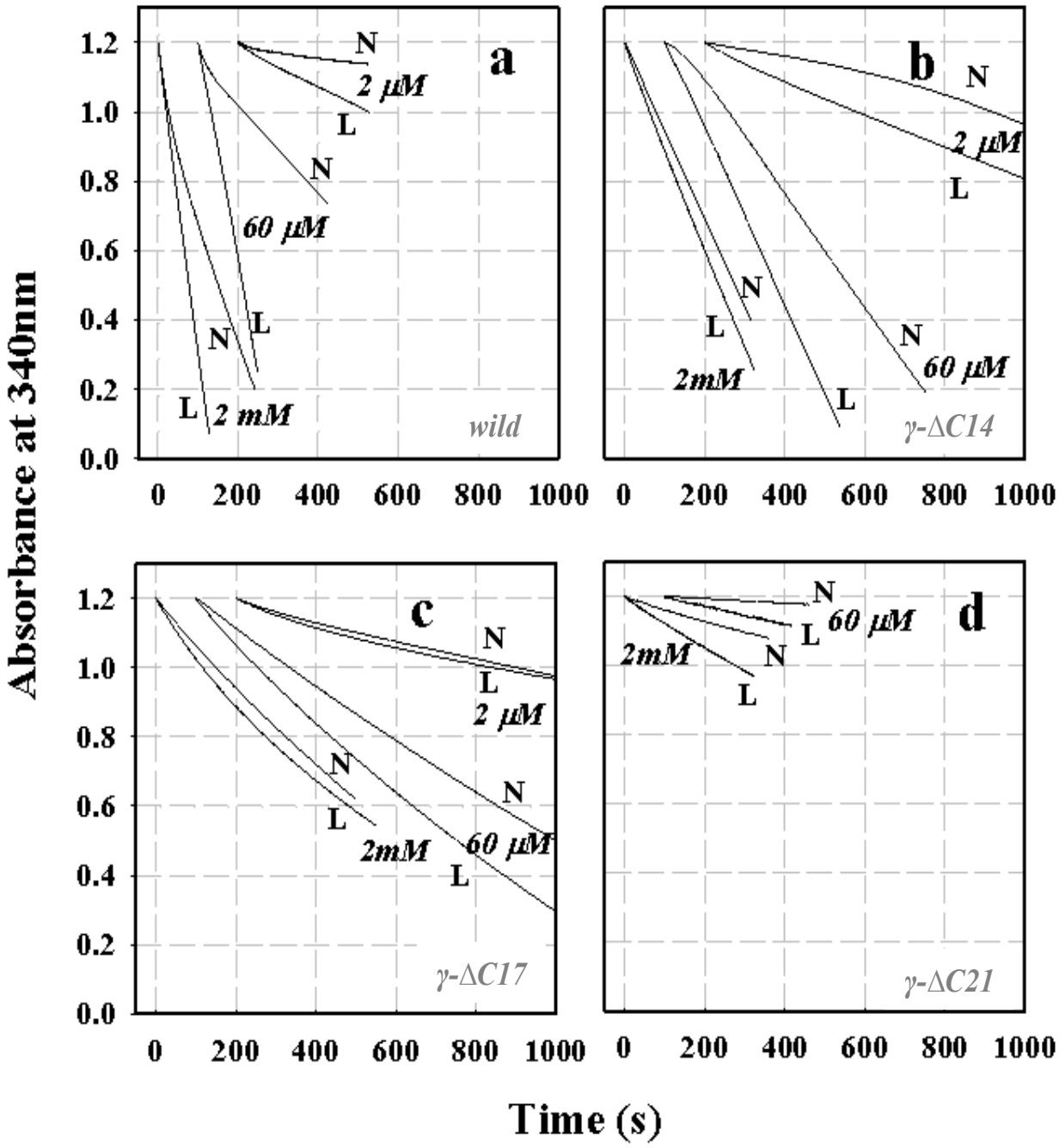

Fig. 4.8 Comparison of time courses of ATP hydrolysis by wild type and mutant F_1 at indicated [ATP]s. (**a**) Wild type; (**b**) γ-ΔC14; (**c**) γ-ΔC17; and (**d**) γ-ΔC21. The symbol N indicates the data in the absence (control) and L indicates the data in the presence of LDAO. The pattern of time courses with LDAO at [ATP] of 600 nM and below is similar to the control. To avoid overlap, the data at various [ATP]s are horizontally shifted by an arbitrary amount. For the measurement with LDAO [F_1] = 5 nM except at 20 and 60 nM ATP (or 200 nM ATP for γ-ΔC21) where [F_1] = 10 nM was used.

4.2.6.2 ATP Hydrolysis Activity

The activity curves as shown in Fig. 4.9 for wild type and mutants in the presence of LDAO follow Michaelis-Menten kinetics and the kinetic parameters in the presence of LDAO are displayed in Table 4.2.

Table 4.2 Kinetic parameters for wild type and mutants in the presence of LDAO derived from Michaelis- Menten equation.

Type of F_1	V_{max} (s^{-1})	K_m (μM)
Wild	288.5	22.0
(γ-ΔC14)	103.0	6.7
(γ-ΔC17)	63.2	5.2
(γ-ΔC21)	23.6	35.7

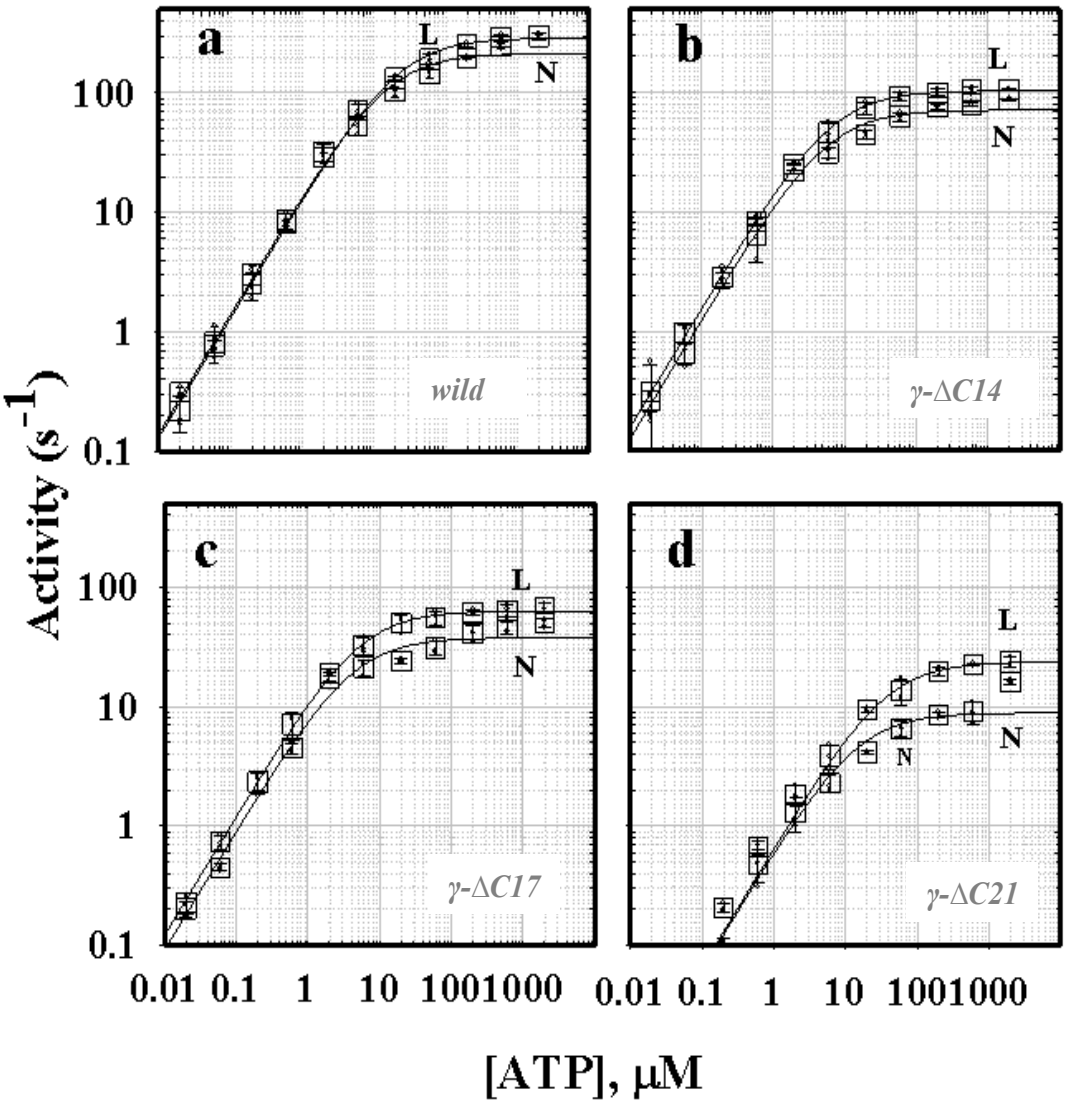

Figure 4.9 Comparison of ATP hydrolysis activity. The symbol N indicates the data in the absence (control) and L indicates the data in the presence of LDAO. (**a**) Wild type; (**b**) γ-ΔC14; (**c**) γ-ΔC17; and (**d**) γ-ΔC21. The circles on the curves are from individual time courses and squares show the average over three points, error bars being a standard deviation. The initial hydrolysis activity estimated at 2–7 s after mixing (2 μM ATP and above), 2–60 s (600 nMATP), or from the entire portion (200 nM ATP and below) of the curve after addition of F_1. Values at 200 nM ATP and below have been corrected for a small decline in absorbance observed in the absence of F_1. The curves show a fit with Michaelis-Menten kinetics: $V = V_{max}$ [ATP]/ (K_m + [ATP]). As seen from the curves, the mutant γ-ΔC14 and γ-ΔC17 are little bit more active in the presence of LDAO compared to the wild type. The maximum increase of initial hydrolysis activity occurs up to 1.3 fold for wild type at 200 μM ATP, 4 fold for γ-ΔC14 at 2 μM ATP comparing initial lag (control) and initial burst (with LDAO, Fig. 4.8**b**), 2.3 fold for γ-ΔC17 at 60 μM ATP comparing initial lag (control) and initial burst (with LDAO, Fig. 4.8**c**) and 2.5 fold for γ-ΔC21 (Fig. 4.8**d**) at 600 μM ATP respectively.

4.2.6.3 Discussion

In F_1, LDAO promotes release of the inhibitory MgADP from the affected catalytic site[29] and produces Michaelis-Menten hydrolysis kinetics[16]. It has been suggested that LDAO activates F_1, either by stimulating binding of ATP to non-catalytic sites that accelerates the release of MgADP from a catalytic site or by directly promoting release of inhibitory MgADP from a catalytic site[34, 45, 47]. The hydrolysis reaction in F_1 is coupled to the rotation of the γ subunit[7]. It is possible that slow isomerization of the F_1.ADP.Mg complex to the inactive F_1*ADP-Mg complex accompanies a movement of the γ subunit into an abortive position for ATP hydrolysis[48]. When ATP binds to non-catalytic sites, the isomerization is slowly reversed by movement of the γ subunit from the abortive position into a position for productive ATP hydrolysis.

Upon reduction of ATP concentration initial burst decreases in wild type or lag increases in some mutants for control data. At low ATP concentrations, ATP may not be abundant enough to saturate the non-catalytic sites. This may be a possible reason why LDAO is not so effective in the low [ATP]s in the case of wild or mutants. The detergent LDAO stimulates both wild type and mutants. The initial slow activation or inhibition in the mutants has been completely removed upon addition of LDAO that leads to simple Michealis-Menten kinetics.

4.2.7 Rotation in the Presence of LDAO

In the previous section it has been shown that the use of LDAO in the hydrolysis assay stimulated ATP hydrolysis activity of both wild type and mutants. The highest concentration of LDAO to elicit a full effect was 0.15 % for γ-ΔC14 mutant. Inactivated states of mutants became activated and followed simple Michealis-Menten kinetics. Being inspired from this result an investigation was done into the effect of LDAO on the rotary torque produced by the wild type and mutant F_1 as described below.

4.2.7.1 Rotation Time Courses

Rotation of wild type and mutant F_1 was observed in the absence and in the presence of LDAO for a continuous period of 60 s or more. The results are summarized in Fig. 4.10. For this study, a saturating ATP concentration (2mM) was used where F_1 (either wild or the mutants) rotates at its highest (time-averaged) speed. In the absence of LDAO, counter clockwise rotation was frequent for both wild type and mutants: about 5 rotating duplexes were found per view field. The number of duplexes as well as their speeds gradually decreased for mutants with the degree of truncation. Both for wild and mutants, some beads in the observation chamber rotated in the counter-clockwise direction, some beads exhibited random fluctuations and some beads were stuck on the glass surface. In the time course of Fig. 4.10 (for wild or mutants) with zero LDAO it is seen that the curves are basically smooth with a small number of pauses, possibly due to surface obstruction or short inhibition. Because the rotation is smooth, the entire time-averaged speed of the bead duplex is higher. For torque estimation (with or without LDAO), the fastest portion of the time course was taken that contained at least seven consecutive revolutions. The highest average speed over seven revolutions is v~4.0 rev/s for wild type; v ~3.0 rev/s for γ-ΔC14; v~2.5 rev/s for γ-ΔC17 and v ~1.0 rev/s for γ-ΔC21.

Occasionally, wild type or mutants also fall into MgADP inhibited states producing pauses that are usually longer. In the presence of 0.15 % LDAO, the trajectories of rotation is not so smooth like zero LDAO and contains many pauses that slow down the average speed of bead duplex as seen in Fig. 4.10. The highest average speed over continuous seven revolutions is v ~3.0 rev/s for wild type; v ~2.2 rev/s for γ-ΔC14; v~1.8 rev/s for γ-ΔC17 and v~0.6 rev/s for γ-ΔC21.

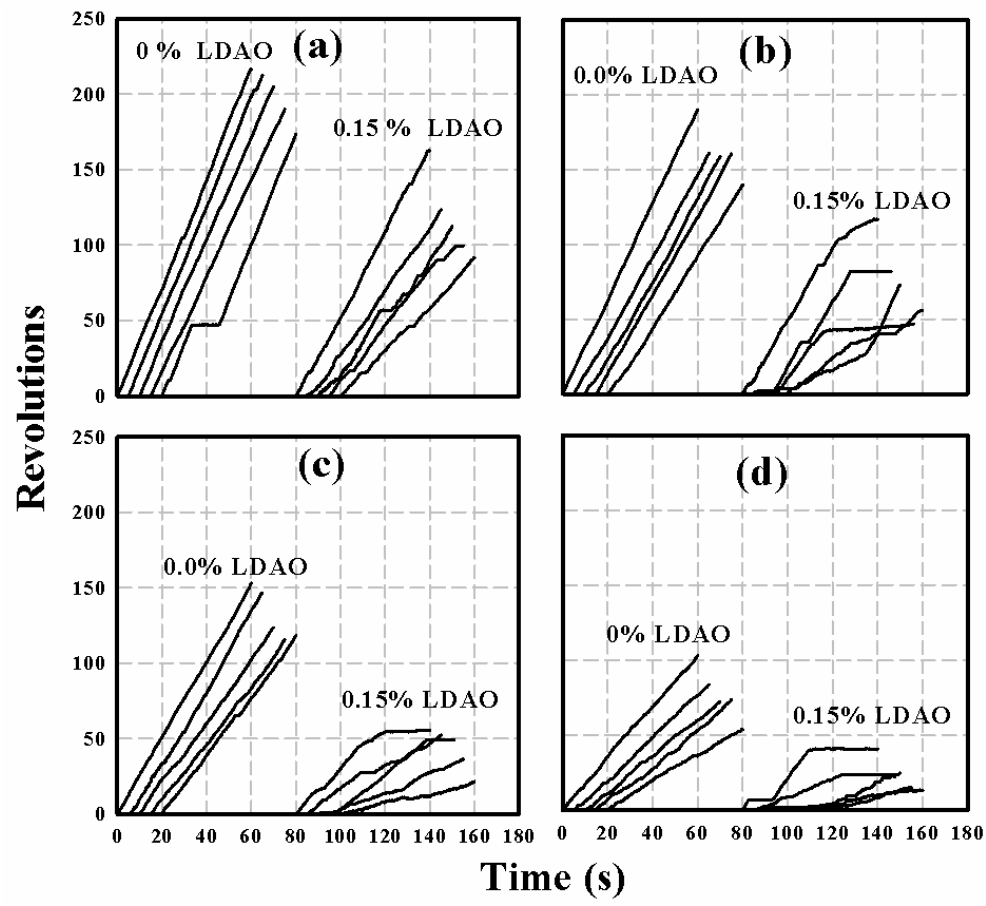

Figure 4.10 Rotation time courses for wild and mutant F_1 at 2 mM [ATP] in the absence as well as in the presence of indicated amount of LDAO. (**a**) Wild type; (**b**) γ-ΔC14; (**c**) γ-ΔC17 and (**d**) γ-ΔC21. Curves are shifted horizontally to distinguish them from each other.

4.2.7.2 Estimation of Torque

In order to compare the torque generated by the wild type or mutants in the absence and in the presence of LDAO, equations 4.1 and 4.2 were used. Like previous section (4.2.3), for both wild and mutants, angular speed of bead duplexes was estimated taking twenty one consecutive steps from seven revolutions to avoid the effect of regular pauses and for the data to be statistically sufficient and an example is shown in Fig. 4.11. The results of torque estimations are summarized in Fig. 4.12. As seen the torque for zero LDAO is ~40 pN-nm for wild and γ-Δ14 mutant; ~35 pN-nm for γ-ΔC17 and ~25 pN-nm for γ-ΔC21 which are consistent with the data presented in section 4.2.3. In the presence of 0.15 % of LDAO, wild or mutant F_1 produces similar torque at 2mM [ATP].

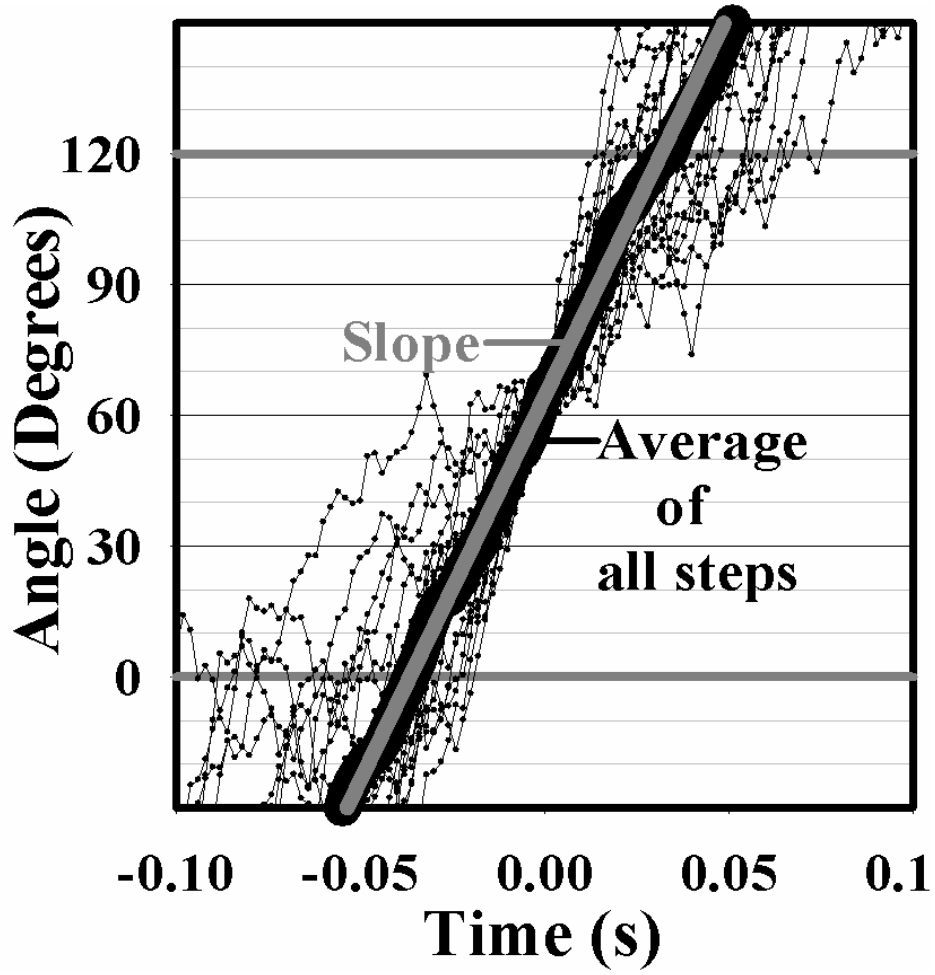

Figure 4.11 The method of estimation of angular speed of a bead duplex attached to the γ subunit of F_1. Here, individual steps (twenty one lines with dots), taken from consecutive seven revolutions of a rotation time course for wild F_1 with zero LDAO at 2mM ATP, are overlaid. The speed of bead duplex was recorded at a rate of 500 frames^{-1}.Angular speed of all rotary bead duplex used for torque estimation of wild and mutant F_1, in the absence or in the presence of LDAO, was calculated using this method.

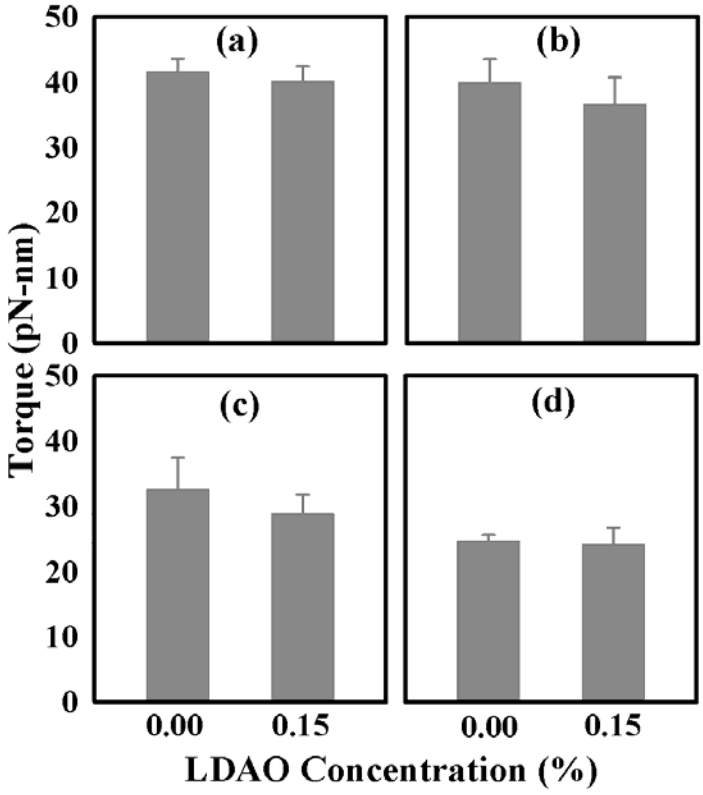

Figure 4.12 Torque of wild and mutant F_1 as a function of LDAO concentration at 2mM [ATP]. (**a**) Wild type; (**b**) γ-ΔC14; (**c**) γ-ΔC17 and (**d**) γ-ΔC21. The box represents torque averaged over three F_1 molecules ± SD.

4.2.7.3 Discussion

The number of rotary beads for wild type or mutants is very low (~only 10 %) compared to without LDAO if 0.49 μm bead is used. A possible reason is the detachment of beads from F_1 by disruption of bead-streptavidin or streptavidin-biotin linkage upon addition of LDAO. Another possibility is that LDAO somehow lets the beads stuck on the surface so that F_1 can not rotate them. It is also possible that most of the F_1 molecules are washed away from the chamber when the observation buffer containing LDAO was infused many times into the chamber due to detergent effect of LDAO. During the course of rotation, beads often detached from the glass surface, indicating disruption of bead-F_1 or F_1-surface linkage. Once the bead was detached it remained stuck on the surface but with zero LDAO the detached bead usually floated in the solution or it is again attached to the glass surface in the chamber. It is most likely that such detachment of either F_1 from glass surface or bead from F_1 might decrease the number of

rotating beads in an observation chamber. Most of the beads (single or duplex) appeared to be rigidly stuck on the glass surface and a few are rotating. Some rotary beads stopped within several minutes.

Previously we have shown that F_1 molecules (wild or these mutants) become stimulated or activated upon addition of LDAO in the ATP hydrolysis assay in which F_1 molecules move freely within the solution. In the case of rotation assay, the F_1 molecules are fixed on the glass surface through histidine tags and they also carry a bead duplex that is huge compared to the size of F_1 and for that extra chemical bonds are used. The detergent LDAO is sticky and may adversely affect such bonds that possibly makes the situation complex compared to hydrolysis assay and we are unable to realize stimulation effects of LDAO during rotation. From the present experiment it appears that the torque of wild and mutant F_1 remains unaffected upon use of LDAO. If an experiment can be designed so that hydrolysis activity and torque measurement can be performed on the same F_1 molecule in the presence of LDAO then a firm conclusion can be drawn. Therefore, further studies still remain for the future.

4.2.8 Hydrolysis Activity in the Presence of Sodium Dodecyl Sulfate (SDS)

The surfactant SDS is commonly used in polyacrylamide gel electrophoresis (SDS-PAGE) to separate proteins. SDS denatures proteins causing the molecules to lose their native conformation. In Fig. 4.3**d** it has been seen that the mutant γ-ΔC21 exhibited relatively poor ATP hydrolytic property, possibly due to its structural instability. SDS denatures protein by dissociating the components of the protein implying that it destabilizes the protein structure. Therefore, ATP hydrolysis by the active mutant (γ-ΔC21) F_1 molecules in the presence of SDS may hint at their structural stability. With this aim in mind, the present investigation of SDS effect on the ATP hydrolysis activity of mainly γ-ΔC14 and γ-ΔC21 mutants has been conducted.

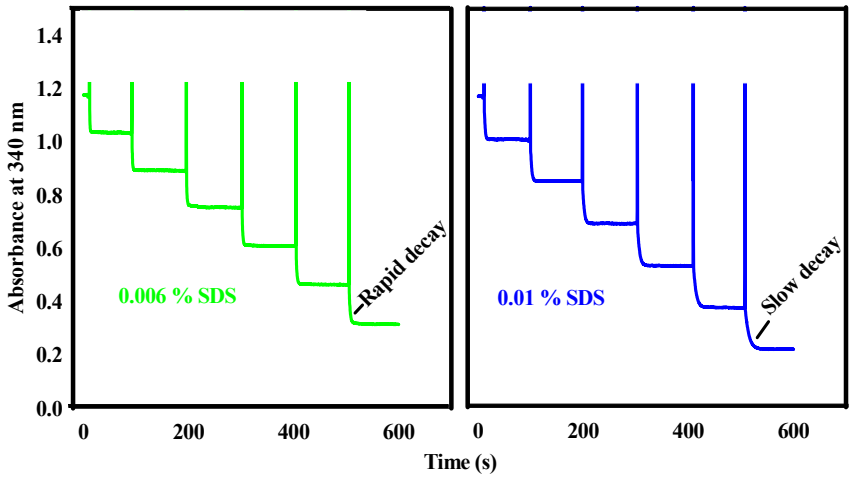

Figure. 4.13 Stability of ATP regenerating system at indicated concentration of SDS. The vertical lines indicate the noise produced during addition of 20 μM ADP. Absorbance decay becomes slow in the curve produced for 0.01 % SDS that indicates the instability of the regenerating solution.

The stability of ATP regenerating system used in this work was checked for 10 minutes before measurement of hydrolysis activity. It has been found that the regenerating system is stable only below 0.01 % of SDS as shown in Fig. 4.13. At 0.01% SDS or more the absorbance decay becomes slower, possibly due to disruption of the system. The hydrolysis activity was measured below this SDS concentration. Different concentrations of SDS (0-0.006 %) were used to examine the activation of F_1. The time courses of ATP hydrolysis at several [SDS]s are displayed in Fig. 4.14. As seen the γ-ΔC14 mutant hydrolyzes 2 mM ATP with a small initial lag that subsequently changes into a linear form (Fig. 4.14**a**) and the γ-ΔC21 mutant hydrolyzes ATP with an initial burst (Fig. 4.14**b**) in the absence of SDS. Use of SDS does not affect so much on the pattern of the time course.

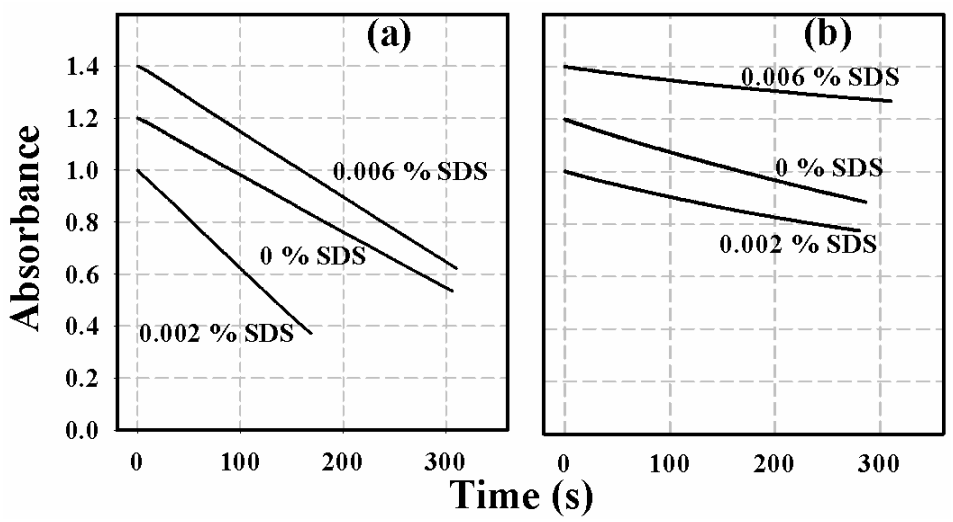

Figure 4.14 Comparison of time courses of ATP hydrolysis by mutant F_1 in the presence or absence of SDS. (**a**) γ-ΔC14 and (**b**) γ-ΔC21. The data at various [SDS]s are vertically shifted by an arbitrary amount to avoid overlap.

The patterns of ATP hydrolysis activity as a function of SDS concentration for these mutants are shown in Fig. 4.15. The activity of F_1 was measured at 2mM ATP which is saturating concentration and at a constant concentration of F_1 (5 nM). The activity curve of γ-ΔC14 mutant F_1 exhibits a peak at 0.002 % of SDS and at higher concentrations it becomes inhibitory (Fig. 4.15**a**). There may be disruption of the interactions between F_1 subunits at higher concentrations so that activity starts decreasing. SDS can also stimulate the activity of some other enzymes[49]. The activity of the mutant γ-ΔC14 increases with the increase of SDS concentration up to a certain limit then activity starts to decrease while the activity of the mutant γ-ΔC21 complex decreases with the increase of SDS. In the SDS activation profile of this mutant the peak is absent (Fig. 4.15**b**). At this moment, the exact reason why or how SDS accelerates the activity of mutant γ-ΔC14 is unknown.

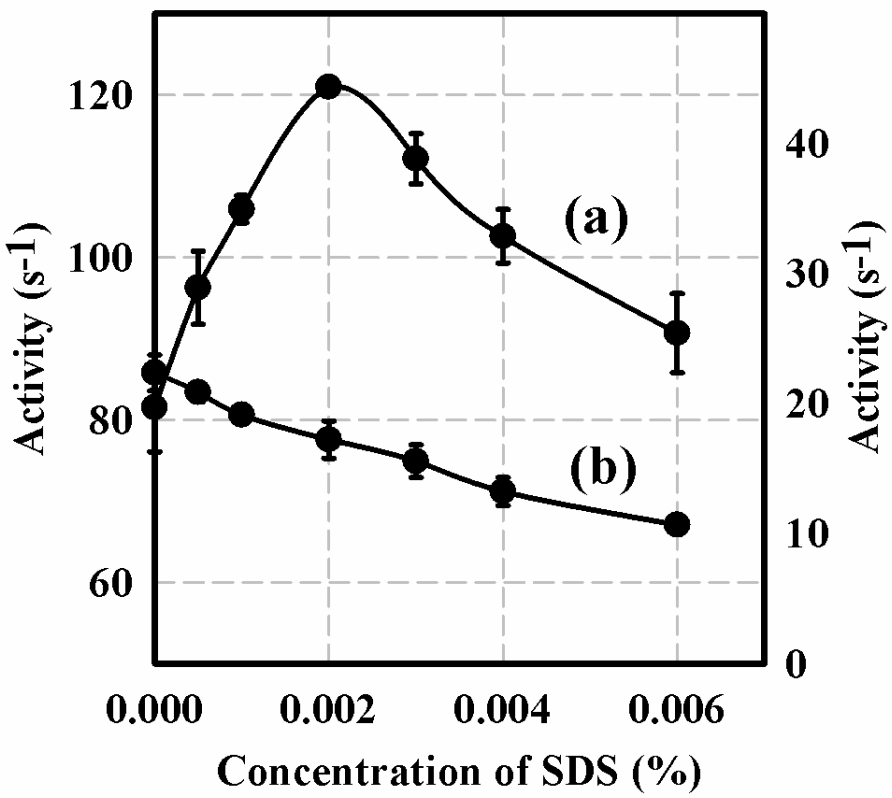

Figure 4.15 Comparison of ATP hydrolysis activity of (**a**) γ-ΔC14 and (**b**) γ-ΔC21 mutant F_1. The circles or triangles show the average over three points, error bars being a standard deviation. The initial hydrolysis activity was estimated from the time course at 2–12 s after mixing of γ-ΔC21 mutant and for 10 s immediately after a very small initial lag for γ-ΔC14 mutant. The right axis applies to the curve for the γ-ΔC14 mutant activity.

4.2.8.1 Discussion

The SDS-induced enzyme activation is related to loosening of protein structure[50]. In the case of F_1, the presence of SDS may confer a more flexible conformation in the γ-ΔC14 mutant F_1 structure and thereby stimulate its activity. This stimulation of activity indicates the structural stability of the mutant. The wild type F_1 has also been stimulated at 0.003 % SDS. The structure of γ-ΔC21 mutant, whose hydrolysis activity was poor, possibly became unstable when it interacts with SDS so that it was deactivated rather than activated. It appears from this study that the mutant γ-ΔC21 hydrolyzed ATP continuously at decreasing rates upon increase of SDS concentration that indicates its structural instability while the other mutant γ-ΔC14 produced a characteristic peak in the activation profile that indicates its structural stability. Therefore, SDS-protein (here mutant

F_1) interactions can be helpful in order to understand the structure-function relationships of proteins.

4.3 Wild Type and Mutant B

In the previous sections it has been shown that the mutants made by truncation of carboxy-terminus of TF_1-γ up to 21 residues (γ-ΔC21 in Fig. 4.17**c**) rotated and produced half or more torque compared to the wild type. Beyond 21, no active sub-complex was obtained. In this section the results of mutant group **B** will be discussed.

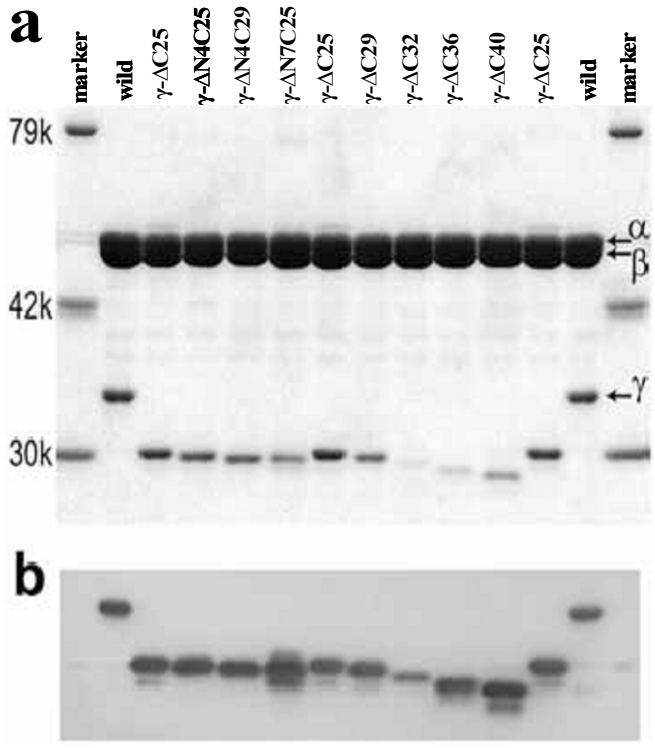

Figure 4.16 Confirmation of γ truncations by polyacrylamide gel electrophoresis. (**a**) 10 % gel containing 0.1 % SDS, stained with Coomassie Brilliant Blue R-250. (**b**) Western blot of **a** stained with an anti-γ antibody. The amount of γ in purified samples was variable depending on preparations; γ-ΔC40 in another preparation showed a barely detectable γ band.

The shorter γ subunits were expressed at levels similar to that of wild type and assembled sub-complexes containing γ, albeit at lower yields for short mutants

(Fig. 4.16) can be obtained. Purified F_1 (assembled sub-complex) with a short γ was unstable and had to be used while fresh.

4.3.1 Rotation and Torque Generation

Rotation of mutants were tested by attaching the β subunits to a glass surface through the histidine residues at the amino-terminus and putting, as a marker, a duplex of 0.29-μm beads on the γ subunit. For carboxy-terminal truncation, rotary beads up to γ-ΔC36 can be found, but none with γ-ΔC40. Amino-terminal truncation was also attempted starting with γ-ΔC25. γ-ΔN4C25 rotated, but γ-ΔN7C25 and γ-ΔN4C29 did not. When a duplex rotated, it did so in the anticlockwise direction as with wild type (observed from above in Fig. 4.17**a**), usually for more than 100 revolutions even with γ-ΔC36 or γ-ΔN4C25 (Fig. 4.18). Finding rotary beads became progressively difficult for shorter mutants. With wild type, ~200 rotating bead duplexes were found per observation chamber when F_1 at 0.5 nM was infused in the chamber.

Mutants were examined within 3-4 days of preparation (kept at room temperature because TF_1 is cold labile) and F_1 at a higher concentration had to be applied to observe rotation. With γ-ΔC25, 20-25 duplexes rotated per chamber at 2 nM F_1; 8-10 duplexes at 10 nM γ-ΔC29; 3-4 duplexes at 20 nM γ-ΔC32; ~2 duplexes at 50 nM γ-ΔC36 if observed within two days (none rotated after four days); 4-5 duplexes at 10 nM γ-ΔN4C25. Rotation could be observed at least for two hours after chamber preparation. Non-rotating mutants (γ-ΔC40, γ-ΔN7C25 and γ-ΔN4C29) were closely examined in 5-6 chambers at various F_1 concentrations up to 100 nM, beginning a few hours after purification.

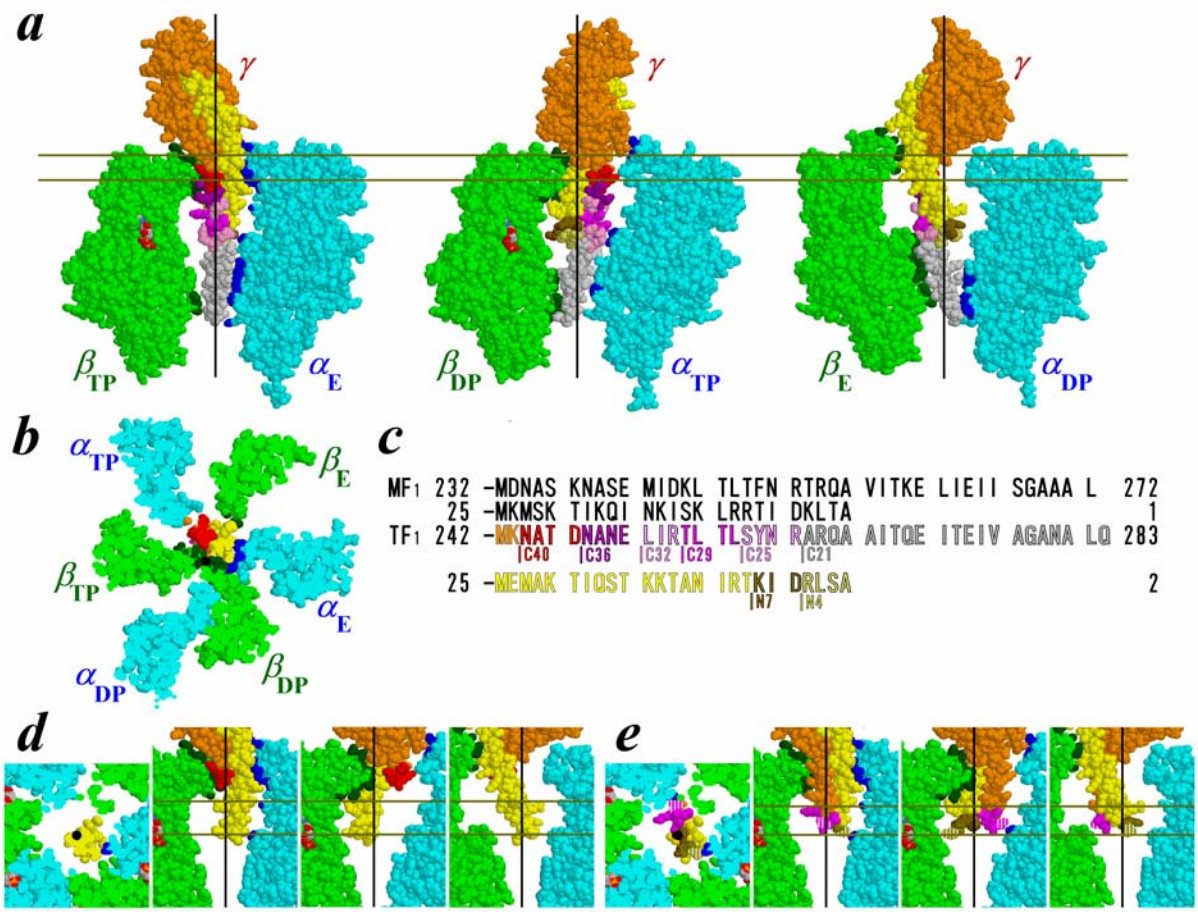

Figure 4.17 An atomic structure[35] of MF_1. Truncations of the γ subunit are shown with the colour scheme in **c**, the N-terminal α-helix shown in yellow. Those atoms of α and β subunits that are within 0.5 nm from an atom of γ (excluding hydrogens) are coloured blue and dark green, respectively. Nucleotides are shown in CPK colours. The black lines in side views and the black dots in bottom views represent a putative rotation axis[10]. (**a**) Side views showing the central γ and an opposing α-β pair. The membrane-embedded F_o portion of ATP synthase would be above the γ subunit. (**b**) Bottom view of the section between the pair of gold lines in (**a**). (**c**) Amino-acid sequences at the carboxy- and amino-termini of γ in MF_1 (ref. 51) and TF_1 (ref. 41 except that numbering in our paper here starts from Met-1, which is absent in the expressed wild-type protein). In γ-ΔN4C25, amino-acid analysis showed that γ-Met-4 was not removed. (**d**, **e**) Central portions of the bottom and side views for γ-ΔC36 and γ-ΔN4C25. In the latter, γ-Met-4 is represented by γ-Lys-4, excluding the ε-amino group to mimic Met; side chains of γ-Met-4 and γ-Leu-258 are shown with stripes because these are close to the cavity wall but unlikely to adopt a rigid conformation.

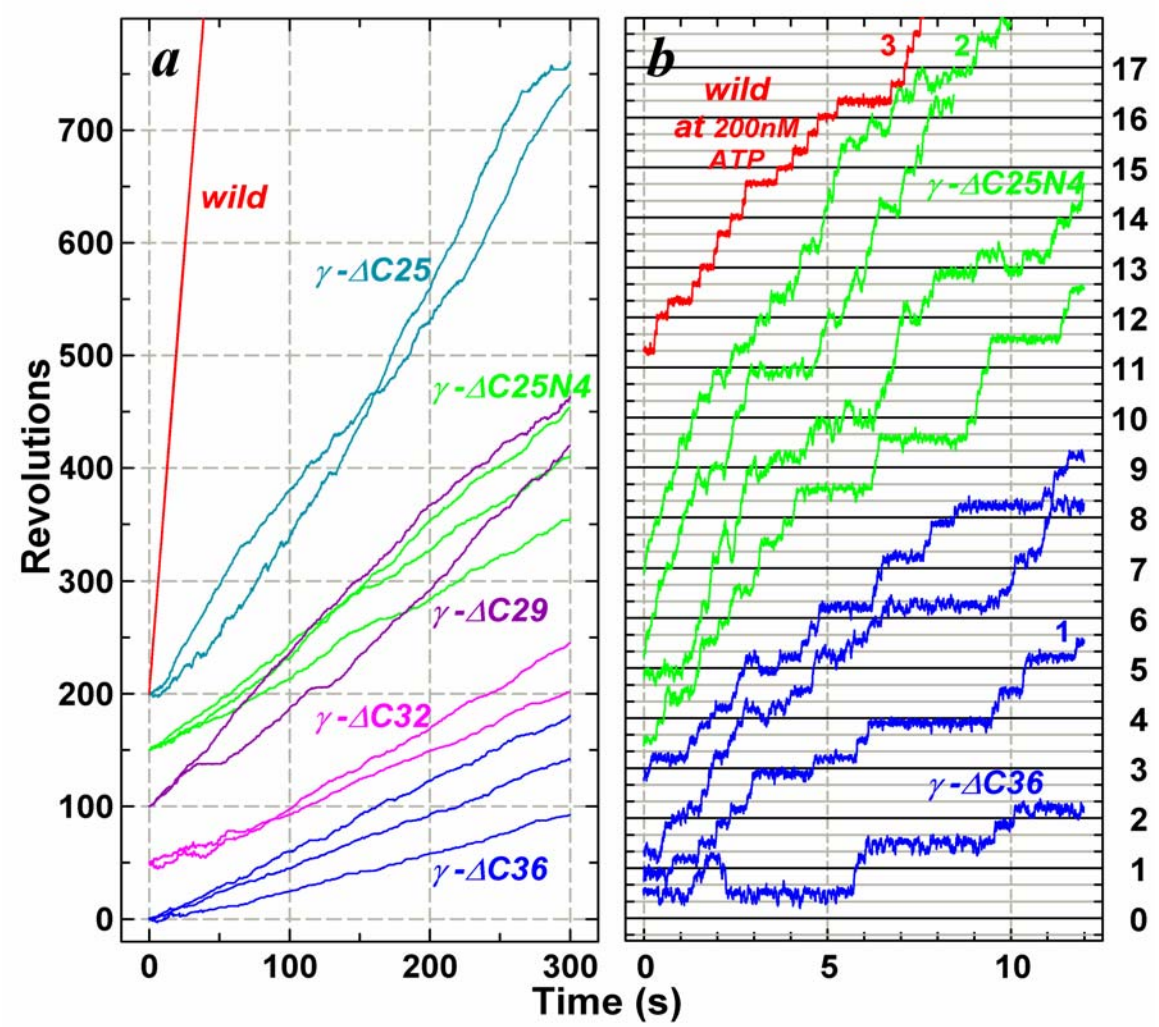

Figure 4.18 Time courses of rotation of 0.29-μm bead duplexes attached to the γ subunit. All rotations were anticlockwise when viewed from above in Fig. 4.17**a**. Horizontal lines in **b** are separated by 120°. ATP concentration was 2 mM, except for the wild type in **b** which stepped due to infrequent binding of ATP at 200 nM (rate constant for ATP binding ~2×10^7 $M^{-1}s^{-1}$). The dwelling angles of the mutants are plotted ~80° ahead of the ATP-waiting dwells of wild type, because long pauses such as those in γ-ΔC29 in **a** also occurred on the same angles and because long pauses in wild type, due to MgADP inhibition, occur at ~80°; this assignment, though, is tentative because we could not determine ATP-waiting angles of the mutants. The bottom curve in **b** shows an exceptional case of reversal over two 120°-steps in a sluggish phase, after which more regular rotation resumed beyond the right-hand axis. Temperature, 2 3°C.

Rotation time courses of beads that rotated relatively fast at 2 mM ATP are shown in Fig. 4.18. For mutants except γ-ΔC25, rotation was failed at lower ATP concentrations. Rotation of wild-type F_1 was basically continuous at the video resolution of 2 ms. At this saturating ATP concentration, a catalytic cycle of ATP hydrolysis under unloaded conditions takes only ~2 ms, and thus the average speed of ~15 revolutions per second (rps) observed here is limited by viscous friction against the bead duplex. Time-averaged speeds of the mutants were an order of magnitude lower, ranging from ~2 rps (γ-ΔC25) to ~0.5 rps (γ-ΔC36). The cause is not the mutants torque being lower, which would result in a lower speed at all moments, but the mutants' tendency to dwell at angles separated by 120° (Fig. 4.18**b**). An interpretation of this 120°-stepping behaviour is that a reaction(s) in the catalytic cycle, the reaction that is to occur at the observed dwelling angles, is sensitive to load and impeded by the bead duplex. Indeed, unlike longer mutants in the previous work (γ-ΔC21 or longer)[52], rotation could not be found when 0.49-μm beads were attached instead of the 0.29-μm beads. Wild type also shows load-dependent stumbling at ~80° ahead of ATP-waiting angles[28]: with a high load such as a duplex of 0.95-μm beads, we often observe momentary pause at this angle, but pauses are less conspicuous with smaller beads. At this angle, ATP is split into ADP and phosphate[53] and one of the hydrolysis products is released, each taking ~1 ms under negligible load[16]. Presumably, thermal barrier against one or both of these reactions is effectively heightened by friction between beads and glass surface (or between beads and F_1), leading to a longer dwell. In the mutants, the barrier may be higher due to inefficient coupling between γ rotation and chemical reactions and/or fluctuation (inclination) of short γ increases the chance of surface interaction, resulting in an effectively higher barrier (note the larger bead fluctuations in the mutants, compared to wild, in Fig. 4.18 and 4.19).

During the stepping motion, the short mutants rotated at half the speed of wild type (Fig. 4.19**a**). To eliminate thermal fluctuations from step records, 30 consecutive steps were averaged to obtain thick cyan curves in the figure. Assuming, as with wild type, that the stepping speed is determined by the balance between the torque of the motor and viscous friction, the torque was calculated as

the slope of the cyan curve (instantaneous rotary speed) times the frictional drag coefficient of the bead duplex. Wild type rotated at a constant speed, implying an angle-independent torque of ~40 pN·nm as previously reported[3]. Torque of the mutants estimated in the central 30°-90° portion of the average curve was ~20 pN·nm (Fig. 4.19**b**), half the torque of wild type.

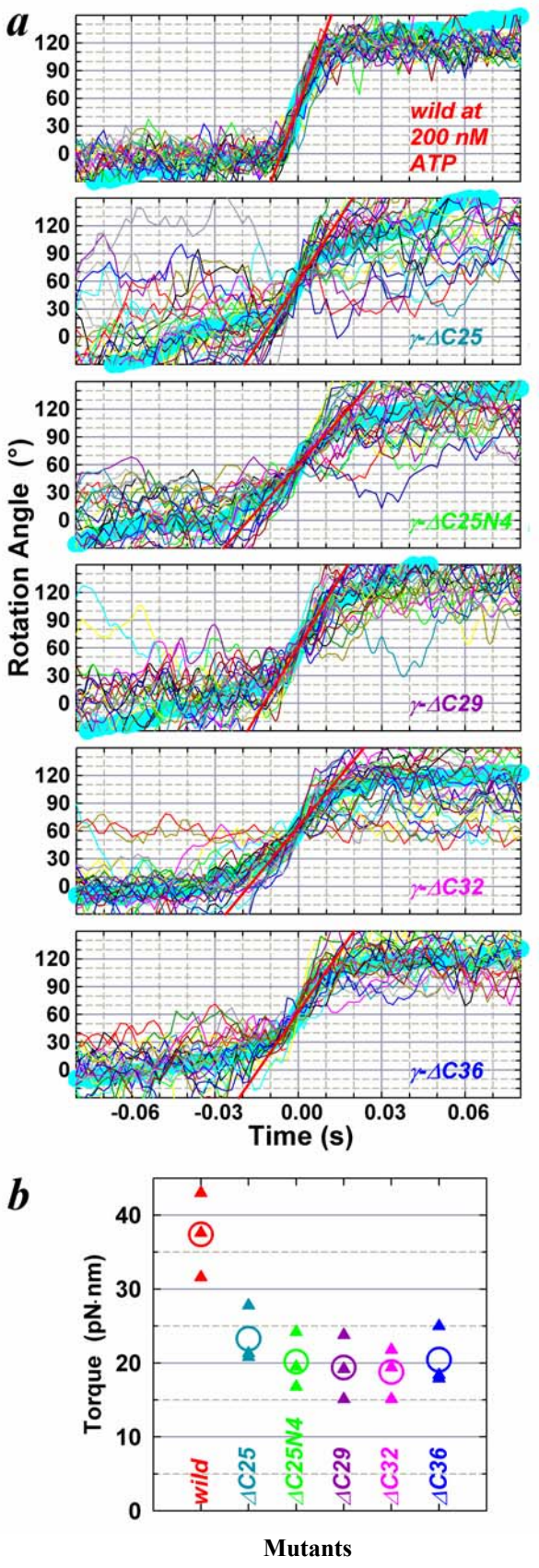

Figure 4.19 Stepping records for torque estimation. (**a**) Thin coloured lines show 30 consecutive steps, thick cyan line being the average. Individual step records have been shifted vertically by a multiple of 120° to obtain the overlap. Time zero for each step record was assigned by eye to the data point closest to 60°. Straight red lines indicate linear fit to the cyan line between 30° and 90°. (**b**) Torque values in three molecules that gave a high torque (triangles) and their means (circles). Torque was calculated as the rotary speed (radian s^{-1}) between 30° and 90° (slope of the red line) times the frictional drag coefficient ξ given by $\xi = 2\times 8\pi\eta a^3 + 6\pi\eta a x_1^2 + 6\pi\eta a x_2^2$ where a is the bead radius (0.145 μm), η the viscosity (~0.93×10^{-3} $N\cdot s\cdot m^{-2}$ at 23°C), and x_1 and x_2 the radii of rotation of inner and outer beads. For clear observation of rotation, we selected those duplexes with $x_2 > 0.2$ μm; x_1 was taken as 0.

Angle dependence could not be determined in the mutants because the steps were too noisy. The apparent sluggishness outside the 30°-90° region likely resulted from simple averaging of noisy and ill-synchronized steps. It is clear, however, that the pivot-less mutants produce half the normal torque at least over half the step angle of 120°.

4.3.2 ATP Hydrolysis Activity

The rate of ATP hydrolysis measured under bulk, unloaded conditions supported the above view. Precise estimation of hydrolysis rate was impossible because mutant γ tended to dissociate from the sub-complex and for this reason, it could not be gone through the time-consuming procedure of removing completely the tightly-bound inhibitory nucleotide[3,4]. Without correcting for these effects, and thus as lower bounds, hydrolysis rates obtained as: ~22 s^{-1} (γ-ΔC25), ~16 s^{-1} (γ-ΔC29), ~20 s^{-1} (γ-ΔCN4C25), ~8 s^{-1} (γ-ΔC32), and ~8 s^{-1} (γ-ΔC36) at 2 mM ATP, which was confirmed to be saturating (same rate at 6 mM ATP). These values are higher than three times the average rotary speeds (expected for the consumption of three ATP molecules per revolution), consistent with the interpretation that infrequent stepping of the mutants is due to a surface effect(s). Hydrolysis activity was measured from initial 20 s of the time courses.

4.3.3 Discussion

Rotation would be clumsy and inefficient without a static axial support and leverage, as in a human attempt to rotate a pen between tips of three fingers. Axial support is a must when force is applied only on one point, as in the proton-driven F_o motor of the ATP synthase which has only one torque-generating unit sitting on the periphery of a cylinder-shaped rotor; indeed the rotor is supported by the F_1 part[4]. In bacterial flagellar motors, too, one force-generating unit at the periphery suffices to produce torque[54], thanks to multiple bearings that hold the rotor. In the truncated F_1 motor here, independent axial support is missing, yet the generated torque is sizable. Much of the torque must be produced by the orifice alone that snugly encloses the γ coiled coil (Fig. 4.17**b**); the shallow orifice works both as a

dynamic support and force generator simultaneously. Through yet unresolved dextrous actions, tips of the three β subunits would rotate the thin rod (radius of γ ~1 nm or less) with an effective linear force as much as ~20 pN or more while preventing backward motion to warrant unidirectional rotation.

4.4 Wild Type and Mutants C

4.4.1 Rotation and ATP Hydrolysis Activity

In the previous section (4.3) it has been shown that mutant group B in which the carboxy-terminus of the γ subunit was truncated just below the orifice, leaving a short, single amino-terminal helix swing freely in the stator cavity. The rotor still rotated in the correct direction with half the normal torque, suggesting that torque may be generated entirely in the orifice. Here mutant group **C** will be discussed in which the shorter γ subunits, the shortest two being almost outside the stator cavity (Fig. 4.20 **F**), are expressed at levels similar to that of wild type and that we can obtain assembled subcomplexes containing a mutated γ, albeit at lower yields for short mutants (Fig. 4.21). Mutant proteins, kept at room temperature, were used immediately, within at most three days.

Rotation of mutants was observed by attaching the β subunits to a glass surface through the histidine residues at the amino-terminus and putting, as a marker, a 40-nm gold bead(s) to the two cysteines on the γ subunit. All, up to γ-ΔN22C43 (Fig. 4.20, **E** and **F**), could rotate the bead in the correct, counterclockwise (viewed from above in Fig. 4.20) direction for >100 revolutions (Fig. 4.22**A**). The probability of finding a rotating bead was low for short mutants: from wild type up to γ-ΔN7C29, on average, a few or more rotating beads per field of view (7.1×7.1 μm^2) were observed when 5-10 nM F_1 was infused in the observation chamber at 2 mM ATP; about 0.5 per view for 10-20 nM γ-ΔN11C32, >10 per chamber (~6×18 mm^2) for 40 nM γ-ΔN14C36, 1-2 per chamber for 40-100 nM γ-ΔN18C40 or 100 nM γ-ΔN22C43. For the last two mutants, surface bead density was already very low, suggesting that most F_1 molecules lacked γ, as evidenced by the faint γ bands

in Fig. 4.21. The beads that rotated relatively smoothly without a serious sign of surface obstruction gave time-averaged rotary speeds which were basically consistent with the rate of ATP hydrolysis measured at 2 mM ATP (Fig. 4.23**D**). The hydrolysis rate leveled off at the value of γ-less mutant $\alpha_3\beta_3$, which shows hydrolysis activity uncoupled to γ rotation[55]. The hydrolysis rate was estimated from the initial 20 s of the time courses (Fig. 4.24)

Time-averaged rate of rotation as well as the rate of ATP hydrolysis was low in the truncated mutants (Fig. 4.23**D**), indicating that the interactions between γ tip and the lower stator support is important for the progress of catalysis. The relatively flat portion in Fig. 4.23**D** between γ-ΔC21 and γ-ΔN7C29 where the tip would be unable to make strong contacts with the lower support indicates similar rotational and hydrolytic properties for these mutants. From γ-ΔN11C32 for which the tip would be completely in the middle of the cavity, we began to observe irregular movements as described below. Elsewhere we have shown that reverse rotation of F_1 by an external force leads to reversal of chemical reactions in the catalytic sites, leading to net ATP synthesis[30]. The reversal by manipulation of γ angle alone implies a γ-dictator mechanism where the γ angle controls which chemical reaction is to take place in the three catalytic sites, ATP binding, hydrolysis, and product releases[3,56]. Leverage by a short γ, without firm pivoting at the bottom, will be inefficient in driving β (and α) subunits over an activation barrier into the conformation appropriate for the next chemical reaction.

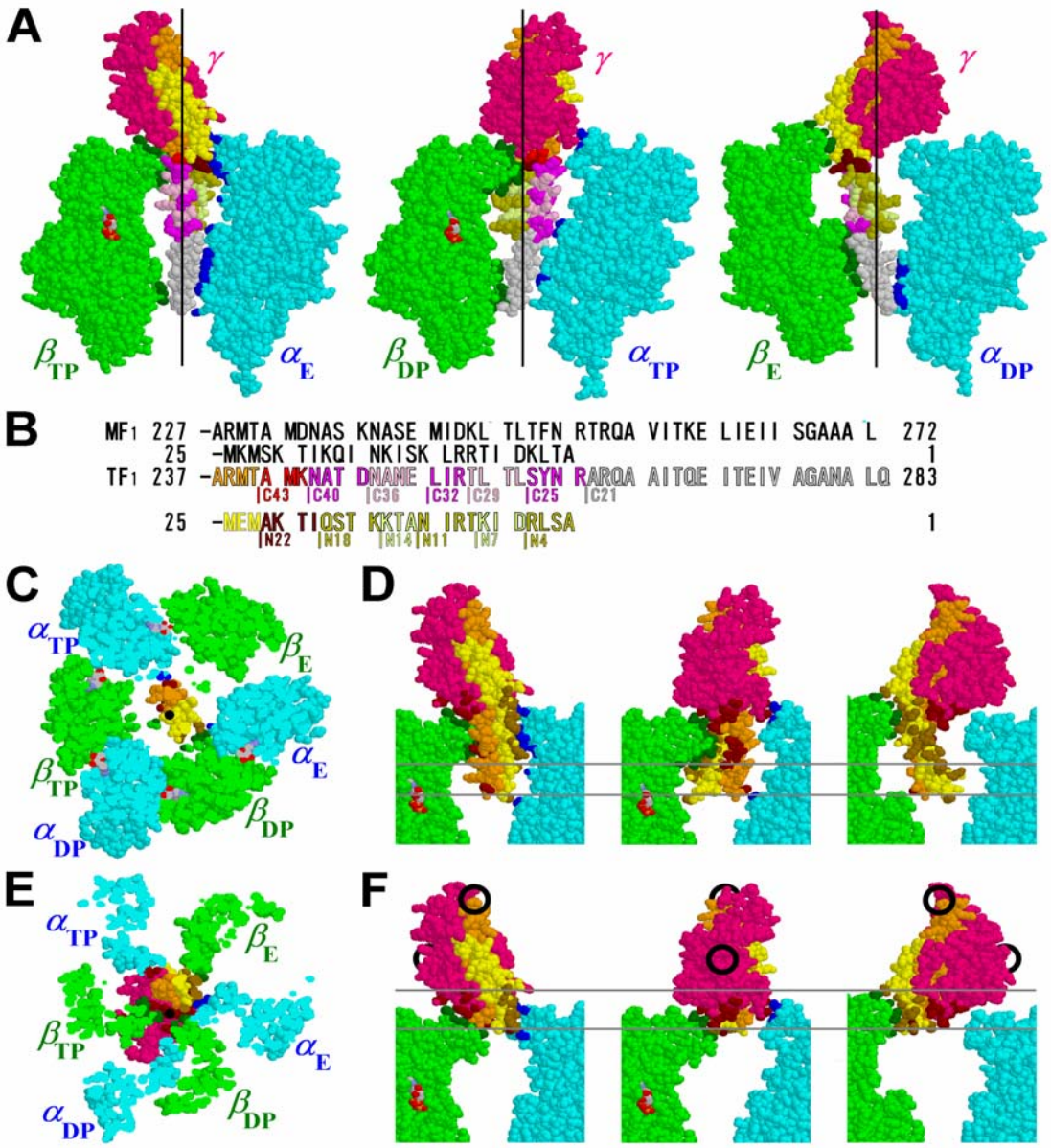

Figure 4.20 An atomic structure[35] of MF_1. (**A**) Side views showing the central γ and an opposing α-β pair. The membrane-embedded F_o portion of ATP synthase would be above the γ subunit. Truncations of the γ subunit are shown with the color scheme in **B**; the N- and C-terminal α-helices are in yellow and orange, respectively. Those atoms of α and β subunits that are within 0.5 nm from an atom of γ (excluding hydrogens) are colored blue and dark green, respectively. Nucleotides are shown in CPK colors. Black lines (and black dots in **C** and **E**) represent a putative rotation axis[10]. (**B**) Amino-acid sequences at the carboxyl- and amino-termini of γ in MF_1[51] and TF_1 ([41], except that numbering in B starts from Met-1, which is absent in the expressed wild-type protein). (**C**) to (**F**) Structures of γ-ΔN4C25 (**C** and **D**) and γ-ΔN22C43 (**E** and **F**). For γ-ΔN4C25, γ-Met-4 is represented by γ-Lys-4, excluding the ε-amino group to mimic Met. For γ-ΔN22C43, γ-Met-22 is represented by γ-Ser-22. **C** and **E** are bottom views of the section between the gray lines in **D** and **F**. Atoms of γ that are within 0.5 nm from an atom of α or β are shown in gold and brown (none on the C-terminal helix of γ-ΔN22C43). Black circles in **F** show approximate locations of biotinylated cysteines.

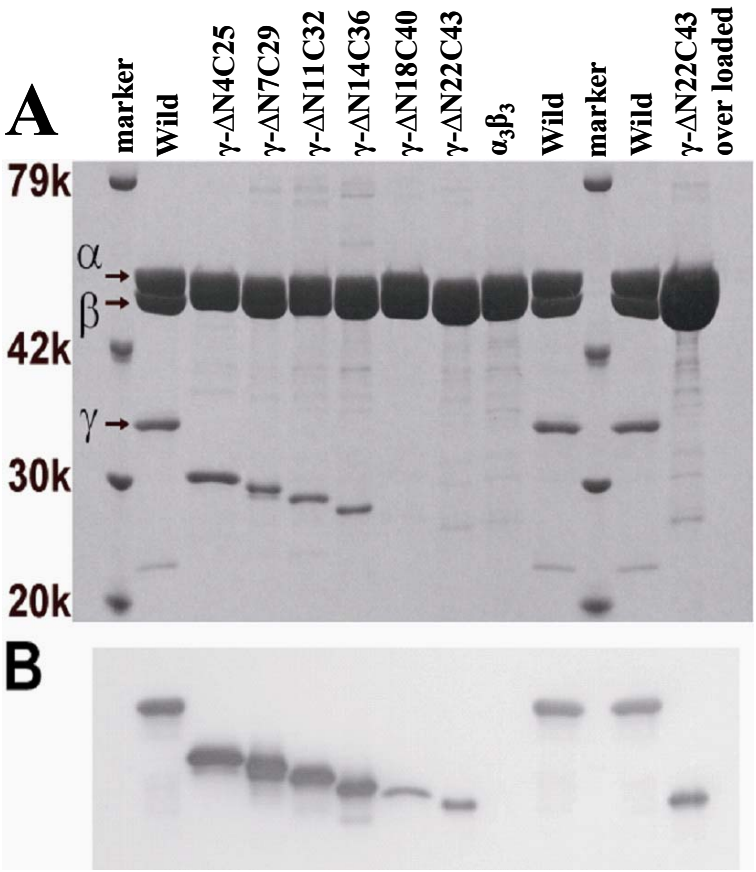

Figure 4.21. Confirmation of γ truncations by polyacrylamide gel electrophoresis. (**A**) 12.5 % gel containing 0.1 % SDS, stained with Coomassie Brilliant Blue R-250. (**B**) Western blot of **A** stained with an anti-γ antibody.

At a sufficiently high camera speed, all rotations appeared stepwise even at 2 mM ATP (Fig. 4.22, **C** and **D**). For wild type, dwells at this saturating ATP concentration are at 80-90° past an ATP-waiting angle, where ATP hydrolysis and phosphate release occur taking ~1 ms each at room temperature[16, 56, 53]. The steps of mutants were more noisy, indicating larger fluctuation of short γ, and thus dwelling angles were not very clear. Also, some mutants showed two or more dwelling angles per 120°. The horizontal lines in Fig. 4.22 **C** and **D** show the angles of the most populated dwells in each mutant.

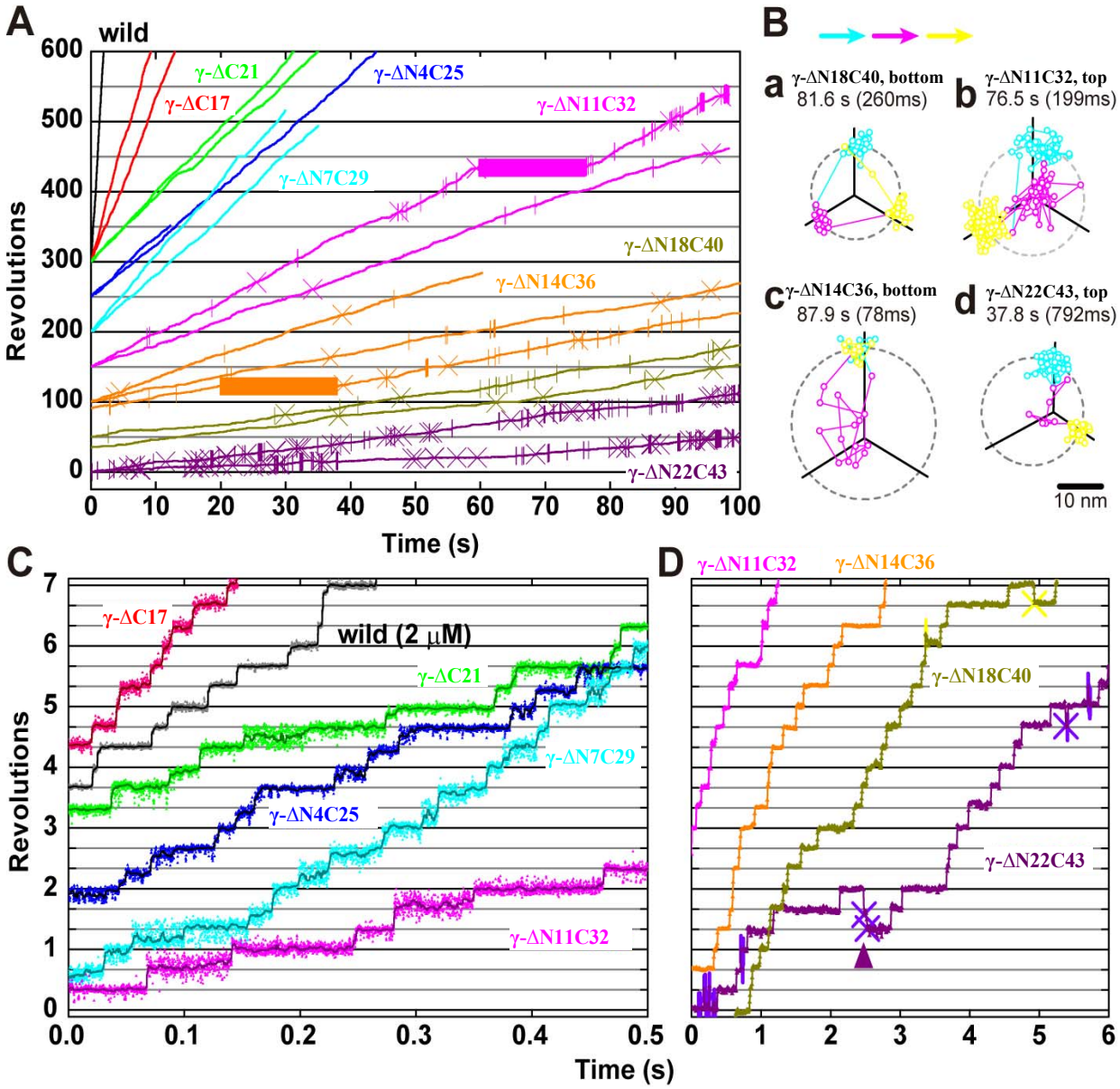

Figure 4.22. Rotation of 40-nm gold beads attached to the γ subunit. Counterclockwise rotations, viewed from above in Fig. 4.20**A**, are plotted as positive revolutions. ATP concentration was 2 mM except for the wild type in **C**. (**A**) Overall time courses for beads that rotated relatively fast. Vertical bars and two horizontal rectangles indicate the period during which irregular motions described in **B** continued. Crosses indicate occurrence of a ~120° backward step, whether rotational or via irregular motion (**B**-**d**). (**B**) Traces of typical irregular motions where the bead tended to dwell near the rotation center. **a**, regular 120° steps; **b**, center then forward; **c**, center and turning back; **d**, center then backward. (**C**) Stepping kinetics observed at 8,000 frames s^{-1}. Thin black lines, after 15-point median filtering. Most-populated angles for each mutant (judged over the entire time courses) are on the horizontal lines separated by 120°; for the wild type at 2 μM ATP, these are ATP-waiting angles. (**D**) Stepping kinetics of the shortest four mutants at 125 frames s^{-1} (records taken at higher speeds have been averaged in 8-ms bins). Vertical bars show moments of irregular motions. Crosses, backward steps; arrow head, succession of two backward steps, a very rare event.

The dwells imply the presence of an activation barrier(s) against a reaction that is to take place at that angle. So far, we have been unable to assign unambiguously the dwelling angles of the mutants and the slow reaction(s) responsible for the dwells.

In addition to the apparently thermal fluctuations, short mutants exhibited moments of irregular behaviors where the bead moved toward and stayed near the rotation axis for tens of milliseconds before going back to the rotary track mostly onto the position 120° ahead (Fig. 4.22**B-b**), occasionally onto the previous position (Fig. 4.22**B-c**), and rarely but significantly onto the position 120° backward (Fig. 4.22**B-d**). Such behaviors tended to be repetitive, but the total time was mostly short and within the width of the vertical bars in Fig. 4.22**A**. Exceptionally long repetitions were also observed (Fig. 4.22**A**, two long horizontal rectangles). The bead position near the rotation axis suggests an F_1 conformation(s) quite different from the one in Fig. 4.20. If the two cysteines on γ (near the black circles in Fig. 4.20**F**) bound the bead, central bead location would require the γ head to become upright, by counterclockwise inclination in Fig. 4.20**F**, right. The tip of γ shaft would then move toward α_{DP}, a movement allowed for a short γ. Or the coiled-coil portion of a short γ may occasionally melts. To be upright, the γ head must reposition itself in the concave orifice, breaking all γ-stator interactions seen in the crystal. The F_1 would be in an un-clutched state. This scenario based on the wild-type MF_1 structure may not be valid, but some major reorganization must underlie the central bead location.

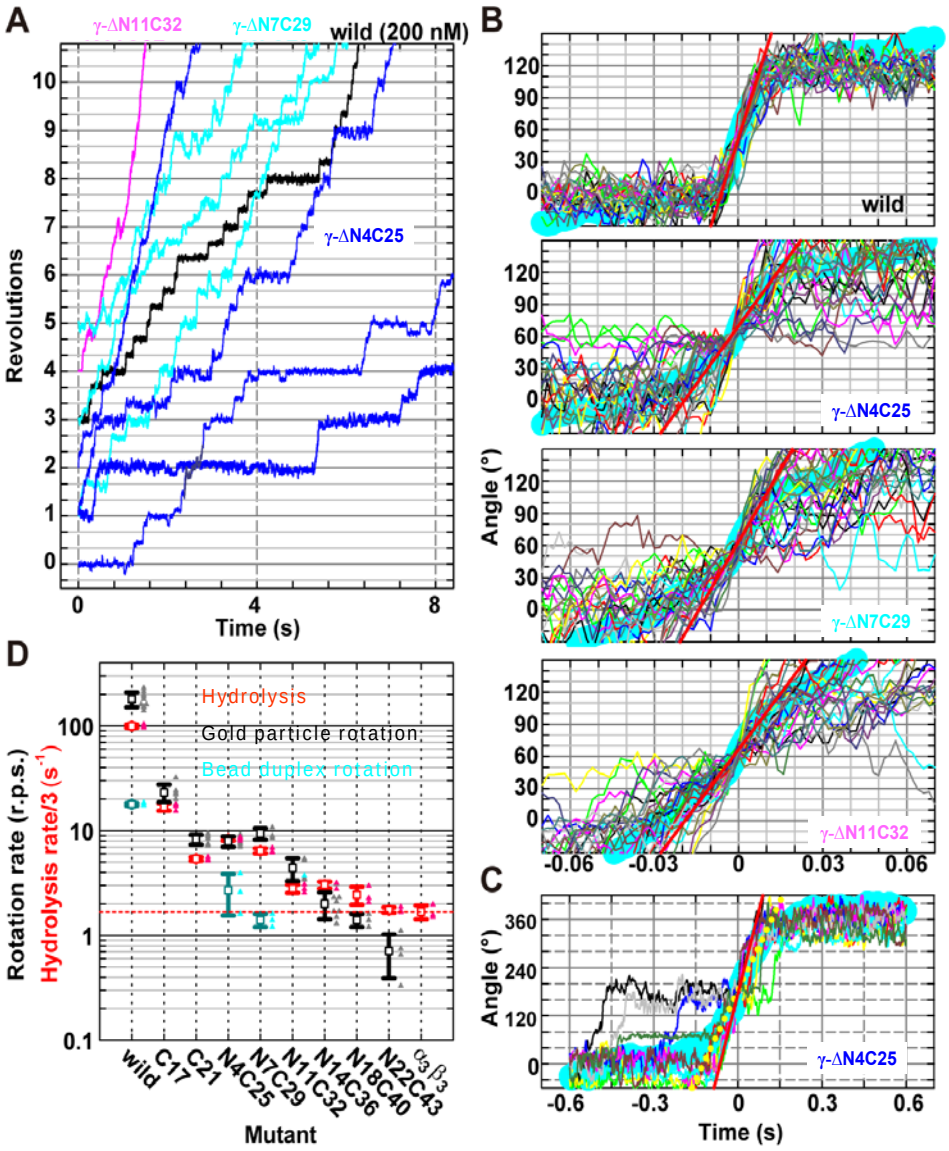

Figure 4.23 Rotation time courses for 0.29-μm bead duplexes at 500 frames s^{-1}. ATP concentration was 2 mM (200 nM for the wild type). (**A**) Overall time courses showing relatively fast rotation or clearer stepping. (**B**) Details of step kinetics. Thin colored lines show 30 consecutive steps, thick cyan lines being the average. Individual step records have been shifted vertically by a multiple of 120° to obtain the overlap. Time zero for each step record was assigned by eye to the data point closest to 60°. Straight red lines fit the cyan line between 30° and 90°. (**C**) Triplets of 120°-steps. Colored thin lines show 10 consecutive triplets in **A**, γ-ΔN4C25, bottom right. Thick cyan line, average; red line, fit between 150° and 210°; yellow dotted line, fit between 60° and 300°. (**D**) Summary of rotation and hydrolysis rates at 2 mM ATP. Black symbols show mean±SD for time-averaged rotation rates of 40-nm gold beads that rotated relatively fast; rates of individual beads over >50 (mostly >100) consecutive revolutions are shown in gray triangles. Dark cyan, mean ± SD for rotation rates of 0.29-μm bead duplexes that rotated relatively fast; cyan, individual rates over 10 revolutions. Red, mean ± SD for the rate of ATP hydrolysis; three determinations in magenta; red dashed line, mean hydrolysis rate of $\alpha_3\beta_3$. Temperature, 23°C.

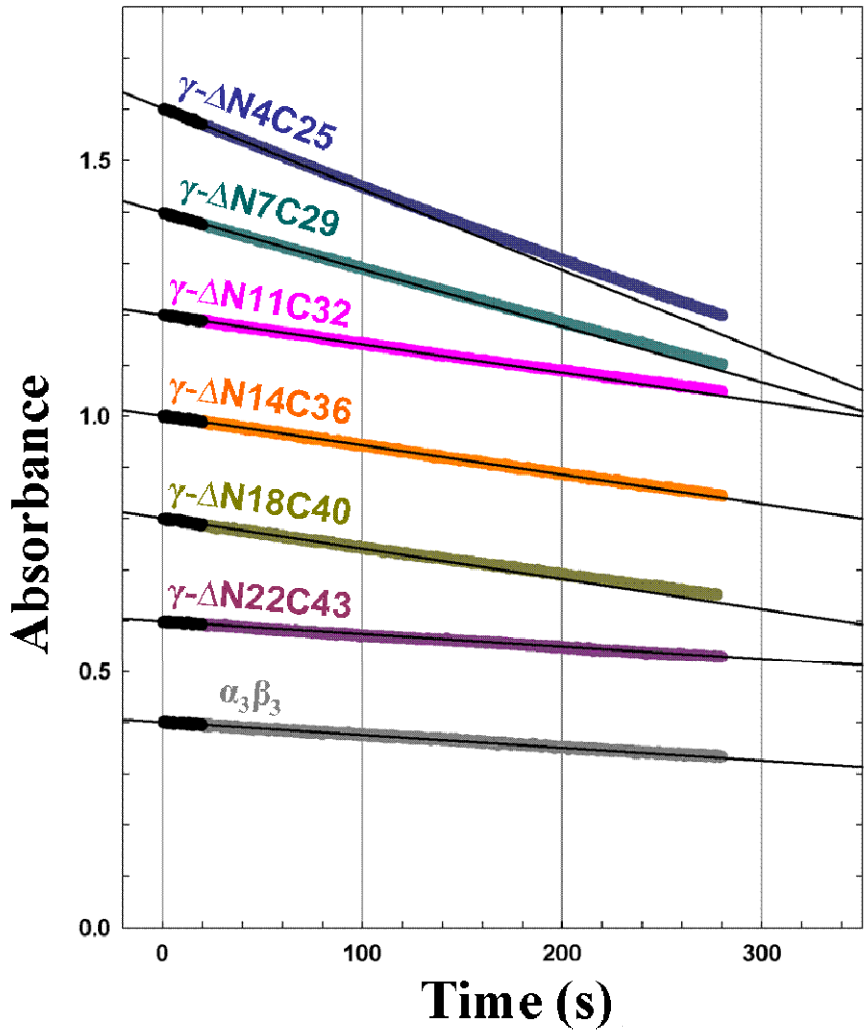

Figure 4.24 Time courses of ATP hydrolysis at 2 mM ATP by 10 nM mutant F_1. A decrease in absorbance by 0.622 corresponds to consumption of 100 μM ATP. Hydrolysis rates were estimated in the initial 20-s portion (black), as shown by the thin black lines. Temperature, 23°C.

The shortest mutant γ-ΔN22C43 exhibited frequent irregular motions and also backward steps (Fig. 4.22**A**). It still rotated mainly in the correct direction, which must be driven by an effective positive torque. For the upper and lower curves in Fig. 4.22**A**, there were 65 and 44 moments of irregular motion in 100 s, respectively, with the total durations of 2.7 s and 2.4 s; there were 368 and 259 forward 120°-steps, compared to 32 and 37 backward steps. The second shortest γ (γ-ΔN18C40), which is also nearly outside the stator cavity, rotated much more steadily.

The effective torque of the mutants was tried to estimate by attaching a larger bead for which the viscous friction is high. Previously we showed[52] that γ-ΔC21 could rotate a duplex of 0.49 μm polystyrene beads with an apparent torque of ~20 pN·nm, about half the torque of wild type; the mutant was unable to rotate a 0.9-μm bead duplex. Here, for γ-ΔN4C25 and shorter mutants, we did not find a 0.49-μm duplex to rotate. With 0.29-μm duplexes, we observed 5-6 rotating duplexes per chamber when 10 nM γ-ΔN4C25 was infused, and 2-3 duplexes per chamber for 10 nM γ-ΔN7C29 (Fig. 4.23**A**). We could record one rotation at 20 nM of fresh γ-ΔN11C32, but further trials even at 100 nM failed. Immediately after infusion, we could find several bead duplexes on γ-ΔN11C32 to rotate, but they were detached from surface in seconds. This was also the case for γ-ΔN7C29, for which many duplexes rotated initially but were detached within a few minutes. The 0.29-μm bead, compared to the 40-nm gold bead, likely bumps the glass (or F_1) surface and is blown away. Also, when the bead is stuck against a surface in one of the dwelling angles where the activation barrier is high for short mutants, the bead may stop there.

The instantaneous rotary speeds of the 0.29-μm bead duplexes during 120° steps (although steps were not always clear) were estimated by averaging 30 consecutive steps (thick cyan curves in Fig. 4.23**B**). Assuming, as with wild type[3,7,28] that the instantaneous stepping speed is determined by the balance between the torque of the motor and viscous friction, we calculated the torque as the slope of the cyan curve times the frictional drag coefficient (0.28-0.34 pN·nm·s for the duplexes examined). Wild type rotated at a constant speed, implying an angle-independent torque of 44±4 pN·nm (mean ± SD, n = 3) as previously reported[3,28]. Torque of the mutants estimated in the central 30°-90° portion of the cyan curve was 23±3 pN·nm for γ-ΔN4C25 (n = 3), 22±2 pN·nm for γ-ΔN7C29 (n = 3), and 18 pN·nm for γ-ΔN11C32 (n = 1). Because the mutants undergo extensive thermal fluctuations, one could object that the 120° excursions in Fig. 4.23**B** may represent occasional large-amplitude fluctuations that are not directly related to the torque of the motor (a diffusion-and-catch mechanism of rotation).

Diffusion and catch, however, also produce an effective torque if they recur in the same direction. In some duplexes, we observed three 120° steps to occur always in succession (Fig. 4.23**A**, bottom right), presumably because the F_1 was obliquely attached to the surface and thus the bead duplex was completely free from the surface except for one angle. From the average rotary speed during the 360° excursions (Fig. 4.23**C**), which cannot be entirely thermal, we obtained a torque of 8.3 pN·nm, which is an underestimate because several of the curves were stuck at the middle. Also, most duplexes in Fig. 4.23A rotated with a time averaged speed exceeding 1 revolution s^{-1} (~6 radian s^{-1}), implying a minimum effective torque of 2 pN·nm. Thus, mutants, of which the γ tip would not touch the bottom support, produce a significant torque. Torque of the shorter mutants could not be estimated, but the unidirectional character of the rotation implies production of an effective torque in the correct direction.

4.4.2 Discussion

Most of man-made rotary machines rely on a rigid axle held by a static bearing(s): thanks to the constraint by the bearing, almost any force acting on the axle is converted to a torque through a lever action. This design principle is simple both conceptually and technically. Rotating a screw with a screw driver is easy when one pushes the driver against the screw, letting the screw head serve as a bearing. Nature seems to have adopted this principle for the bacterial flagellar motor[54] and the proton-driven F_o motor of the ATP synthase[4]: their rotor axis is held stationary by stator bearings, and thus force from one driving unit, acting on only one point on the rotor, suffices to produce torque. Thus, when Walker and colleagues revealed the atomic structure of F_1[9] in which the C-terminal helix of γ is held by the hydrophobic sleeve (Fig. 4.20), many researchers agreed that F_1 would rotate. Our previous mutant γ-ΔC21, slightly longer than γ-ΔN4C25 in Fig. 4.20 **D**, lacked snug fit with the sleeve, but alternating point contacts with the cavity wall could still help pivoting action. For the shortest mutants γ-ΔN18C40 and γ-ΔN22C43 here, however, the concepts of static bearings and lever action through a rigid axle no longer apply. Had it been Fig. 4.20 **F** that Walker group

revealed, no one would have predicted rotation. Yet the shortest mutants rotate in fact.

Rotating the shortest γ is not at all an easy job, like rotating an unsupported pen between three (six) fingers, suspending the pen vertically at the very top. The six upper tips of the α and β subunits must play three roles in a highly concerted fashion: moving the rotor in the correct direction, serving as a fulcrum to convert the motion into torque, and, most important, keeping the truncated rotor from escaping. All these require contacts between the rotor and tips, but static contacts do not allow full rotation. The grip must be dynamic, yet continuous: a failure for a moment will allow Brownian motion to carry the rotor away. A possible hint at torque production mechanism is the twist of γ seen in some crystal structures[57], implicating torque generation in the upper half of the stator cylinder while the bottom holds the γ tip, but the rotary angle between different crystals is at most ~30°, compared to the basic step angle of 120°. The rest might be covered by Brownian rotation. Biased diffusion may indeed be the driving mechanism for the short γ, as in the single-head linear motor KIF1A[58] that cannot rely on alternating firm grips allowed for two-head motors. Unlike KIF1A which undergoes broad-range diffusion, however, diffusion of the truncated γ is largely within 120° and most 120° steps are made in the forward direction (~90 % in γ-ΔN22C43 and >99 % in γ-ΔN18C40). The orifice somehow blocks backward diffusion, ensuring generation of an effective torque. Dexterous operation of the six orifice tips, yet to be clarified, must provide a new paradigm for the make of molecular machines.

CHAPTER 5
CONCLUSIONS

CHAPTER 5
CONCLUSIONS

The experiments done in this thesis revolutionize current understandings of the mechanism of rotation of F_1, demanding an entirely new direction particularly on the role of the γ-subunit. Existing models of rotation such as the push-pull mechanism must be abandoned. In this mechanism, the tip of γ-subunit held in the bottom of the stator cylinder essentially acts as a pivot for the conical rotation. However, all truncation mutants constructed in this work rotated in the correct direction, though the average rotary speeds were low compared to wild type and some mutants exhibited moments of irregular motion. This implies that neither a pivot nor an axle is needed for rotation of F_1. Rotation may be like rotating an unsupported pen between three (six) fingers, holding the pen at a very end in the case of the shortest mutants (as mentioned in the section 4.4.2 of chapter 4).

In the structure of MF_1, the tip of the carboxy-terminus of the γ-subunit held by the bottom of the stator cylinder was suggested to play important roles in rotation of γ-subunit. Here most of the interaction between rotor and stator for the shortest rotary mutants is absent. The rotary characteristics of the group **A** mutants did not differ greatly from those of the wild-type over the ATP concentrations of 20 nM-2mM, the most conspicuous effect being 50 % reduction in torque and 70 % reduction in the rate of ATP binding. The ATP hydrolysis activity estimated in bulk samples was up to 10-fold lower compared to the wild type. Group **B** mutants and several of group **C** mutants produced ~50 % of wild type torque but the hydrolysis activity was reduced to ~3 % in some mutants. The time-averaged rate of rotation as well as the rate of ATP hydrolysis were low in the mutants, indicating that the interactions between tip and the bottom stator support is important for the rapid progress of catalysis. A mutant in group **C** lacking most of the rotor shaft and with the remaining rotor portion merely sitting on the concave entrance of the stator cylinder still rotates in the correct direction for >100 turns implying effective torque generation. This suggests that most of the interactions

between the rotor and the stator cylinder, hitherto considered important, are not essential for rotation.

What we have done in this work is to destroy the wild-type F_1 motor that apparently relies on the simple concept of a rigid axle and static bearings. There is no reason to expect the broken motor to rotate. Why did Nature care to implement such an exceeding robustness in the rotary mechanism of F_1? A probable answer is that she first invented a less efficient, possibly clumsy device and then proceeded to sophistication. If so, ring-shaped AAA+ ATPases may all, in principle, be capable of producing torque, as suggested for helicases[59]. The spiral staircase encircling a strand of DNA in a recently solved helicase structure[60] may represent another sophistication. Swing of the dynein stalk[61] might also rely on a rotary mechanism.

REFERENCES

REFERENCES

1. Boyer, P. D. 1993. The binding change mechanism for ATP synthase—some probabilities and possibilities. *Biochim. Biophys. Acta*. **1140**:215-250.

2. Kinosita, K. Jr., R. Yasuda, H. Noji and K. Adachi. 2000. A rotary molecular motor that can work at near 100 % efficiency. *Philos. Trans. R. Soc. Lond. B. Biol. Sci.* **355**:473-489.

3. Kinosita, K. Jr., K. Adachi and H. Itoh. 2004. Rotation of F_1-ATPase: how an ATP-driven molecular machine may work. *Annu. Rev. Biophys. Biomol. Struct.* **33**:245-268.

4. Yoshida, M., E. Muneyuki and T. Hisabori. 2001. ATP synthase—a marvellous rotary engine of the cell. *Nat. Rev. Mol. Cell Biol.* **2**:669-677.

5. Boyer, P. D. and W. E. Kohlbrenner. 1981. The present status of the binding-change mechanism and its relation to ATP formation by chloroplasts. *In* Energy Coupling in Photosynthesis. B. R. Selman and S. Selman-Reimer, editors. Elsevier, Amsterdam. 231-240.

6. Oosawa, F. and S. Hayashi. 1986. The loose coupling mechanism in molecular machines of living cells. *Adv. Biophys.* **22**:151-183.

7. Noji, H., R. Yasuda, M. Yoshida and K. Kinosita Jr. 1997. Direct observation of the rotation of F_1-ATPase. *Nature.* **386**:299-302.

8. Kinosita Jr, K., R. Yasuda, H. Noji, S. Ishiwata, and M. Yoshida. 1998. F_1-ATPase: a rotary motor made of a single molecule. *Cell* **93:**21-24.

9. Abrahams, J. P., A. G. W. Leslie, R. Lutter and J. E. Walker. 1994. Structure at 2.8 Å resolution of F_1 -ATPase from bovine heart mitochondria. *Nature.* **370**:621-628.

10. Wang, H. and G. Oster. 1998. Energy transduction in the F_1 motor of ATP synthase. *Nature*. **396:**279-282.

11. Shirakihara, Y., A. G. W. Leslie, J. P. Abrahams, J. E. Walker, T. Ueda, Y. Sekimoto, M. Kambara, K. Saika, Y. Kagawa and M. Yoshida. 1997. The crystal structure of the nucleotide-free $\alpha_3\beta_3$ subcomplex of F_1-ATPase from the thermophilic *Bacillus* PS3 is a symmetric trimer. *Structure*. **5**:825-836.

12. Kaibara C., T. Matsui, T. Hisabori and M. Yoshida. 1996. Structural asymmetry of F_1-ATPase caused by the γ subunit generates a high affinity nucleotide binding site. *J. Biol. Chem.* **271:**2433-2438.

13. Yasuda, R., H. Noji, K. Kinosita Jr and M. Yoshida. 1998. F_1-ATPase is a highly efficient molecular motor that rotates with discrete 120° steps. *Cell*. **93**:1117-1124.

14. Adachi, K., R. Yasuda, H. Noji, H. Itoh, Y. Harada, M. Yoshida and K. Kinosita Jr. 2000. Stepping rotation of F_1-ATPase visualized through angle-resolved single-fluorophore imaging. *Proc. Natl. Acad. Sci. USA*. **97**:7243-7247.

15. Nishizaka, T., K. Oiwa, H. Noji, S. Kimura, E. Muneyuki, M. Yoshida and K. Kinosita Jr. 2004. Chemomechanical coupling in F_1-ATPase revealed by simultaneous observation of nucleotide kinetics and rotation. *Nat. Struct. Mol. Biol.* **11**:142-148.

16. Yasuda, R., H. Noji, M. Yoshida, K. Kinosita Jr and H. Itoh. 2001. Resolution of distinct rotational substeps by submillisecond kinetic analysis of F_1-ATPase. *Nature*. **410**:898-904.

17. Hara, K. Y., H. Noji, D. Bald, R. Yasuda, K. Kinosita Jr and M.Yoshida. 2000. The role of the DELSEED motif of the β subunit in rotation of F_1-ATPase. *J. Biol. Chem.* **275**:14260-14263.

18. Iwamoto, A., J. Miki, M. Maeda and M. Futai. 1990. H^+-ATPase γ subunit of *Escherichia coli*: role of the conserved carboxyl-terminal region. *J. Biol. Chem.* **265**: 5043-5048.

19. Sokolov, M., L. Lu, W. Tucker, F. Gao, P. A. Gegenheimer and M. L. Richter. 1999. The 20 C-terminal amino acid residues of the chloroplast ATP synthase γ subunit are not essential for activity. *J. Biol. Chem.* **274**:13824-13829.

20. Müller, M., O. Pänke, W. Junge and S. Engelbrecht. 2002. F_1-ATPase, the C-terminal end of subunit γ is not required for ATP hydrolysis-driven rotation. *J. Biol. Chem.* **277**:23308-23313.

21. Berg, J.M., L. Stryer and J.M. Tymoczko. Biochemistry. 2002. W.H. Freeman and Company, New York, 5th edition: p-204.

22. Matsui, T. and M. Yoshida. 1995. Expression of the wild-type and the Cys-/Trp-less a $\alpha_3\beta_3\gamma$ complex of thermophilic F_1-ATPase in *Escherichia coli*. *Biochim. Biophys. Acta.* **1231**:139-146.

23. Monticello, R. A., E. Angov and W. S. A. Brusilow. 1992. Effects of inducing expression of cloned genes for the F_o proton channel of the *Escherichia coli* F_1F_o ATPase. *J. Bacteriol.* **174**:3370-3376.

24. Yanisch-Perron, C., J. Vieira and J. Messing. 1985. Improved M13 phage cloning vectors and host strains: nucleotide sequences of the M13mp18 and pUC19 vectors. *Gene*. **33**:103-119.

25. Tartof, K. D. and C. A. Hobbs. 1987. Improved media for growing plasmid and cosmid clones. *Bethesda Res. Lab. Focus.* **9**:12-12.

26. Adachi, K., H. Noji and K. Kinosita Jr. 2003. Single molecule imaging of the rotation of F_1-ATPase. *Methods Enzymol*. **361B**:211-227.

27. Noji, H., D. Bald, R. Yasuda, H. Itoh, M. Yoshida and K. Kinosita Jr. 2001. Purine but not pyrimidine nucleotides support rotation of F_1-ATPase. *J. Biol. Chem.* **276**:25480-25486.

28. Sakaki, N., R. Shimo-Kon, K. Adachi, H. Itoh, S. Furuike, E. Muneyuki, M. Yoshida and K. Kinosita Jr. 2005. One rotary mechanism for F_1-ATPase over ATP concentrations from millimolar down to nanomolar. *Biophys. J.* **88**:2047-2056.

29. Matsui, T., E. Muneyuki, M. Honda, W. S. Allison, C. Dou and M. Yoshida. 1997. Catalytic activity of the $\alpha_3\beta_3\gamma$ complex of F_1-ATPase without noncatalytic nucleotide binding site. *J. Biol. Chem.* **272**:8215-8221.

30. Itoh, H., A. Takahashi, K. Adachi, H. Noji, R. Yasuda, M. Yoshida and K. Kinosita Jr. 2004. Mechanically driven ATP synthesis by F_1-ATPase. *Nature*. **427**:465-468.

31. Hirono-Hara, Y., H. Noji, M. Nishiura, E. Muneyuki, K. Y. Hara, R. Yasuda, K. Kinosita Jr and M. Yoshida. 2001. Pause and rotation of F_1-ATPase during catalysis. *Proc. Natl. Acad. Sci. USA.* **98**:13649-13654.

32. Pänke, O., D.A. Cherepanov, K. Gumbiowski, S. Engelbrecht and W. Junge. 2001. Visco-elastic dynamics of actin filaments coupled to rotary F_1-ATPase: angular torque profile of the enzyme. *Biophys. J.* **81**:1220-1233.

33. Kinosita, K. Jr, R. Yasuda and H. Noji. 2000. F_1-ATPase: a highly efficient rotary ATP machine. *Essays Biochem.* **35**:3-18.

34. Jault, J.-M., C. Dou, N. B. Grodsky, T. Matsui, M. Yoshida and W. S. Allison. 1996. The $\alpha_3\beta_3\gamma$ subcomplex of the F_1-ATPase from the thermophilic bacillus PS3 with the βT165S substitution does not entrap inhibitory MgADP in a catalytic site during turnover. *J. Biol. Chem.* **271**:28818-28824.

35. Gibbons, C., M. G. Montgomery, A. G. W. Leslie and J. E. Walker. 2000. The structure of the central stalk in bovine F_1-ATPase at 2.4 Å resolution. *Nat. Struct. Biol.* **7**:1055-1061.

36. Hausrath, A. C., G. Grüber, B. W. Matthews and R. A. Capaldi. 1999. Structural features of the γ subunit of the *Escherichia coli* F_1-ATPase revealed by a 4.4-Å resolution map obtained by x-ray crystallography. *Proc. Natl. Acad. Sci. USA.* **96**:13697-13702.

37. Gumbiowski, K., D. Cherepanov, M. Müller, O. Pänke, P. Promto, S. Winkler, W. Junge and S. Engelbrecht. 2001. F-ATPase: forced full rotation of the rotor despite covalent cross-link with the stator. *J. Biol. Chem.* **276**:42287-42292.

38. Greene, M. D. and W. D. Frasch. 2003. Interactions among γR268, γQ269 and the β subunit catch loop of *Escherichia coli* F_1-ATPase are important for catalytic activity. *J. Biol. Chem.* **278**:51594-51598.

39. Ni, Z.-L., H. Dong and J.-M. Wei. 2005. N-terminal deletion of the γ subunit affects the stabilization and activity of chloroplast ATP synthase. *FEBS J.* **272**:1379-1385.

40. Nakamoto, R. K., K. Shin, A. Iwamoto, H. Omote, M. Maeda and M. Futai. 1992. *Escherichia coli* F_o F_1-ATPase. Residues involved in catalysis and coupling. *Ann. N. Y. Acad. Sci.* **671**:335-344.

41. Ohta, S., M. Yohda, M. Ishizuka, H. Hirata, T. Hamamoto, Y. Otawara-Hamamoto, K. Matsuda and Y. Kagawa. 1988. Sequence and over-expression of subunits of adenosine triphosphate synthase in thermophilic bacterium PS3. *Biochim. Biophys. Acta.***933:**141-155.

42. Milgrom Y.M. and P.D. Boyer. 1990. The ADP that binds tightly to nucleotide-depleted mitochondrial F_1-ATPase and inhibits catalysis is bound at a catalytic site. *Biochim. Biophys. Acta.* **1020:**43-48.

43. Guerrero K.J., Z.X. Xue and P.D. Boyer. 1990. Active/Inactive state transitions of the chloroplast F_1-ATPase are induced by a slow binding and release of Mg^{2+}. Relationship to catalysis and control of F_1-ATPases. *J. Biol. Chem.* **265:**16280-16287.

44. Kato Y., T. Sasayama, E. Muneyuki and M. Yoshida. 1995. Analysis of time-dependent change of *Escherichia coli* F_1-ATPase activity and its relationship with apparent negative cooperativity. *Biochim. Biophys. Acta*. **1231:**275-281.

45. Jault J. M., T. Matsui, F. M. Jault, C. Kaibara, E. Muneyuki, M. Yoshida, Y. Kagawa and W. S. Allison. 1995. The $\alpha_3\beta_3\gamma$ complex of the F_1-ATPase from thermophilic *Bacillus* PS3 containing the αD261N substitution fails to dissociate inhibitory MgADP from a catalytic site when ATP binds to noncatalytic sites, *Biochemistry.* **34:**16412-16418.

46. Lotscher, H-R, C. deJong and R.A, Capaldi. 1984. Interconversion of high and low adenosinetriphosphatase activity forms of *Escherichia coli* F_1 by the detergent lauryldimethylamine oxide. *Biochemistry.* **23:**4140-4143.

47. Paik S.R., J-M. Jault and W.S. Allison. 1994. Inhibition and inactivation of the F_1 adenosinetriphosphatase from *Bacillus* PS3 by dequalinium and activation of the enzyme by lauryl dimethylamine oxide. *Biochemistry.* **33:**126-133.

48. Alison W.S., J-M. Jault, C. Dou and N.B. Grodosky. 1996. Does the γ subunit move to an abortive position for ATP hydrolysis when the F_1.ADP.Mg complex isomerizes to the inactive F_1*.ADP.Mg complex? *J. Bioen. Biomem.*, **28:** 433-436.

49. Shibatani, T. and W. F. Ward. 1995. Sodium dodecyl sulfate (SDS) activation of the 20S proteasome in rat liver. *Arch. Biochem. Biophys.* **321:**160-166.

50. Muga, A., J.L. Arrondo, T. Bellon, J. Sancho and C. Barnabeu. 1993. Structural and functional studies on the interaction of sodium sodium dodecyl sulfate with beta- galactosidase. *Arch. Biochem. Biophys.* **300:**451-457.

51.Walker, J. E., I. M. Fearnley, N. J. Gay, B. W. Gibson, F. D. Northrop, S. J. Powell, M. J. Runswick, M. Saraste and V. L. J. Tybulewicz. 1985. Primary structure and subunit stoichiometry of F_1-ATPase from bovine mitochondria. *J. Mol. Biol.* **184:** 677-701.

52. Hossain, M. D., S. Furuike, Y. Maki, K. Adachi, M. Y. Ali, M. Huq, H. Itoh, M. Yoshida and K. Kinosita Jr. 2006. The rotor tip inside a bearing of a

thermophilic F_1-ATPase is dispensable for torque generation. *Biophys. J.* **90:**4195-4203.

53. Shimabukuro, K., R. Yasuda, E. Muneyuki, K. Y. Hara, K. Kinosita Jr and M. Yoshida. 2003. Catalysis and rotation of F_1 motor: Cleavage of ATP at the catalytic site occurs in 1 ms before 40° substep rotation. *Proc. Natl. Acad. Sci. USA.* **100**: 14731-14736.

54. Berg, H. C. 2003. The rotary motor of bacterial flagella. *Annu. Rev. Biochem.* **72:** 19-54.

55. K. Miwa, M. Yoshida, 1989. The $\alpha_3\beta_3$ complex, the catalytic core of F_1-ATPase. *Proc. Natl. Acad. Sci. U.S.A.* **86:**6484-6487.

56. Adachi K., K. Oiwa, T. Nishizaka, S. Furuike, H. Noji, H. Itoh, M. Yoshida and K. Kinosita Jr. 2007. Coupling of Rotation and Catalysis in F_1-ATPase Revealed by Single-Molecule Imaging and Manipulation. *Cell,* **130:**309-321.

57. Kabaleeswaran V., N. Puri, J. E. Walker, A. G. W. Leslie and D. M. Mueller. 2006. Novel features of the rotary catalytic mechanism revealed in the structure of yeast F_1-ATPase. *EMBO J.* **25**:5433-42.

58. Okada Y., H. Higuchi and N. Hirokawa.2003. Processivity of the single-headed kinesin KIF1A through biased binding to tubulin. *Nature.* **424**:574–577.

59. Patel, S. S. and K.M. Picha. 2000. Structure and function of hexameric helicases. *Annu. Rev. Biochem.* **69:**651-697.

60. Enemark, E. J. and L. Joshua-Tor. 2006. Mechanism of DNA translocation in a replicative hexameric helicase. *Nature*. **442:**270-275.

61. Burgess S. A., M. L. Walker, H. Sakakibara, P. J. Knight and K. Oiwa. 2003. Dynein structure and power stroke. *Nature.* **421**:715-718.

Achievement for this dissertation

Papers

1) **Axle-less F_1-ATPase Rotates in the Correct Direction**
Science, **319**, 955-958, 2008.
Shou Furuike*, Mohammad Delawar Hossain*, Yasushi Maki, Kengo Adachi, Toshiharu Suzuki, Ayako Kohori, Hiroyasu Itoh, Masasuke Yoshida and Kazuhiko Kinosita Jr.(*Equal contribution)

2) **Hydrolysis Activity of Mutants of F_1-ATPase: a Comparative Study Using Spectrophotometric Method**
Research Journal of Chemistry and Environment, 2008 in press.
Mohammad Delawar Hossain.

3) **Rotation of F_1-ATPase with a Truncated Rotor in the Presence of Lauryldimethylamine Oxide**
Research Journal of Biotechnology, **2**(2), 09-13, 2007.
Mohammad Delawar Hossain and M. Yusuf Ali.

4) **Stimulation of Hydrolysis Activity of Rotary Protein F_1-ATPase with Gamma Subunit Truncations by Lauryldimethylamine Oxide**
Research Journal of Biotechnology, **2**(1), 33-37, 2007.
Mohammad Delawar Hossain.

5) **The Rotor Tip Inside a Bearing of a Thermophilic F_1-ATPase Is Dispensable for Torque Generation**
Biophysical Journal, **90**, 4195-4203, 2006.
Mohammad Delawar Hossain, Shou Furuike, Yasushi Maki, Kengo Adachi, M.Yusuf Ali, Mominul Huq, Hiroyasu Itoh, Masasuke Yoshida and Kazuhiko Kinosita Jr.

Presentations

1) **Studies of γ Subunit Truncated F_1-ATPase**

A poster presented at the annual meeting of the Biophysical Society of Japan, Dec.21-23, 2007, Pacific Yokohama, Yokohama City, JAPAN. Abstract book, vol.47, SUPPLIMENT 1, p.S244, 2007.

Mohammad Delawar Hossain, Shou Furuike, Yasushi Maki, Kengo Adachi and Kazuhiko Kinosita Jr.

2) **Rotation of Some Mutants of Thermophilic F_1-ATPase**

A poster presented at the joint Meeting of Australian Physiological Society and Australian Biophysical Society held in Newcastle City Hall, Newcastle, AUSTRALIA during 2-5 December, 2007. Published in the Proceedings of the Australian Physiological Society, vol.38, 79P, 2007.

Mohammad Delawar Hossain, Shou Furuike, Yasushi Maki, Kengo Adachi and Kazuhiko Kinosita Jr.

3) **F_1-ATPase with a Truncated Rotor**

A poster presented at the Fifth East Asian Biophysics Symposium & Forty-Fourth Annual Meeting of the Biophysical Society of Japan, Nov.12-16, 2006, Okinawa Convention Center, Okinawa, JAPAN. Abstract book: vol.46, SUPPLIMENT 2, p.S347, 2006.

Mohammad Delawar Hossain, Shou Furuike, Yasushi Maki, Kengo Adachi, M. Yusuf Ali, Mominul Huq and Kazuhiko Kinosita Jr.

4) **Generation of Torque by F_1-ATPase with Truncated γ Subunit**

A poster presented at the conference on Frontiers in Chemical Biology: Single Molecules, March 26-29, 2006, Churchill College, University of Cambridge, ENGLAND. Abstract book: p.P06, 2006.

Mohammad Delawar Hossain, Shou Furuike, Yasushi Maki, Kengo Adachi, M. Yusuf Ali, Mominul Huq and Kazuhiko Kinosita Jr.

5) **A study on the $\alpha_3\beta_3\gamma$ Complex of F_1-ATPase with Short γ Subunit**

An oral presentation at the Motility Meeting, January 6-8, 2006, University of Tokyo, JAPAN.

Mohammad Delawar Hossain, Shou Furuike, Yasushi Maki, Kengo Adachi, M. Yusuf Ali, Mominul Huq and Kazuhiko Kinosita Jr.

6) **Rotation of F_1-ATPase with γ Subunit Truncations**

A poster presented at the Annual Meeting of the Biophysical Society of Japan, Nov. 23-25, 2005, Sapporo Convention Center, Hokkaido, JAPAN. Abstract book: vol.45, SUPPLIMENT 1, p.S164, 2005.

Mohammad Delawar Hossain, Shou Furuike, Yasushi Maki, Kengo Adachi, M. Yusuf Ali, Mominul Huq and Kazuhiko Kinosita Jr.

7) **Single Molecule Studies of F_1-ATPase with γ Subunit Truncations**

A poster presented at the Workshop on Biopolymers: Thermodynamics, Kinetics, and Mechanics of DNA, RNA and Proteins, 30 May-3 June, 2005, The Abdus Salam International Center for Theoretical Physics (ICTP), Trieste, ITALY. Abstract book: p.46, 2005.

Mohammad Delawar Hossain, Shou Furuike, Yasushi Maki, Kengo Adachi, M. Yusuf Ali, Mominul Huq and Kazuhiko Kinosita Jr.

8) **Rotation and Hydrolysis Activities of F_1-ATPase with γ Subunit Truncations**

A poster presented at the Annual Meeting of the Biophysical Society of Japan, Dec.13-15, 2004, Kyoto International Conference Center, JAPAN. Abstract book: vol.44, SUPPLIMENT 1, p.S225, 2004.

Mohammad Delawar Hossain, Shou Furuike, Yasushi Maki, Kengo Adachi, M. Yusuf Ali, Mominul Huq and Kazuhiko Kinosita Jr.

9) **A Study on the $\alpha_3\beta_3\gamma$ Complex of Thermophilic F_1-ATPase and Mutants Made by Truncation at the C-terminus of the γ Subunit**

A poster presented at the Autumn Meeting of The Physical Society of Japan, September 12-15, 2004, Aomori University, JAPAN. Abstract book: vol.59, Issue 2, p.258, 2004.

Mohammad Delawar Hossain, Shou Furuike, Yasushi Maki, Kengo Adachi, M. Yusuf Ali, Mominul Huq and Kazuhiko Kinosita Jr.